APPLICATION OF MICROWAVE DIAGNOSTICS TO COPPER CHLORIDE AND CARBON DIOXIDE LASERS

Thesis by

Emilio Sovero

In Partial Fulfillment of the Requirements

for the Degree of

Doctor of Philosophy

California Institute of Technology

Pasadena, California

1977

(Submitted May 26, 1977)

A mis padres y Kyra
por el apoyo que
siempre me han brindado

ACKNOWLEDGMENTS

I would like to express my thanks to my advisor, Professor Fred Culick for his guidance throughout these years. His encouragement and patience are greatly appreciated. His dedication is an example I will always try to follow.

I am also particularly indebted to Professor Fred Shair for his generosity in letting me use his lab facilities. During the early phase of the carbon dioxide experiment we had many discussions which helped me understand the experimental techniques I used.

The experimental work with the copper chloride laser benefited from the support given by Mr. Gary Russell and Dr. J. Chen of the Jet Propulsion Laboratory where the experiments were carried out.

I would like to express my appreciation to all those who have helped me in one way or another: Dr. Alan Vetter, Mr. Erich Siegel, Mr. Don Laird, George Nekrachevitch Jr., Joseph Godley, Jim Bennett, James Yocom, Yuk Lun Chang and Dr. Alexis Livanos.

Thanks are also due to Mr. Frank Linton for technical assistance rendered through the years and for his expertise in the preparation of the illustrations on such a short notice.

I could have never finished this dissertation for the deadline had it not been for Mrs. Ruth Stratton who cheerfully adjusted to my schedule by doing all the typing in record time and with no sacrifice in quality.

I would like to thank the California Institute of Technology for the Graduate Assistantships and Tuition Scholarships I was awarded.

ABSTRACT

Part A

A problem restricting the development of the CuCl laser has been the decrease in output power with increases of tube temperature above 400°C. At that temperature the CuCl vapor pressure is about .1 torr. This is a small fraction of the buffer gas pressure (He at 10 torr).

The aim of the project was to measure the peak radiation temperature (assumed related to the mean energy of electrons) in the laser discharge as a function of the tube temperature. A 24 gHz gated microwave radiometer was used.

It was found that at the tube temperatures at which the output power began to deteriorate, the electron radiation temperature showed a sharp increase (compared with radiation temperature in pure buffer).

Using the above result, we have postulated that this sudden increase is a result of Penning ionization of the Cu atoms. As a consequence of this process the number of Cu atoms available for lasing decrease.

Part B

The aim of the project was to study the dissociation of CO_2 in the glow discharge of flowing CO_2 lasers.

A TM_{011} microwave (3 gHz) cavity was used to measure the radially averaged electron density $\bar{n}_e$ and the electron-neutral collision frequency in the laser discharge. An estimate of the electric field is made from these two measurements. A gas chromatograph was used to measure

the chemical composition of the gases after going through the discharge. This instrument was checked against a mass spectrometer for accuracy and sensitivity.

Several typical laser mixtures were used: CO_2-N_2-He (1,3,16), (1,3,0), (1,0,16), (1,2,10), (1,2,0), (1,0,10), (2,3,15), (2,3,0), (2,0,15), (1,3,16) + H_2O and pure CO_2. Results show that for the conditions studied the dissociation as a function of the electron density is uniquely determined by the STP partial flow rate of CO_2, regardless of the amount of N_2 and/or He present. The presence of water vapor in the discharge decreased the degree of dissociation.

A simple theoretical model was developed using thermodynamic equilibrium. The electrons were replaced in the calculations by a distributed heat source.

The results are analyzed with a simple kinetic model.

TABLE OF CONTENTS

PART A

MEASUREMENT OF ELECTRON RADIATION TEMPERATURE IN DOUBLE-PULSED COPPER CHLORIDE LASERS

I. INTRODUCTION TO COPPER VAPOR LASERS

Interest in the copper vapor laser stems from the need to develop efficient lasers in the visible part of the spectrum. These lasers are representative of the "self-terminating" type in which the transition involved terminates in a metastable level. Its duration is limited by the properties of the transition itself. Stimulated emission lasts only until the populations of the two levels become equal. Pulsed operation with high practical efficiencies (1%) have been achieved with this type of laser.

In this introductory chapter, the general characteristics of the pure copper and the copper chloride lasers are discussed. In particular, the unexpected decay in power output of the copper chloride laser with increasing oven temperature (above 400°C) is to be emphasized. If the cause of this limitation were to be removed, higher volumetric efficiencies would then be possible; the present limit is about 35 μJ per cubic centimeter of active medium. The primary reason for undertaking the experimental work to be described here has been to understand better the reasons for the lower power output above 400°C.

1.1 Lasers Operating in the Visible

In the visible part of the spectrum many types of lasers are known. Table 1.1 is a summary of the principal characteristics of some of the most common CW lasers and the ruby laser. In lasers where a metastable is involved in populating the upper state population, such as for the He-Ne and He-Cd lasers, little or no increase in peak power

TABLE 1.1 Commonly used lasers operating in the visible portion of the spectrum

type	wavelength	avg. power	efficiency
Ruby	6943Å @ 77°K	pulsed	.02%
He-Ne	6328Å	50 mW	.1 %
He-Cd	4416 & 3250Å	75 & 15 mW	.01 & .005%
Ar^+	5287 to 3336Å (several lines)	5 W	.02%
Kr^+	8588 to 3335Å (several lines)	2 W	.01%

can be obtained by pulsing. That type of laser can be usually operated at highest efficiency under CW conditions. The efficiencies of those lasers is usually very small, 0.1% or less. This is due mainly to the low quantum efficiency η of the lasing transition; η is defined as the fraction of the energy of the upper laser level which is utilized in the laser action.

A second class of lasers exists which uses a different transition scheme to be studied here. Lasers of this type include lead, copper, mercury, manganese and nitrogen among others; see Ref. 1.1 for an early and useful review. In atomic systems based on this mechanism the major part of the excitation energy is normally expended in the excitation of the first resonance level. The first resonance level usually has the largest electron-impact cross section. Therefore, it would be desirable to use the first resonance level as the upper laser level. The utilization of a metastable level as the lower laser level then makes it possible to attain efficient population inversion under pulsed conditions (until the lasing action builds up the metastable population). Electron-impact excitation of the forbidden transitions are usually much smaller than those of the allowed transitions. This type of transition is called "self terminating" because the lifetime of the lower level is considerably longer than the upper level. Thus the inversion lasts only until the populations of the two laser levels become equal. (Part of the upper level population is therefore unused in this type of transition.) Excitation may be provided by electron-atom collisions, while inelastic

atom-atom collisions relax the lower levels. If the requirement is dropped that the excitation and relaxation proceed simultaneously, then a class of efficient pulsed lasers becomes possible which is cyclic in operation (Ref. 1.2). Collisional excitation and relaxation occur sequentially rather than simultaneously. Therefore each process may be considered separately and optimized virtually independently of each other. Copper chloride lasers, as opposed to copper vapor lasers, need two additional steps in the cycle: dissociation and recombination of copper chloride. Thus a typical cycle in the copper chloride laser would consist of dissociation of copper chloride into copper and chlorine; excitation of the copper atoms to the upper laser level; lasing transition of the excited copper to the lower metastable level; and finally, recombination of copper and chlorine to form copper chloride.

Calculation of the quantum efficiency of these lasers place an upper limit of 38% in the case of copper atoms. This efficiency is more than two orders of magnitude larger than the lasers shown in Table 1.1. Of course this is only a theoretical maximum, but nevertheless suggests the potential of this type of laser.

1.2 Copper Lasers

The energy levels for the copper atom are shown in Figure 1.1. Copper has two closely spaced resonance levels $^2P_{1/2}$ (3.79 eV) and $^2P_{3/2}$ (3.82 eV). Population inversion may be expected for three transitions to metastable levels $^2D_{3/2}$ and $^2D_{5/2}$, but $^2P_{3/2} \rightarrow {}^2D_{3/2}$

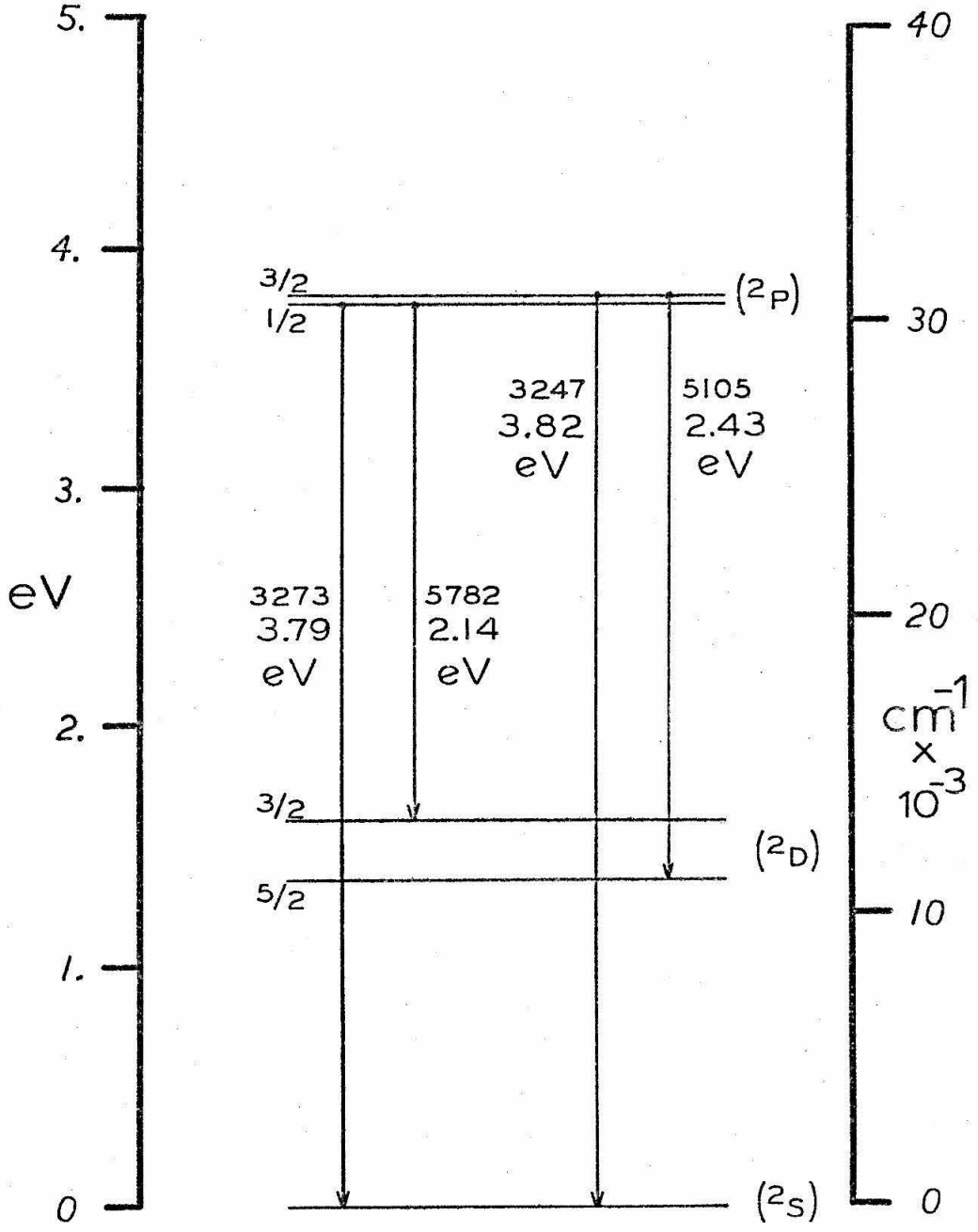

FIGURE I.I.- Energy Levels of Copper.

transition is not observed. The transition $^2P_{3/2} \rightarrow {}^2D_{5/2}$ emits at 5105.54Å, while the $^2P_{1/2} \rightarrow {}^2D_{3/2}$ at 5782.13Å.

This type of three-level structure lends itself to the efficient production of a transient population inversion in a high voltage discharge. Copper has the further advantage of having no energy levels other than the upper and lower laser levels between the ground state to 1 eV above the upper laser level. This contributes to high practical efficiencies by minimizing the number of competing parallel paths for energy loss.

In the design of practical systems to take full advantage of these transitions two things are particularly important: (1) a rapidly rising discharge current pulse. This requirement arises from the need to populate the upper laser level faster than its relaxation rate. This creates an overall increase in the population inversion (i.e., lasing transitions). This process continues only up to the point at which no more copper atoms are available for pumping in the ground state. (2) A sufficient number of copper atoms must be present in the discharge medium. In a pure copper laser, this is accomplished by heating copper metal to a very high temperature, so that sufficient number of copper atoms vaporize. Sputtering of electrodes and exploding wires give a less controlled source. The use of a copper compound with a higher vapor pressure than copper alone permits operation at lower temperatures, but a means to dissociate the compound must be provided.

Laser emission corresponding to the transitions shown in Figure 1.1 was achieved (Refs. 1.2 and 1.3) in pure copper vapor lasers. Copper was deposited in a tube made of alumina, and the tube was filled with a buffer gas, helium, at 1 to 3 torr. The tube was then heated to about 1500°C by an external heater. This temperature corresponds to a copper vapor pressure of .4 torr and a copper atom concentration of $2 \times 10^{15} cm^{-3}$. In a tube 80 cm long, 5 cm I.D., the peak power of the 5106Å line exceeded 40 KW for pulses 16 nsec in duration (Ref. 1.4). The efficiency was calculated to exceed 1%. At 1 kHz repetition rate, the average power was .5 watt.

Isaev et al (Ref. 1.5) used a copper vapor laser of similar construction. However, the heating was done by the discharge itself. Repetition rates of up to 20 kHz were used. At 18 kHz with the discharge capacitor at 18 KV, peak power of 170 KW and efficiency of 1% was obtained. The temperature was estimated to be around 1500°C. Copper was vaporized from small samples in the cavity. Helium pressure was several dozen torr.

Other self heating copper (Refs. 1.6 and 1.7) and lead (Ref. 1.8) lasers have been described. Although simpler to design, the high operating temperatures make them cumbersome to work with. The effects of the partial pressure of copper atoms and the discharge current cannot be isolated because the current itself influences the vaporization of the metallic copper.

A different method of introducing the copper atoms in the optical cavity has been described (Ref. 1.9). It consists of an

exploding copper wire scheme. Pumping is accomplished with a 20 KV pulsed discharge. The main advantages of this method are operation at room temperature and wider pulses (65 nsec); however, an elaborate focusing arrangement and low pressures (10^{-5}torr) are needed; low power output is obtained (30 watts peak @ 5106Å) and only single shot operation is possible.

A method developed at the Jet Propulsion Laboratory (Ref. 1.10) is based on introducing copper in the form of a halide, copper chloride. The relatively high vapor pressure of this compound made operation at less than 400°C possible. A more detailed description of the double pulsed laser used in the present work will be given in later discussion of the experimental work (§3.1 and 3.2).

Briefly, copper chloride is deposited in the laser tube. It is appropriate to note here that the choice of material for the tube is not as limited as in the case with pure copper vapor lasers; although quartz is preferred, pyrex can also be used as tube material. The laser tube is enclosed in an oven and heated, typically to 400°C. The vapor pressure of copper chloride at this temperature has been calculated to be about .2 torr, yielding a copper atom density of $1.5 \times 10^{15} cm^{-3}$. Both helium and neon at 10 torr have been used as buffer gases.

At least two discharge pulses (20 KV, 300 amp peak) are needed for operation. The first pulse dissociates the copper chloride, and the second pumps copper atoms from the ground state to the upper laser level. Laser emission takes place at the beginning of the second current pulse and lasts for about 15 nsec. The output energy

density per pulse is 30 $\mu J/cm^{-3}$ at a repetition rate of 17 Hz.

It is possible to have a continuous train of pulses in which each pulse acts as a pumping and dissociating pulse. As in the case of self heating copper (pure) lasers, the active medium is heated by the discharge itself. In a tube 30 cm long, with an inside diameter of 1 cm, the best performance was obtained with the 5106Å line, at 20 kHz. The average efficiency was 1% and the energy and power density per pulse were 35 $\mu J/cm^{-3}$ and 1.7 kW/cm^{-3}, respectively. The laser pulse width was 20 nsec. The buffer gas used was helium at 10 torr.

Copper iodide has been used in a similar fashion (Ref. 1.12). Since the vapor pressure of this compound is higher, the operating temperatures are also correspondingly higher (600°C); repetition rates of 8 kHz have been achieved, with an output energy density per pulse of 9 $\mu J/cm^{-3}$. Transverse excitation has been demonstrated (Ref. 1.13) with copper iodide.

Although it appears that the continuously pulsed laser is the type with the most potential applications (due to its higher efficiencies and average power), many of its operating parameters are coupled. Thus the simpler operation of the double pulsed copper chloride laser makes it attractive for the study of the lasing mechanism.

1.3 Characteristics of the Copper Chloride Laser

Copper chloride at the operating temperature of the laser (400°C) is largely in the solid phase. The vapor in equilibrium at this temperature is composed of a monomer CuCl and a trimer Cu_3Cl_3 with no

dimer present. At 1000°K the monomer comprises only $1.4 \times 10^{-3}\%$ of the vapor (Ref. 1.14). Since typical operating temperatures of the laser are below this level, the amount of monomer present in the laser medium is assumed negligible. The vapor pressure of copper chloride in equilibrium with its solid phase can be calculated from data provided by Brewer (Ref. 1.14) and the Clausius Clapeyron equation. The calculated vapor pressure as a function of temperature is given by

$$\ell n(P) = C_1/T + C_2^* \ell n(T) + C_3 \quad \begin{cases} P \text{ in torr} \\ T \text{ in } °K \end{cases}$$

$$C_1 = -2.254 * 10^4$$

$$C_2 = -7.892$$

$$C_3 = 81.414$$

With the vapor pressure of copper chloride it is then possible to calculate the number density of copper atoms available if all the copper chloride atoms were dissociated. A graph of copper atom density versus temperature is shown in Figure 1.2, taken from Ref. 1.16.

Buffer gases used to date include helium, neon and argon. Partial pressures range from 5 to 40 torr, the optimum based on power output being in the vicinity of 10 torr.

Buffer gas flow serves mainly as a mechanism to remove gaseous impurities released by the copper chloride powder after heating. Sealed off operation has been demonstrated to be possible if precautions are taken to remove all impurities from the laser tube

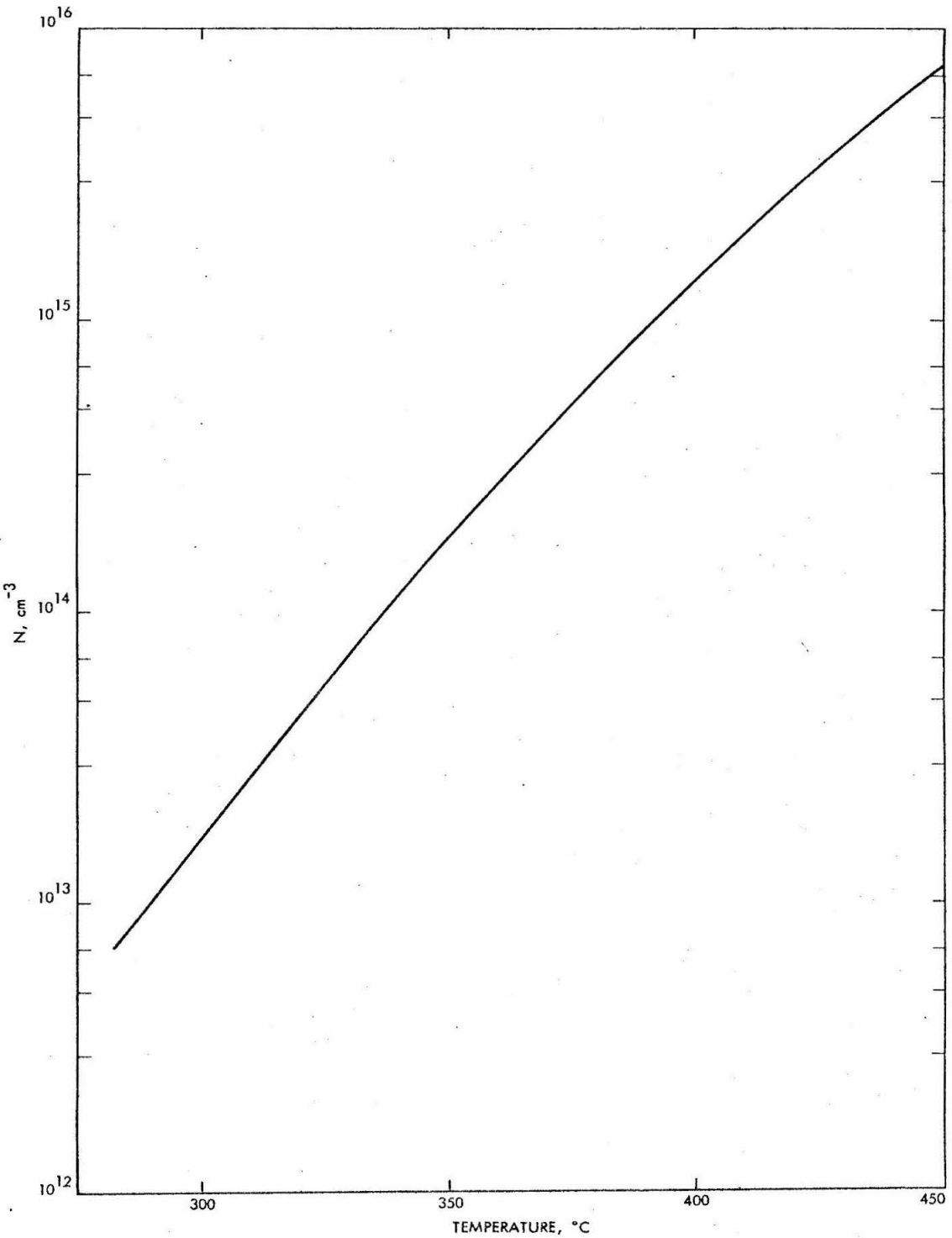

Figure 1.2.– Density of Copper Atoms from Saturated Cu_3Cl_3 Vapor as a Function of Temperature. (ref. 1.16)

before sealing (Ref. 1.15). Performance is comparable to flowing double pulsed lasers. However, degradation in performance has been observed after a few weeks of operation.

The copper chloride laser in the double pulsed mode requires two discharge pulses separated by some fixed delay. The pulses are generated by discharging capacitors across the laser tube with fast high voltage switches (thyratrons). Since the initial charge of the capacitors and their capacitance value is known, and if losses in the circuit are ignored, the input energy per pulse is easily calculable as $1/2\ CV^2$. The delay between pulses is generated by delaying the trigger signal to the high voltage switches with standard digital circuits. Typically this delay has been found to be of the order 30 μsec to 100 μsec, depending on the tube diameter. Figure 1.3 shows the laser output vs delay between pulses of a 30 cm by 2.5 cm I.D. laser tube.

Both minimum and maximum delays have been explained by absorption measurements (Ref. 1.16). After the first pulse the copper chloride is almost completely dissociated. However, a large number of metastable copper atoms in the lower levels of the lasing transition are also created at this time. The metastable population decays at a faster rate than the recombination of copper and chlorine atoms, so after a few microseconds a state of potential inversion is possible if all the ground state copper atoms were to be pumped to the upper laser level. This finite lifetime of the metastable population determines the existence of a minimum delay before a pumping pulse can

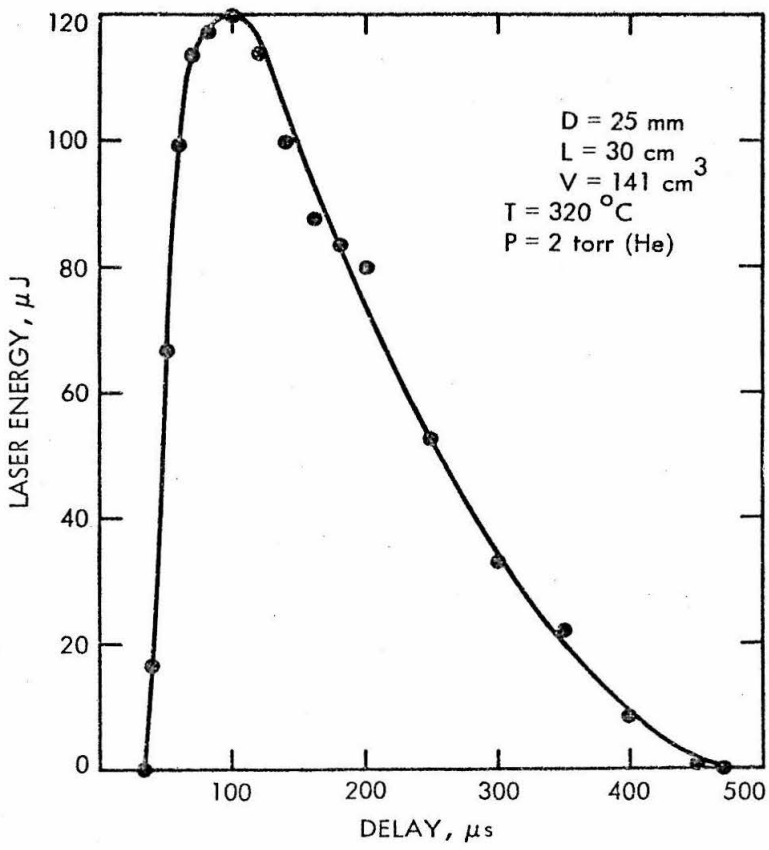

Fig.1.3 Laser energy as a function of delay between current pulses (ref. 1.16)

be applied. This minimum delay is sharply defined and depends on the diameter of the tube. The metastables decay at a faster rate in smaller diameter tubes. This dependence is attributed to diffusion phenomena.

It is the lifetime of the lower metastable level which puts an upper limit to the repetition rate in continuously pulsed lasers using pure copper, copper chloride or copper iodide. It is necessary to allow the metastables created by the lasing action to decay back to the ground state before a pumping pulse may be applied again.

Although not as sharply defined, there exists a maximum delay for the pumping pulse, beyond which no lasing action is observed. This is attributed to the removal of available copper atoms by recombination with chlorine.

1.4 Behavior of the Double Pulsed Copper Chloride Laser as a Function of Temperature

Figure 1.4 shows the peak output power of a copper chloride laser versus temperature. The increase in output power with temperature has been attributed to the similar increase in number density of copper atoms shown in Figure 1.2. It was expected that as the temperature was increased further, the accompanying increase in copper chloride vapor pressure would result in an increase in total output power for the same active volume, due to the higher copper atom density available (Figure 1.2). However this is not the case; after a temperature of about 400°C the output power decreases with increasing temperature. No satisfactory explanation for this phenomenon has been advanced to date.

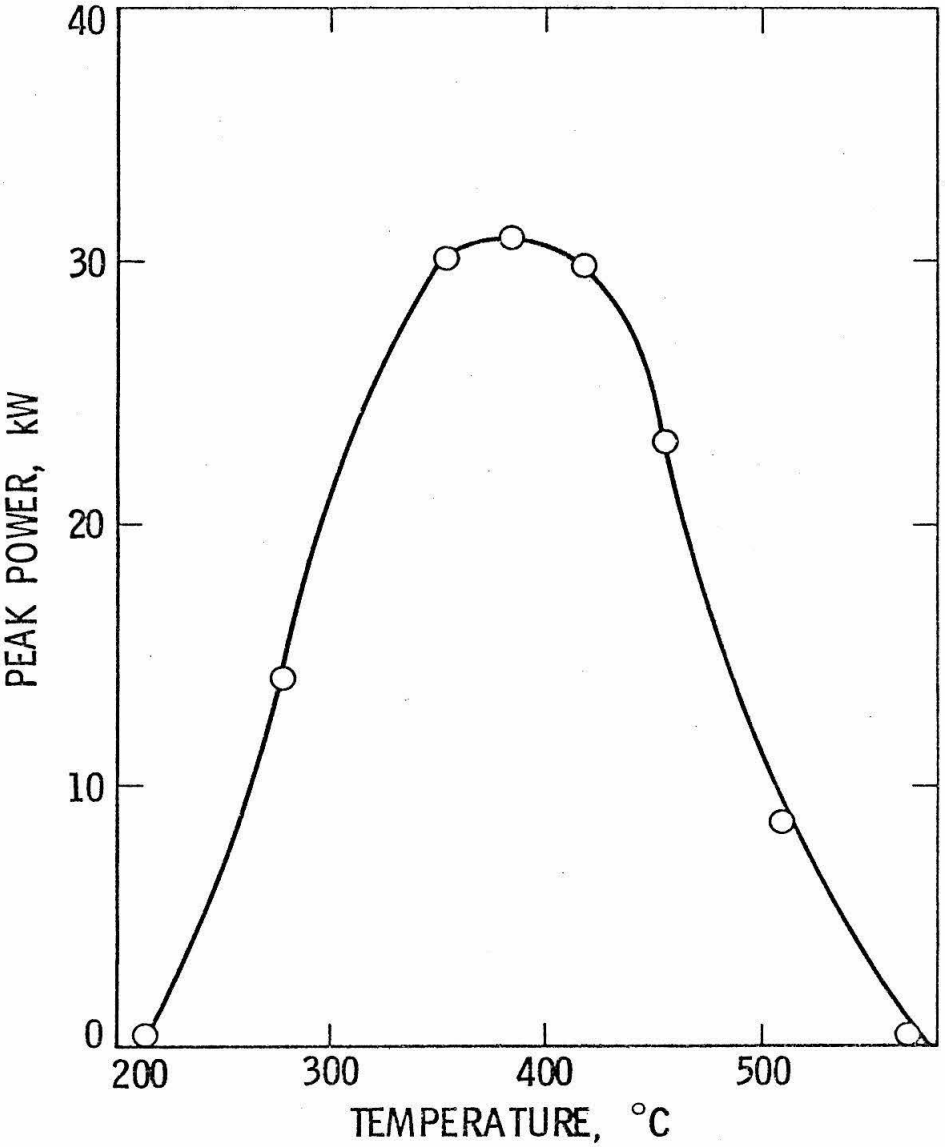

FIG 1.4: TYPICAL LASER OUTPUT VS. TUBE TEMPERATURE (Ref. 1.16).

The excitation of the copper atoms after dissociation by the first pulse is accomplished by direct electron impact excitation. Simple calculations of excitation rates (Ref. 1.17), assuming Maxwellian electron distribution and cross sections calculated by classical methods (Ref. 1.18), indicate that the upper level excitation rate is highly dependent on the average electron energy.

A study of electron temperatures during the pumping pulse in the double pulsed laser might clarify the phenomenon of decreasing power with increasing temperature. If this limitation could be removed, the power density per unit of active volume would increase. This would result in more powerful lasers.

1.5 Present Measurements of Electron Temperature

To measure the electron average energy, a gated microwave radiometer method was chosen, as this was the most reliable for the conditions encountered in a double pulsed copper chloride laser.

A radiometer measures the radiation intensity coming from a body. If the assumption is made that the emission is produced by a black-body, it is then possible to calculate the temperature of such a body from Planck's law. The radiometer system incorporated boxcar averaging techniques in order to improve the signal-to-noise ratio. The rise time of the system is estimated to be 20 nsec.

Broadly, the results found in the present work are the following. If the laser tube is operated normally in all respects except with no copper chloride present, a plot of peak radiation temperature

(during the second or pumping pulse) versus tube temperature exhibits the monotonically decreasing behavior to be expected. If copper chloride is then placed in the tube, similar results are obtained for laser temperatures below 400°C, but for temperatures above that the behavior is markedly different. Above 400°C the electron radiation temperature increases with increasing laser temperature giving a "U" shaped curve, more pronounced for helium than for neon buffer.

This strong influence of copper chloride on the electron radiation temperature has been attributed to Penning ionization (Ref. 1.19) of copper atoms by metastable helium or neon atoms created by the dissociation (first) current pulse. Since copper atoms are thus ionized, fewer are then available for lasing. This mechanism provides a possible reason for the decrease in laser output above certain laser tube temperature.

References

1.1 G. G. Petrash, "Pulsed Gas Discharge Lasers", Soviet Physics Uspekhi 14, N6, 747 (1972).

1.2 W. T. Walter, M. Pilch, N. Solimene, G. Gould, "Pulsed Laser Action in Atomic Copper Vapor", Bull. Amer. Phys. Soc. 11, 113 (1966).

1.3 W. Walter, N. Solimene, M. Pilch, G. Gould, "Efficient Pulsed Gas Discharge Lasers", IEEE J. Quant. Elect. QE-2, 474 (1966).

1.4 W. Walter, "40 KW Pulsed Copper Laser", Bull. Amer. Phys. Soc. 12, 90 (1967).

1.5 A. A. Isaev, M. A. Kazaryan, G. C. Petrash, "Effective Pulsed Copper Vapor Laser with High Average Generation Power", JETP Lett. 16, 27 (1972).

1.6 R. S. Anderson, L. W. Springer, B. G. Bricks, T. W. Karras, "A Discharge Heated Copper Vapor Laser", IEEE J. Quant. Elect. QE-11, 172 (1975).

1.7 R. S. Anderson, B. G. Bricks, L. W. Springer and T. W. Karras, "A Discharge Heated Copper Vapor Master Oscillator Power Amplifier", IEEE J. Quantum Elect. QE-11, 56D (1975).

1.8 R. S. Anderson, B. G. Bricks, T. W. Karras, L. W. Springer, "Discharge heated lead vapor laser", IEEE J. Quantum Elect. QE-12, 313 (1976).

1.9 J. F. Asmus and N. K. Moncur, "Pulse broadening in a MHD copper Vapor Laser", Appl. Phys. Lett. 13, 384 (1968).

1.10 C. J. Chen, N. M. Nerheim, G. R. Russel, Appl. Phys. Lett. 23, 514 (1973).

1.11 C. J. Chen and G. R. Russell, "High Efficiency, Multiple Pulsed Copper Vapor Laser Utilizing Copper Chloride as a Lasant", Appl. Phys. Lett. 26, 504 (1975).

1.12 I. Liberman, R. V. Babcock, C. S. Liv, T. V. George and L. A. Weaver, "High Repetition Rate CuI Laser", Appl. Phys. Lett. 25, 334 (1974).

1.13 I. Smilanski, L. A. Levin and G. Erez, "A Copper Laser Using CuI Vapor", IEEE J. Quant. Elect. QE-11, 919 (1975).

1.14 L. Brewer, "The Fusion and Vaporization Data of the Halides" in The Chemistry and Metallurgy of Miscellaneous Materials: Thermodynamics, L. L. Quill, Ed. (McGraw-Hill Book Co. Inc., 1950), Ch. 7.

1.15 N. M. Nerheim, Jet Propulsion Laboratory, Private communication.

1.16 Visible Wavelength Laser Development, Final Report, Aug. 1975 to DARPA by Jet Propulsion Laboratory.

1.17 D. A. Leonard, "A Theoretical Description of the 5106Å Pulsed Copper Vapor Laser", IEEE J. Quant. Elect. QE-3, 380 (1967).

1.18 M. Gryzinski, "Classical Theory of Atomic Collisions. I. Theory of Inelastic Collisions", Phys. Rev. 138, A336 (1965).

1.19 A. von Engel, "Ionization in Gases by Electrons in Electric Fields", Encyclopedia of Physics, Vol. XXI, S. Flügge, Ed. (Springer-Verlag, 1956).

II. METHODS OF MEASURING AVERAGE ELECTRON ENERGY

Many of the useful characteristics of plasmas are due to the interaction of the electrons with the other particles in the plasma. For instance, the electron-neutral collisions are the main excitement mechanism in many gas lasers.

Except in very special systems, a complete theoretical description of the plasma parameters such as electron density, collision frequency, electron energy distribution or average energy is not possible. It is therefore necessary to rely on experimental techniques to provide the required information for the characterization of the plasma.

In this chapter three methods for measuring electron temperatures are briefly reviewed: Langmuir probes; spectroscopic observation of visible radiation; and microwave radiometry. It has been found that for transient phenomena in medium pressure gases (10 to 40 torr) microwave radiometry is the most accurate method. Since radiometer measurements are based on the assumption of partial equilibrium, the thermalization time must be substantially less than the time scale for the desired measurements.

2.1 Measurement of the Average Electron Energy

In the absence of an electric field, a swarm of electrons in a gas attains thermal equilibrium with the gas molecules. When an electric field is applied and the swarm drifts along E at the drift velocity, the electrons acquire energy from the field at a rate which can greatly

exceed the rate of loss determined by the elastic and inelastic collisions. The mean energy thus increases until the rate of loss balances the rate of gain.

Only in the case when elastic collisions predominate (low E/P, the ratio of electric field and pressure) can the mean energy be easily calculated (Ref. 2.1)

$$\langle \varepsilon \rangle = \frac{eE*\ell_1}{P(3\lambda)^{1/2}} \qquad (2.1)$$

where the symbols are defined as

- E electric field
- e electron charge
- P gas pressure
- ℓ_1 mean free path at 1 torr
- λ mean fractional loss per collision (elastic)

In all other cases it is necessary to obtain the mean energy experimentally. The most commonly used methods include electrical probes, spectroscopy, and microwave radiometry.

2.2 Electrical Probes

By a probe we mean a small metallic electrode, which is immersed in a plasma. Generally the probe is connected across a potential source to a reference electrode, which in many cases serves simultaneously as the cathode or the anode of a discharge tube. The current flowing to the probe is measured as a function of the applied voltage. The resulting relation between the probe current and the

probe voltage is called the "characteristic". Under the most favorable conditions, the potential and the velocity distribution of electrons of the undisturbed plasma in the immediate neighborhood of the probe can be derived from characteristics. Compared with many other diagnostic tools the probe is distinguished by the possibility of direct local measurement of plasma parameters. This advantage of probes, however, is closely connected to their main shortcomings. The local measurement requires the probe to be inserted into the plasma being investigated by means of a probe holder whose surface area in most cases is many times larger than the probe itself. The probe system forms a "wall" in addition to the already existing plasma boundaries and at least in its close proximity the plasma parameters may deviate seriously from those in the absence of the probe.

Since the original work by Langmuir (Ref. 2.2) and later by Druyvesteyn (Ref. 2.3) on the theory of the single probe, the experimental techniques and the theory of probes has been refined by many workers. A significant development was the invention of the double probe technique by Johnson and Malter (Ref. 2.4). This method is useful when the space potential is not well defined (e.g., high-frequency discharges, afterglows, and the upper atmosphere).

The range of applicability of simple probe theory is limited to cases in which the mean free path of the electrons is much greater than the probe dimensions and the Debye shielding length. The first limitation implies gas pressures below one torr while the second

guarantees that the quasi-neutrality of the plasma will not be significantly disturbed by the probe. The Debye length is given by

$$h = \left(\frac{kT_e}{4\pi e^2 n_e}\right)^{1/2} \simeq 6.9\left(\frac{T_e}{n_e}\right)^{1/2} \text{ cm.} \qquad \begin{matrix} T_e[=]\ ^\circ K \\ n_e[=]\ cm^{-3} \end{matrix} \qquad (2.2)$$

in which the temperature is expressed in °K, and n_e is the electron density, cm^{-3}.

Systems deviating significantly from these limits can still be studied with probes by taking into consideration all the other phenomena which were neglected in the simple probe theory. Results obtained with probes in the high pressure range ($\lambda \simeq r_{probe}$) have been subject to questioning.

2.2.1 Time Resolution of Probes

In order to study transient phenomena it is necessary to record the probe characteristic in a time shorter than the time scale of changes in the plasma. However, there exists a limit to the rate at which this can be done. This limit is set by the finite time required by the ions for their redistribution within the sheath. Practical time resolutions are of the order of one microsecond. Some improvement can be obtained by pulsing, sampling, and averaging techniques. As one tries to improve the time resolution, the hardware aspect of the experiment becomes crucial, the capacitance impedance of the probe plasma system becomes significant and masks the true characteristics.

In conclusion it can be said that electrical probes are most useful in studying low pressure plasmas of characteristic times greater than about 1 microsecond.

2.2.2 Probes in the Copper Chloride Laser

The use of probes to study the characteristics of laser plasmas is well established. Probes are particularly well suited for CW gas lasers, carbon dioxide (Refs. 2.5, 2.6, 2.7) for instance. Although these lasers operate outside the low pressure limit of the simple probe theory, due to the stable nature of the plasma, it is possible to modify the theory to account for any departures from the ideal.

In the case of copper chloride lasers, the plasma is also outside the low pressure limit (pressure greater than 1 torr), however, more serious difficulties preventing the use of probes are:

The time resolution required (better than 100 nsec) is outside the practical limit of probes.

The laser tube is operated well below the boiling point of copper chloride, as a result copper chloride is likely to form deposits in the cooler parts of the tube. Due to higher heat conductivity, metal probes and their electrical connections which act as radiators are more likely to be cooler than surrounding glass. Any amount of deposits will mask the true nature of the probe response. Since the amount of deposits is uncontrollable, its effect on the probe response is unpredictable.

2.3 Spectroscopic Measurements of the Electron Temperature

Another method of obtaining the plasma parameters is based on the observed characteristics of the spectral lines or bands, or continuous radiation.

One such method consists in measuring the relative intensity of two lines of the same atom. From these the electron temperature can be derived, provided the electron excitation functions for both lines are known and are markedly different from each other. This method assumes that all the excitation transitions occur by electron impact from the ground state. Helium or neon lines cannot be used with this method since excitation by electrons may not be only from the ground state, but also from metastable states. This rules out this method for copper chloride lasers, since they use either helium or neon. In theory the time resolution of this system should be limited only by the detector and the time constant of the excitation process.

The second order Stark effect of lines from an isolated upper level can also be used to evaluate T_e. The ratio of shift to width of a spectral line is a strong function of T_e. The method is adequate for temperatures below 12 eV (94,200°K). The time resolution of this method is limited by the speed and accuracy at which a line spectrum may be obtained.

The very noisy, both electrically and optically, environment of the laser system suggests that it would be more difficult to use spectroscopic techniques in the copper chloride laser plasma. Many problems are anticipated in trying to measure such small optical signals.

2.4 Microwave Radiometry

It is a consequence of the laws of thermodynamics that the radiation of a perfect black body is a function of temperature and wavelength only. Planck's formula is the quantitative expression of this law. From the diagnostic point of view, the measurement of thermal (incoherent) radiation provides information on the electron temperature of the plasma (Ref. 2.8).

The radiation temperature of a plasma is defined as (Ref. 2.9):

$$kT_r = \frac{-\int \eta_\omega(p)\ f(p)\ d^3p}{\int \eta_\omega(p)\ \frac{\partial f(p)}{\partial \varepsilon}\ d^3p} \tag{2.3}$$

where $\eta_\omega(p)$ is the differential rate at which energy is emitted spontaneously per unit solid angle per unit bandwidth by an electron with momentum p and $p + \Delta p$, $f(p)$ is the electron distribution function, ε the electron energy, k is the Boltzmann constant, and ω is the frequency in radians, at which the observation is made. This radiation temperature is related to the intensity received at the radiometer by the source function S_ω (Ref. 2.9).

$$S_\omega = \frac{\omega^2}{8\pi^2 c^2}\, kT_r \tag{2.4}$$

The formulas (2.3) and (2.4) are derived in Appendix A.

If the source is in equilibrium it is theoretically possible to determine T from intensity measurements directly. In practice it is usually more convenient to use a reference source at the same

frequency and of known temperature to calibrate the radiometer.

The radiation temperature of a plasma is related to the electron temperature (average energy) only when the electron distribution is Maxwellian and/or when $\eta_\omega(p)$ varies as p^2 (see Appendix A) as in the case of helium for electron energies greater than 1 eV. Although very few cases satisfy exactly either of the above two conditions, in practice they approach them close enough that significant information can be gained from the radiation temperature (Refs. 2.10 and 2.11).

A significant advantage of radiometry over electrical probes is that the plasma is not disturbed by the probing system. Additionally, there is no fundamental limitation on the values the plasma pressure could have.

2.4.1 Radiometer Design

A radiometer is a receiver used in the detection of noise-like signals spread over a relatively large band of frequencies (microwaves in the case of plasmas). The design of a suitable radiometer is governed by the expected frequency spectrum, amplitude and temporal structure of the signal. For relatively narrow bandwidths, the thermal emission of a plasma can be considered constant: the amplitude is approximately independent of frequency. In theory, it would then be favorable to make the bandwidth of the receiver very wide to pass as much power to the detector as possible. However, this increase in bandwidth also increases the minimum detectable signal, thereby reducing the signal quality and the signal-to-noise ratio. Only in the case of very strong emission can this method be used.

The signal levels expected (10^{-15} watts) in glow discharges render direct detection of the emission impractical. To bring the signal to detectable levels, amplification in excess of one hundred decibels is necessary. The noise figure of the amplifier (or amplifiers) required for this purpose exceeds this signal level by several orders of magnitude.

The Dicke radiometer (Ref. 2.12) solves this problem by periodically switching between a known source (T_r) and an unknown (T_x). By then synchronously detecting the amplified signal, noise reduction is at a maximum when the reference and the unknown signal are of equal amplitude (on the average). Thus the usual arrangement (Fig. 2.1) consists of two input branches: one for the unknown source and the other for a reference source in series with a calibrated attenuator. A switch then alternatively connects the two branches to the radiometer (at a repetition rate f). The attenuator is adjusted until the Fourier component, at frequency f, of the resulting signal is zero. At this point the signal received from the two input branches is of the same magnitude. It is then straightforward to calculate the unknown temperature T_x from the reference T_r and the attenuation factor α :

$$T_x = \alpha T_r$$

With this system, sensitivities of a few degrees are possible.

2.4.2 Time-Resolved Measurements

The Dicke radiometer is very useful when studying steady phenomena such as D.C. glow discharges with characteristic times longer than the

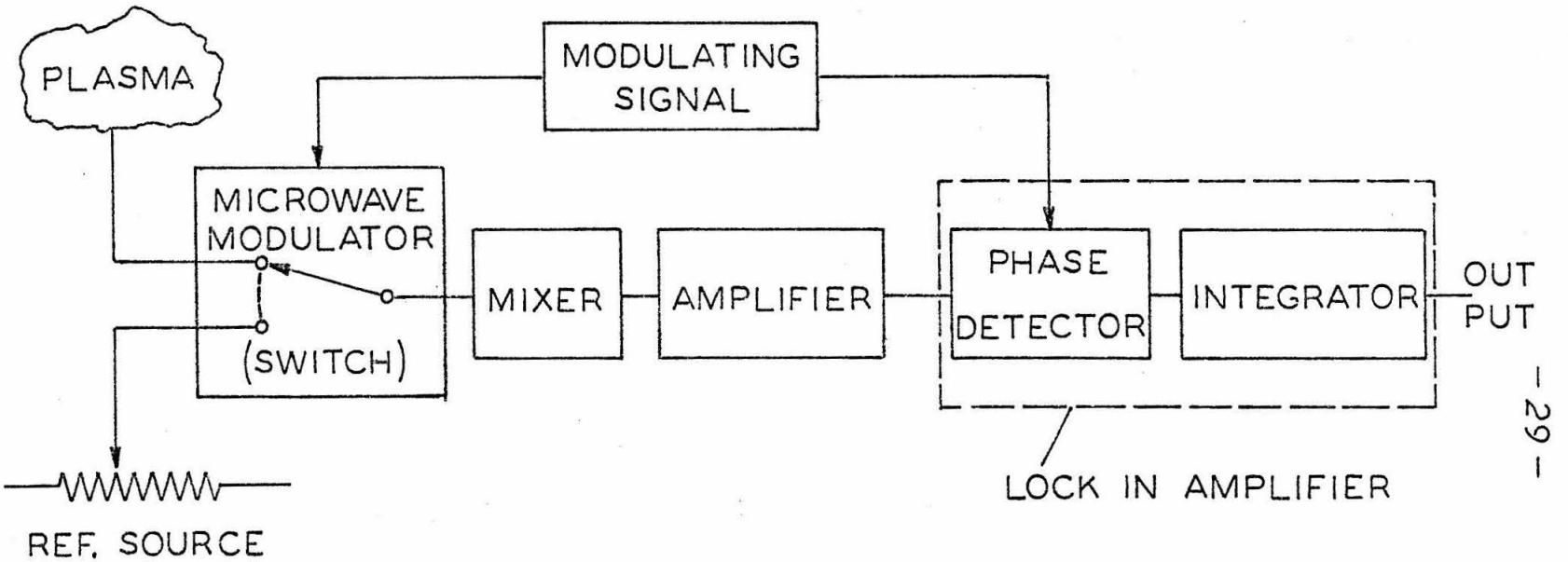

FIG. 2.1 SCHEMATIC DIAGRAM OF DICKE RADIOMETER

integration time of the radiometer which is of the order of minutes. In pulsed systems, the radiation emission changes rapidly and the Dicke instrument is of little use.

A modification of the Dicke radiometer can be made with only a modest loss in sensitivity, which allows time-resolved measurements in repetitive phenomena. A gate signal of very short duration (compared with the times involved in the experiment) is used to sample and hold (until the next sample is acquired) alternatively a reference source and the transient plasma emission. If the gate signal is synchronized with the plasma event it is then possible to obtain a point by point comparison of the transient signal to the reference source. The transient signal can then be reconstructed. This method was used in Refs. 2.13 and 2.14, and with some modifications is the method used in the present study.

The boxcar averager is an instrument ideally suited to accomplish all these signal processing functions. The boxcar averager operates in the following manner. A repetitive waveform and a synchronous trigger are presented to the boxcar averager. At precisely the selected moment an electronic gate opens for a very short selected time period and then closes. The balance of the waveform is ignored. Since many repetitions of the waveform are sampled, the output of the boxcar averager will be proportional to the average level of the input signal during sampling. However, the noise which accompanies the waveform is attenuated, since the average value of random noise is zero. If more than one point on the waveform is to be examined,

or if the entire waveform is of interest, the gate is scanned across the entire waveform.

Although the use of microwave radiometry in the study of pulsed discharges has been established in the past few years (Refs. 2.13, 2.14, 2.15), the time resolution of the measurements has been rather limited, of the order of 10 μsec typically. In pulsed lasers the time region of interest is usually the time while the current is flowing through the plasma. Of particular interest in metal vapor lasers is the leading edge of the current pulse, since it is during that period that lasing takes place. All these events occur in less than .2 μsec, so it was necessary in the present work to develop a radiometer system capable of resolving events in that time scale.

Transient measurements of radiation temperature are based on the assumption that the electron distribution rapidly relaxes to the equilibrium Maxwellian distribution. The time constant τ_{ee} for energy relaxation by electron-electron interaction is a rough measure of the relaxation time. This time constant is given by (Ref. 2.16)

$$\tau_{ee} \simeq \frac{[U_e(eV)]^{3/2}}{7.7 \times 10^{-5}[n_e(cc^{-1})]} \text{ sec} \qquad (2.6)$$

As a typical example, for an electron temperature of 10 eV and electron density $n_e \doteq 10^{14} cm^{-3}$, the time constant is 4.1 nsec. This is a factor of ten less than the shortest characteristic time in the experiment. We therefore assumed that radiation coming from the laser tube is generated by a nearly Maxwellian plasma.

According to equation (2.6), as the measured radiation temperature increases (related to the average electron energy) the time required to approach equilibrium also increases. This behavior introduces some uncertainty in the results due to the larger departure from the Maxwellian distribution.

References

2.1 F. Llewellyn-Jones, "The Glow Discharge and an Introduction to Plasma Physics (Methuen & Co. Ltd., London, 1966), p. 39.

2.2 I. Langmuir and H. M. Mott-Smith, Phys. Rev. 28, 727 (1926).

2.3 M. J. Druyvesteyn, Z. Phys. 64, 790 (1930).

2.4 E. O. Johnson and L. Malter, Phys. Rev. 76, 1411 (1949).

2.5 P. O. Clark and M. R. Smith, Appl. Phys. Lett. 9, 367 (1966).

2.6 P. Bletzinger and A. Garscadden, Proc. IEEE 59, 675 (1971).

2.7 M. Z. Novgorodov, A. G. Sviridov and N. N. Sobolev, IEEE J. Quantum Electr. QE-7, 508 (1971).

2.8 M. A. Heald and C. B. Wharton, Plasma Diagnostics with Microwaves (John Wiley & Sons Inc., New York, 1965).

2.9 G. Bekefi, Radiation Processes in Plasmas (J. Wiley & Sons Inc., New York, 1966).

2.10 G. Bekefi and S. C. Brown, J. Appl. Phys. 32, 25 (1961).

2.11 D. Wildman, QPR No. 106, Research Laboratory of Electronics, M.I.T., p. 121.

2.12 R. H. Dicke, Rev. Sci. Instrum. 17, 268 (1946).

2.13 J. C. Ingraham and S. C. Brown, Phys. Rev. 138, A1015 (1965).

2.14 R. L. Stenzel and R. W. Gould, Rev. Sci. Instrum. 40, 1461 (1969).

2.15 M. Sugawara and B. C. Gregory, Phys. Rev. 2, A439 (1970).

2.16 I. Shkarofky, T. Johnson and M. Bachynskii, The Particle Kinetics of Plasmas (A and W Co., Reading, 1966).

III. APPARATUS AND INSTRUMENTATION

This chapter describes the apparatus used in the experiments. Attention is drawn to the laser tube design. Sealed-off operation was possible but lack of reproducibility prevented its use. A flow system that flows only through the ends of the tube (2 inlet and 2 outlet ports) and not through the active region was used.

A low inductance double-pulsed power supply capable of repetition rates up to 18 Hz is described, and also the radiometer system with associated calibrations.

3.1 Laser Tube, Gas and Vacuum System

The laser tube was made of quartz with ground glass taper joints at each end. The tubes were sealed for low pressure operation by means of end pieces constructed with matching taper joints. Fused silica windows were fused to the end pieces at the Brewster angle. Each end piece was made with both a gas inlet and an exhaust port. Figure 3.1 is a diagram of a laser tube. The laser was usually operated with a continuous flow of buffer gas through the end pieces but with no net flow of gas through the tube. This design was found to provide the most uniform density of copper chloride in the active medium. The main function of the buffer gas flow is to carry away any gaseous impurities generated by the copper chloride powder. Unless extreme care is taken to prevent contamination, sealed-off performance degrades after about half an hour to an hour of operation. It has been found that the flow rate is not critical to the short term operation of the laser.

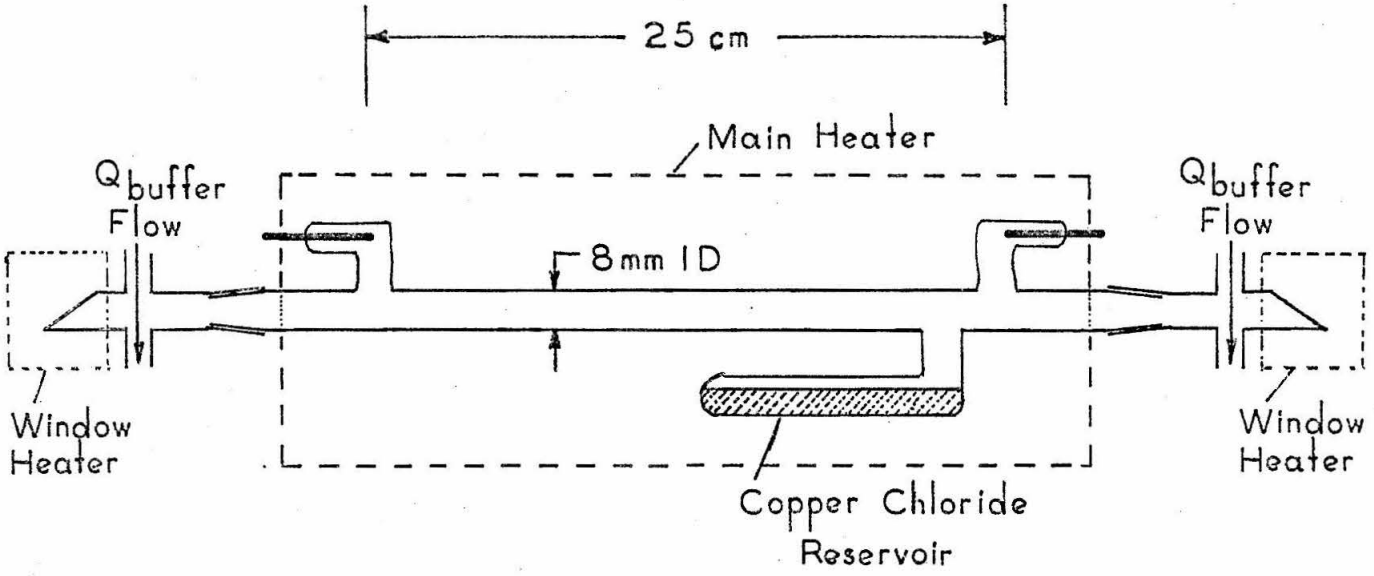

FIG. 3.1 Laser tube used in the experiment

The gases used as buffers were helium (99.95%) and neon (99.7%). The active region of the laser was enclosed in a 12 inch Mellen heater. The end caps with the windows which were outside the oven were heated separately with heating tape. The power supplied to the heaters was controlled manually with autotransformers (VARIAC).

The temperature in the tube was monitored with two iron-constantan thermocouples. One was placed next to the reservoir of copper chloride while the other monitored the temperature of the tube in the active region of the laser. The temperature reported as the tube temperature in these experiments is the arithmetic average of these two readings (the hottest and coolest part). This is, of course, not precisely the temperature of the medium in the laser. The error is estimated to remain constant, yielding relative values of temperature with an accuracy of about 1-3%

3.2 Power Supply

A double-pulse power supply designed and built at the Jet Propulsion Laboratory was used. Figure 3.2 shows a simplified circuit diagram of the supply. Reduced to the bare essentials, the circuit consists of a charging system (25 KV, 25 ma), a capacitor (being charged continuously) and a high voltage fast switch for each of the two pulses. The capacitor C_1 is charged to a set voltage; when that voltage is reached the control circuit discharges the capacitor through the laser tube. Then after a short delay (10-200 μsec) the second capacitor (C_2), also fully charged by its own charging circuit, at this time is discharged.

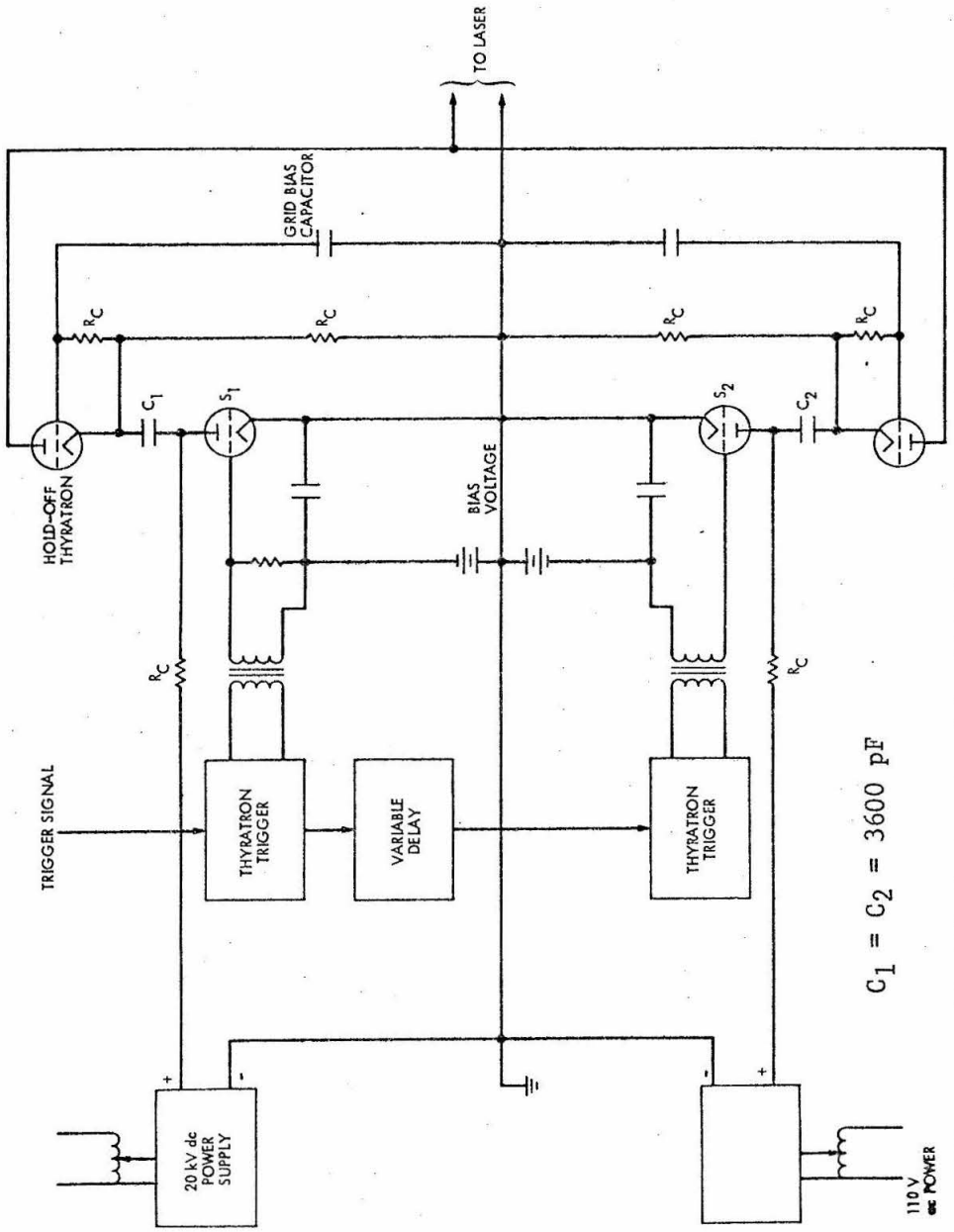

Fig. 3.2 Modified circuit of double-thyratron-switched power supply. The hold-off thyratrons prevented premature firing of switch S_2

This produces two current pulses of about 200 nsec in duration (more or less, depending on the value of capacitance) separated by an adjustable delay. The maximum repetition rate of these double pulses is limited by the time required to fully charge the capacitors (on the order of milliseconds) before the control circuits can activate the discharge mechanism. To allow the use of a wide range of capacitance values the repetition rate was limited to 17 Hz. To minimize the effects of stray inductances, the capacitors and high voltage switches (thyratrons) were assembled around the laser oven. The term "saddle power supply" will be used when referring to this power supply. Current rise times of about 7.5×10^9 amperes/sec were obtained.

The laser had tungsten pin electrodes located in branches of the main tube. The active region (the region of the discharge located within the optical cavity) was approximately 25 cm long and 8 mm I.D.

3.3 Radiometer System

A schematic diagram of the radiometer system is shown in Figure 3.3. The characteristics of the components are summarized in Appendix B. In order to detect the microwave emission from the laser tube it is necessary to match the discharge tube to the K-band waveguide (the radiometer used operated in this band). This is accomplished with a brass fitting (Fig. 3.4) in which a waveguide section crosses the axis of the laser tube at a ten degree angle. It is assumed that the microwave radiation in the cavity is in equilibrium with the plasma radiation and that the measured radiation leaking into the waveguide

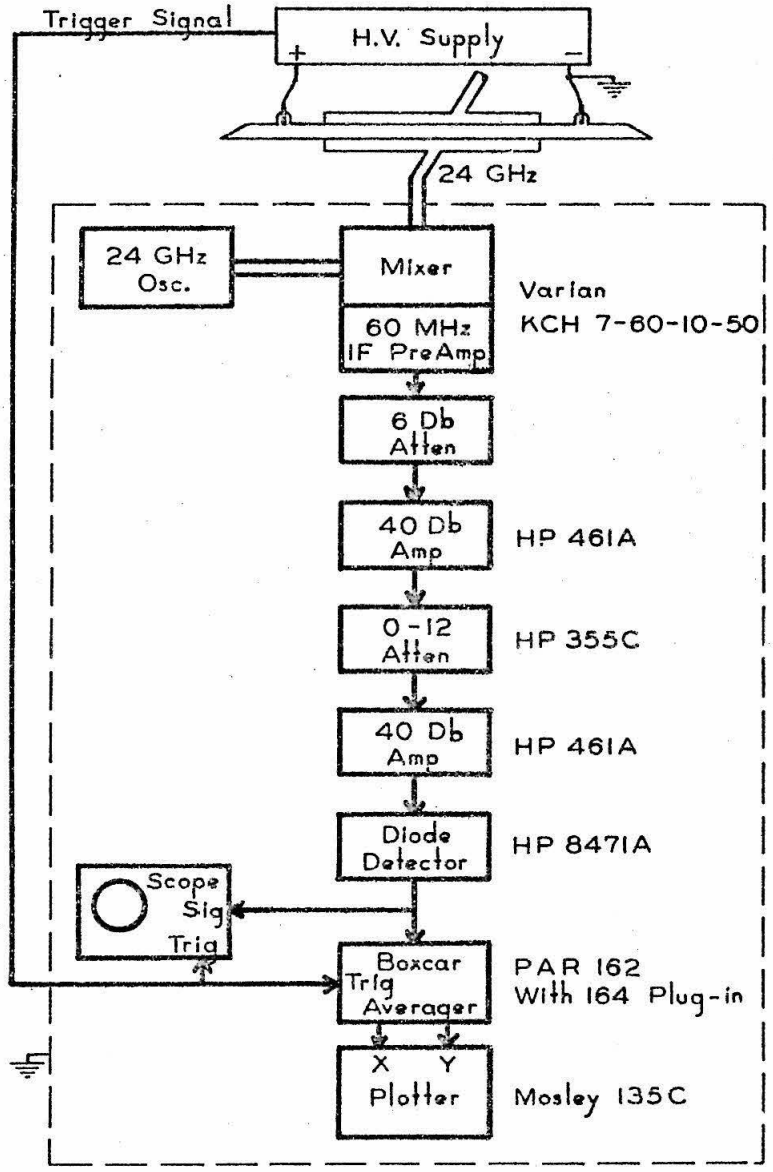

Fig.3.3: RADIOMETER SYSTEM

FIG. 3.4 Plasma to Waveguide Coupler

is a true sample of radiation in the plasma tube. Due to the high operating temperatures it was necessary to nickel-plate the brass fitting in order to prevent corrosion.

The signal emitted by the plasma and coupled to the waveguide is fed to a mixer which shifts it in frequency to a 20 MHz band, centered at 60 MHz. The signal is then further amplified and then rectified by a diode detector. A boxcar averager (P.A.R. 162 with P.A.R. 164 plug-in) samples this signal synchronously. The sampled signal is averaged internally and its resultant value displayed in the vertical axis of an X-Y plotter. A ramp signal which is synchronized with the trigger and sampling pulse provides a horizontal axis for the reconstruction of an average signal. The entire instrumentation was enclosed in a grounded copper screen room to prevent any R.F. interference.

The entire system had a bandwidth of 12 MHz, which is equivalent to a time resolution or response time of 28 nsec. This bandwidth was determined by noting that all other instruments in the system had wider bandwidths than that of the preamplifier in the microwave mixer which was 12 MHz. The sampling gate of the boxcar averager was set to 30 nsec.

3.4 Calibration of the Instruments

The following calibrations of the instruments are required.

1. The correlation between the radiation temperature and strength of the output signal. The laser discharge tube is operated in D.C. mode with pure helium gas; the discharge current and gas pressure are known. The radiation temperature under this condition is well established both by theoretical prediction (Ref. 3.1) and experimental verification

(Ref. 3.1). The output signal is measured. Thus the strength of the output signal can be correlated with the radiation temperature under the same geometrical and electronic conditions. The calibration has also been checked with a neon standard noise source. The agreement between the two calibrations is satisfactory.

2. The signal delay time in the electronic circuit. Because the time scale in the present measurement and the signal delay time in the electronic circuit are of the same order, the correction of the time measurement for the signal delay time is required. The signal delay time in the circuit between the input of the microwave mixer to the input of the boxcar averager is measured by using the scheme depicted in Figure 3.5. The high voltage pulses break down the discharge tube, causing the electron density in the tube to increase rapidly. The transmission of microwaves across the tube is cut off abruptly when the electron number density reaches the cut-off point. This cut-off point is observed simultaneously with a dual beam oscilloscope, Tektronix 7844 with 7A19 and 7A24 vertical amplifiers. This instrument is capable of resolving events down to 1 nsec. Since the delay introduced by a foot of coaxial cable is 1.5 nsec, care was taken to compensate for the different lengths of cable used. Thus the signal delay time in the electronic circuit is obtained.

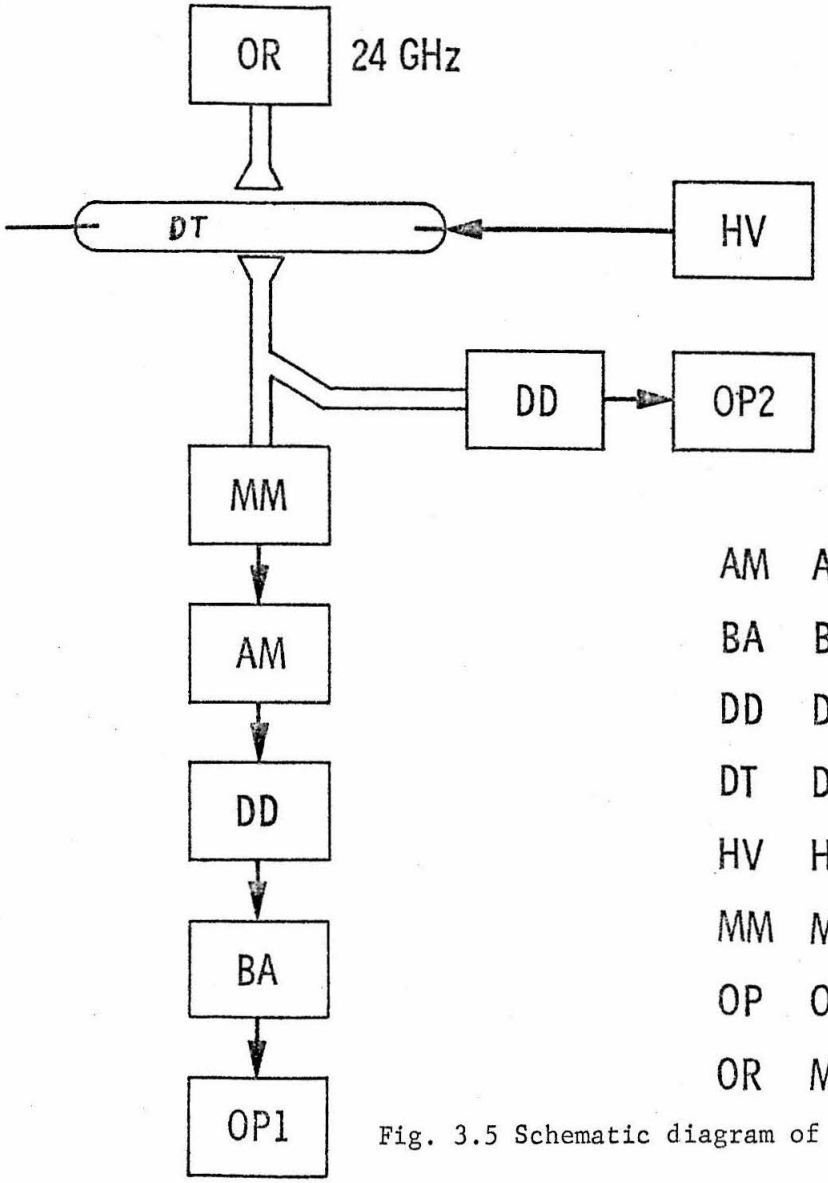

AM AMPLIFIER 60 MHz, 62-74 dB

BA BOXCAR AVERAGER

DD DIODE DETECTOR

DT DISCHARGE TUBE

HV HIGH VOLTAGE PULSE

MM MICROWAVE MIXER, IF = 60 MHz, 23 dB GAIN

OP OSCILLOSCOPE, TECHRONIX 7704

OR MICROWAVE OSCILLATOR, 24 GHz

Fig. 3.5 Schematic diagram of the instrumentation for time delay measurement.

References

3.1 G. Bekefi and S. C. Brown, J. Appl. Phys. 32, 25 (1961).

IV. EXPERIMENTAL RESULTS

To insure reproducibility of the results a weekly schedule was established. This schedule is described along with the graphs of peak radiation temperature (during the second pulse) versus laser tube temperature for helium and neon, with and without copper chloride in the system. The data obtained show a definite effect on the radiation temperature by the presence of copper chloride vapor in the system.

4.1 Experimental Procedures

The data acquisition was adjusted to the following schedule. On Friday the laser tube was disassembled and cleaned with nitric acid. It was then washed, dried, and loaded with new copper chloride powder. The laser tube was then reassembled, heated to 250°C and pumped continuously until Monday. It is believed that with this procedure all the impurities were driven off the copper chloride powder, since the use of distilled copper chloride (as opposed to that commercially available) yielded no appreciable difference in the behavior of the laser. On Monday a buffer gas was supplied to the laser and the temperature of the laser was slowly increased. With the power supply operating, radiometer readings were taken of the radiation temperature during the second pulse (the first pulse dissociates the copper chloride, the second excites the dissociated copper atoms). It was thus possible to obtain a set of curves of radiation temperature vs time (Fig. 4.1).

A curve was plotted for each temperature interval of about 30°C between 300°C to 500°C. In order to avoid any transient effects the

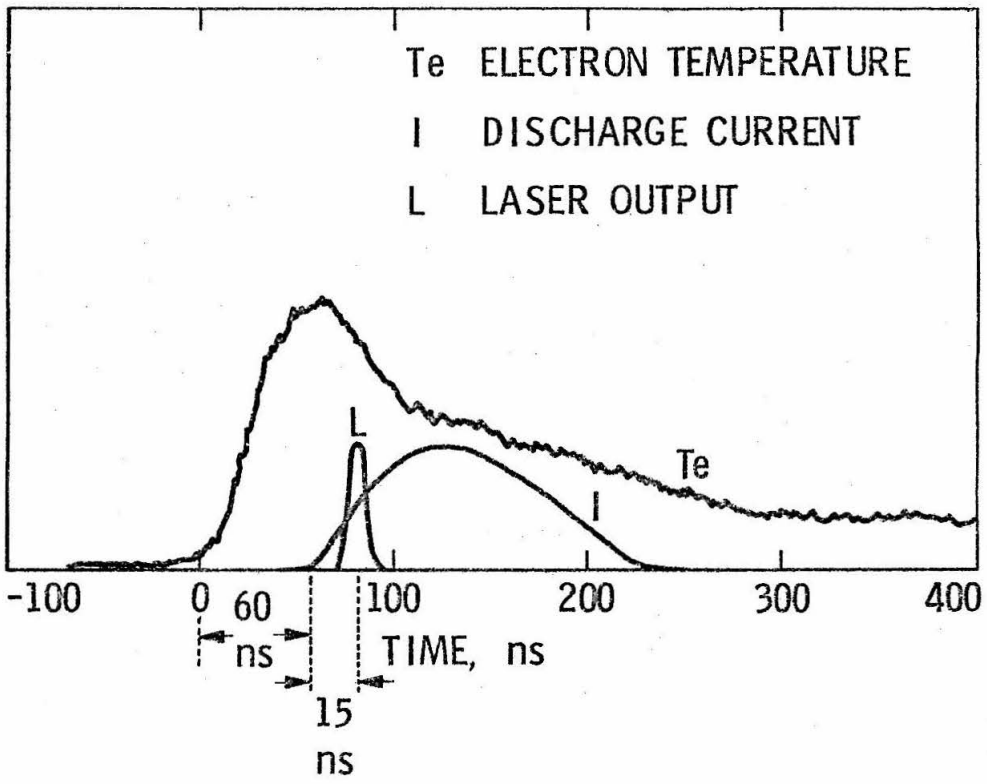

FIG. 4.1 Temporal relation among electron temperature, current peak, and laser output.

temperature was changed very slowly; as a result only one set of curves was taken per day. A load of copper chloride usually lasted for over a week of daily operation (if the operating time above 450°C was limited). However, in this study the operation was limited to four days (Monday to Thursday). Data were taken on the first three days, while the fourth day was dedicated to testing the instruments and apparatus.

The delay time from the first to the second pulse was set at 33 μsec for helium and 55 μsec for neon. This delay was chosen as the optimum delay in each case (see Figure 1.3). The power supply settings were the same in both cases: a 3600 pF capacitor was charged to 20 KV for the second pulse.

4.2 Dependence of Radiation Temperature on the Temperature of the Laser Tube

The peak of the radiation temperature, shown in Figure 4.1, roughly coincides with the laser emission under all conditions. Figure 4.1 also shows that the initial rise in radiation temperature precedes the steep current pulse rise by about 60 nsec. The peak current value was around 300 amperes. A more careful observation of the current pulse (Ref. 4.1) has shown that there is a small current (of the order of amperes) not observed within the resolution of our system, flowing for about 40 nsec before the steep rise in current.

Peak radiation temperatures as a function of the laser tube temperature for pure helium (no copper chloride present) and neon are shown in Figures 4.2 and 4.3. Despite the scatter in the experimental

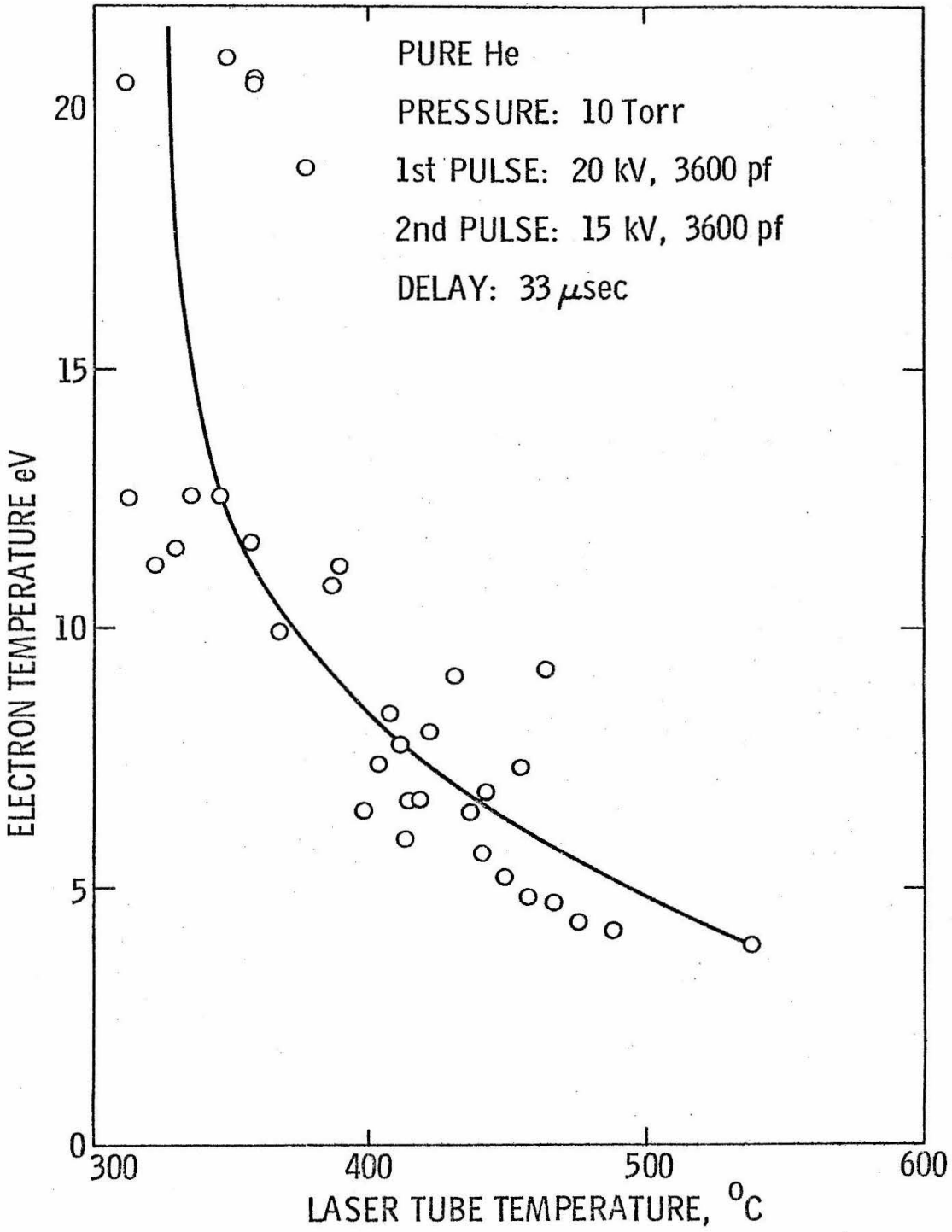

Fig. 4.2 Radiation temperature vs. laser tube temperature for pure He.

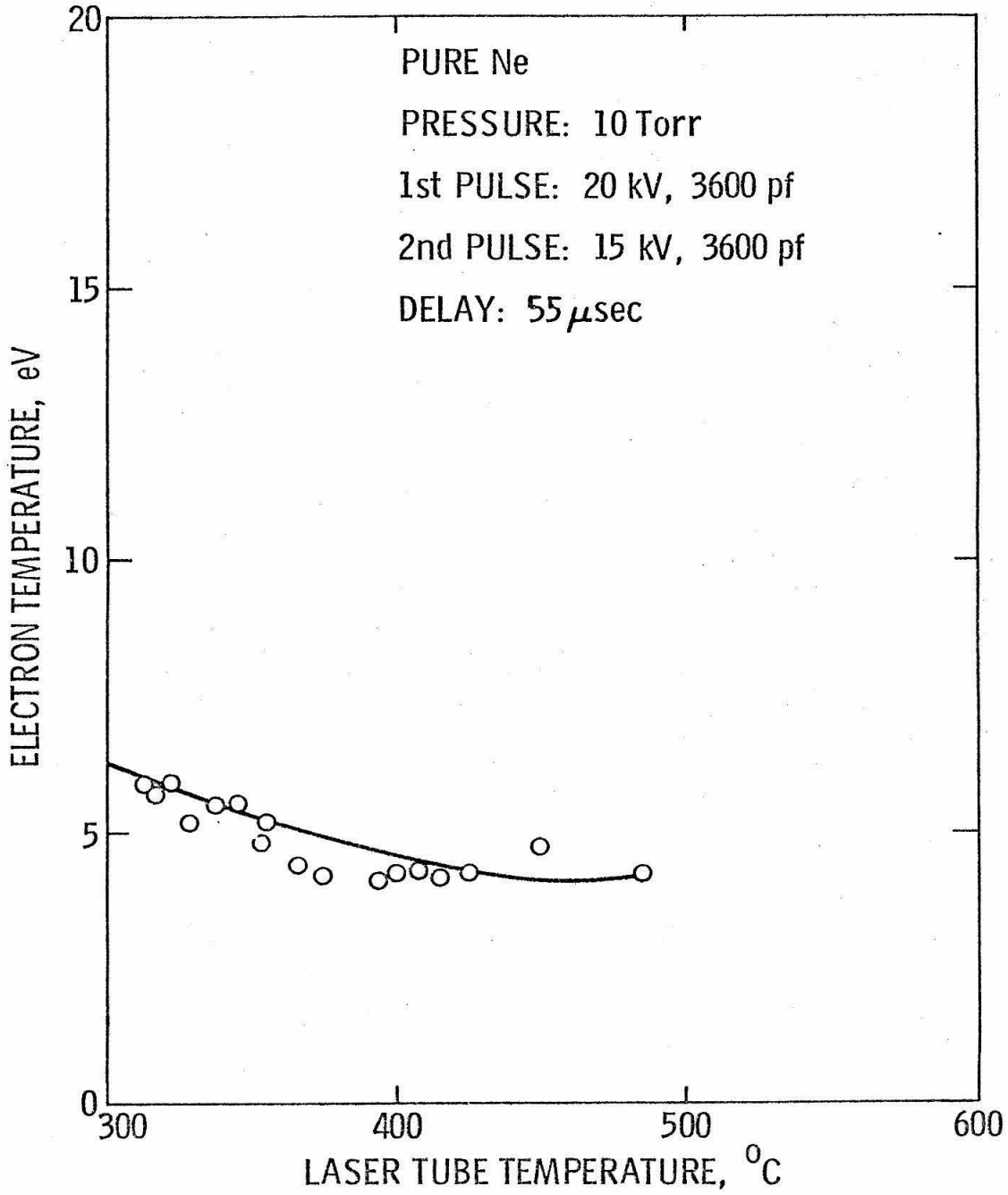

Fig. 4.3 Radiation temperature vs. laser tube temperature for pure Ne.

data, there is a definite decrease in radiation temperature with increasing laser temperature. These trends agree with theoretical calculations for these gases (Ref. 4.2).

The maximum radiation temperature as a function of the laser tube temperature for mixtures of copper chloride and buffer gases helium or neon is shown in Figures 4.4 and 4.5, respectively. It can be seen that at the lower laser tube temperatures the descending portion of the radiation temperature curves agree in trend with the theory advanced by Von Engel (Ref. 4.2), while the ascending portion of the electron temperature is contrary to theory. Both curves exhibit a minimum electron temperature at the laser temperature of about 400°C, which is also the optimum temperature for maximum laser output for the experimental arrangement used.

4.3 Observations

It is worthwhile noting three qualitative observations:

(a) When the delay between the first and second pulse was varied from 20 to 200 μsec, the peak radiation temperature seemed unaffected.

(b) Measurements of the electron density in the afterglow of the first pulse indicate that the electron density remains high ($n_e > 10^{14} cc^{-1}$) throughout the interval between the first and second pulse, for delays up to 60 μsec.

(c) Emission from the laser takes place after 10 nsec of the start of the current pulse under all conditions studied. This corresponds to approximately the peak of the microwave emission (radiation temperature, Fig. 5.1). This maximum, however, is not as well defined.

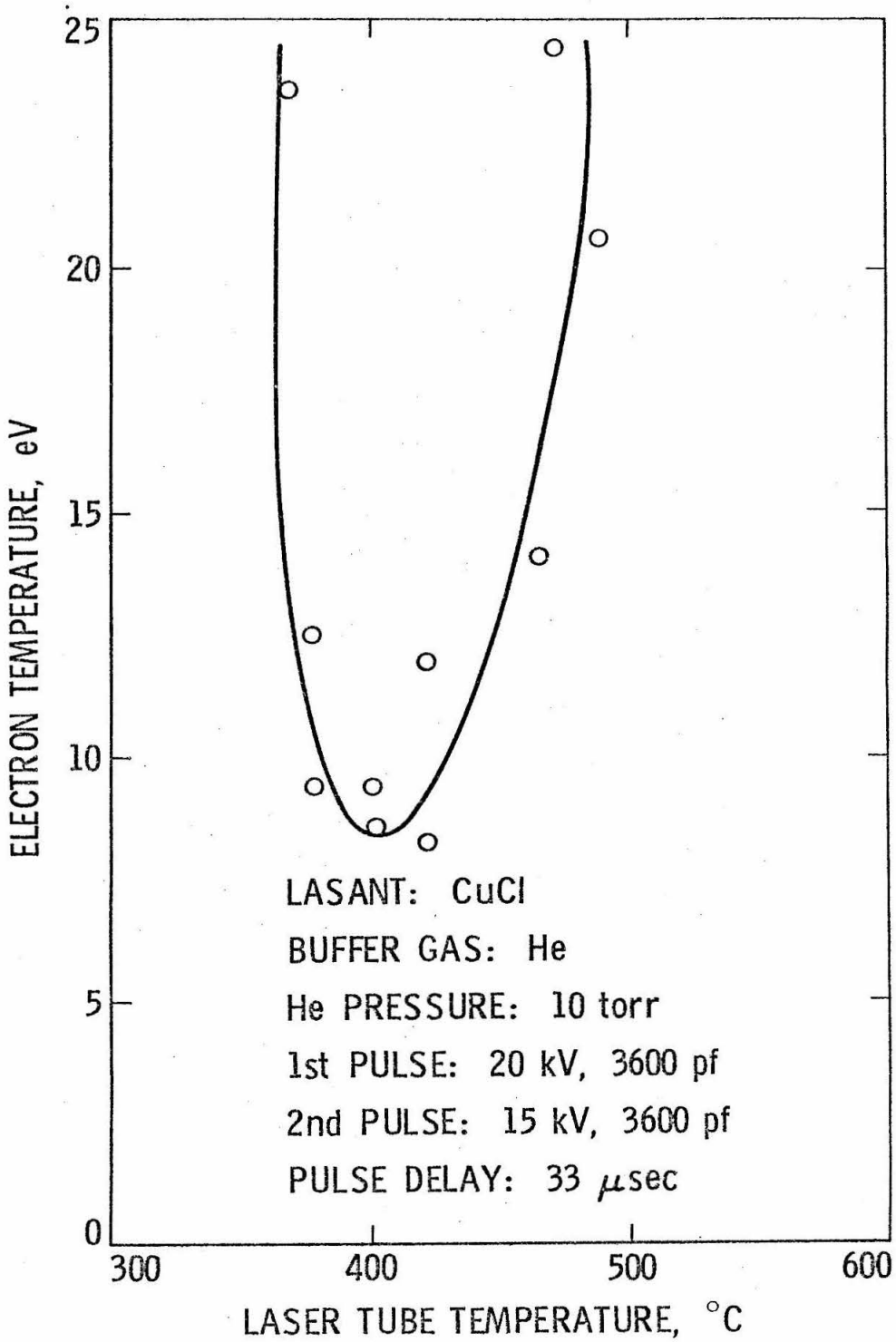

Fig. 4.4 Radiation temperature vs. laser tube temperature for mixture of copper chloride and He.

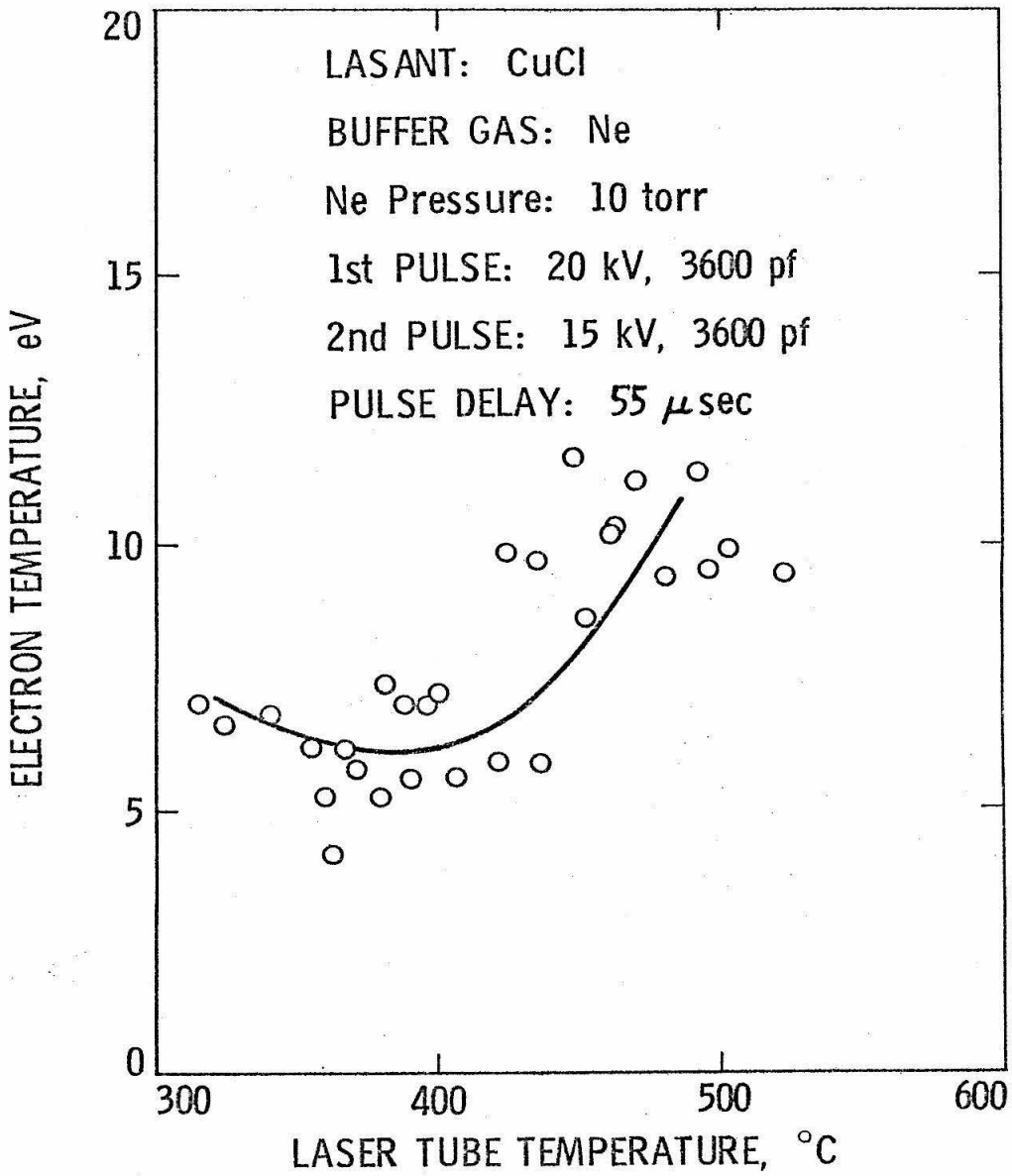

Fig. 4.5 Radiation temperature vs. laser tube temperature for mixture of copper chloride and Ne.

References

4.1 A. Vetter, Jet Propulsion Laboratory, Pasadena (Private communication).

4.2 A. Von Engel and M. Steenbeck, Electrische Gasentladungen, Ihre Physik und Technik (Springer-Verlag, Berlin, 1932), Vol. 2, p.86.

V. DISCUSSION OF THE RESULTS

The behavior of the peak radiation temperature vs gas temperature in the copper chloride laser is discussed. The lack of lasing action at high oven temperatures is evidently related to the rise in radiation temperatures. Penning ionization is proposed as a possible reason for this rise; however, only qualitative arguments can be presented at this time.

5.1 The Possible Causes of Electron Temperature Increase

From Figures 4.2, 4.3, 4.4 and 4.5 it is apparent that the increase of the electron temperature at higher laser tube temperatures is due to the interaction of buffer bases (He or Ne) and the lasing medium in the tube. The detailed mechanism of the interaction, at this time, is not known. Possible causes may be Penning ionization and charge exchange ionization of the copper and/or chloride atoms. The reactions can be represented as

He metastable Penning ionization

$$He(2^1S,2^3S) + X \rightarrow He(^1S) + (X^+)^* + e \rightarrow He(^1S_0) + X^+ + e + \Delta E_1 \cdots \quad (5.1)$$

Charge exchange ionization

$$He^+ + X \rightarrow (X^+)^* + He \rightarrow X^+ + He + \Delta E_2 \cdots \quad (5.2)$$

where X stands for Cu or Cl. Similar reactions may be written with Ne replacing He. In reaction (5.1) a He atom in the metastable state

having excitation energy of about 20.3 eV, collides with the copper (chlorine) atom which has an ionization potential of 7.7 eV (13 eV). The collision results in a ground state He atom, a highly excited copper ion having an excitation energy of ΔE_1 = 12.6 eV (20.3 - 7.7 eV), and a low energy electron. The excitation energy ΔE_1 is then released when the ion is de-excited. In reaction (5.2) the He ion exchanges charge with the copper (chlorine) atom, yielding a ground state He atom and a highly excited Cu (Cl) ion. The excitation energy in the Cu ion is ΔE_2 = 16.8 eV which is equal to the difference between the ionization potential of He (24.5 eV) and that of Cu (7.7 eV). For chlorine, ΔE_2 is 11.5 eV. The Cu (Cl) ion excitation energy is released through de-excitation. The energy of the metastable level of neon is 16.6 eV; therefore the excess energy ΔE_1 in relation (5.1) is approximately 4 eV less than in the case of helium. Evidence of the above reactions has been demonstrated by a previous study of the Cu^+ laser (Ref. 5.1). The energies (ΔE_1 and ΔE_2) are then transferred to the electron gas and ultimately radiated by collisional processes (Ref. 5.2).

There are no experimental or theoretical data known to the author for the rates of the reactions expressed in (5.1) and (5.2) for copper or chlorine in the literature. However, the published cross sections for Penning ionization of the metastable state for He with various target species listed in Ref. 5.3 are higher than $10^{-15} cm^2$ (with the exception of H_2). The cross section for Penning ionization

of the metastable state for Ne is about 50% less than that of He. The charge exchange cross section can only be inferred from the data for the other elements (Ref. 5.4) to be about $10^{-16}cm^2$. The numbers quoted here are uncertain and are used only for a qualitative illustration. The reaction characteristic time τ_p and τ_c for the Penning and charge exchange ionization, respectively, can be estimated by using the quoted numbers with the expression

$$\tau = \frac{1}{qnv} \tag{5.3}$$

where q is the ionization cross section ($10^{-15}cm^2$ for τ_p, 10^{-16} for τ_o); n is the number density of He metastable states or ions (estimated to be 3×10^{16}, roughly 10% of the He atom density); and v is the thermal speed of the reactants ($2 \times 10^5 cm/sec$).

Thus

$$\tau_p \equiv 80 \text{ nsec}$$

$$\tau_c \equiv 1 \text{ } \mu sec$$

τ_p is within the time scale of the present experiment. Thus, Penning ionization may be the dominant process in this present experiment.

In comparing Figs. 4.2, 4.3, 4.4, and 4.5 it can be seen that when the tube temperature is increased from 400°C to 500°C the increases of electron temperature due to the interaction between the copper and the buffer gases are 18 eV for He and 8 eV for Ne. The magnitude of the increase in electron temperature for a given metastable number density is proportional to the product of the cross section for Penning ionization and the difference between the energy

of the metastable level and the ionization level of Cu (or Cl). For Ne, the energy of the metastable level (16.6 eV) is smaller than that for He (20.3 eV), and the Penning ionization cross section for Ne is probably less than that for He. The measured increases of electron temperature, assumed due to Penning ionization, for the two buffer gases have qualitatively borne out this assumption. As the tube temperature is increased, the electron temperature rises more when helium is used as the buffer gas because more energy is lost to the electron gas in the process described by reaction (5.1).

5.2 Explanation of Laser Output as a Function of Laser Tube Temperature

The typical laser output as a function of laser tube temperature is shown in Figure 1.4. From the results discussed in the preceding section, the characteristic of the copper laser represented by the curve in Figure 1.4 can be explained as follows. At lower laser tube temperature (in the vicinity of 300°C) the copper number density is low ($5.5 \times 10^{12} cm^{-3}$). The lack of copper atom number density explains the lower laser output in this range of laser tube temperatures. At higher laser tube temperatures (in the vicinity of 500°C) the number density of copper is 6×10^{15} following the dissociation of copper chloride.

For the elevated electron temperatures (with He, 25 eV and with Ne, 13 eV) according to Figures 4.4 and 4.5 the copper should be fully ionized, depleting the density of copper atoms. To support this argument, the ionization characteristic times for ionization of

copper atoms are estimated. The experimental value of the ionization rate of copper atoms by electron collisions is not available. However, the ionization rate by electron collision as a function of electron temperature may be calculated by using the Gryzinski classical formulation (Ref. 5.5) with a Maxwellian electron velocity distribution. The electron temperatures are 25 and 13 eV for He and Ne buffer gases, respectively. The characteristic times for ionization of copper atoms is given by

$$\tau = \frac{1}{kn_e} \tag{5.4}$$

where k is the ionization rate constant and n_e is the electron number density. The results derived in Ref. 5.6 for a Maxwellian distribution with average energy 25 eV and 13 eV give as the rate constant k, 10^{-7} and $3 \times 10^{-8} cm^3/sec$ respectively. If we assume an electron density of at least $10^{15} cm^{-3}$, the characteristic times would then be 33 nsec for neon and 10 nsec for helium. These are in the range of characteristic times for the experiments. Thus, with these high average electron energies, it is quite possible that a large fraction of the copper atoms will indeed be ionized on the time scale at which the pulsed laser is operated.

The optimum laser power is obtained in the laser tube at a temperature of about 400°C. The corresponding electron temperatures, as shown in Figs. 4.4 and 4.5, are about 6 to 7 eV. At these electron energies the ionization rate (ionization characteristic time is about 10^{-6}sec) is not high enough to deplete the copper atom number density and cause deterioration of the laser output.

References

5.1 J. R. McNeil and G. J. Collins, Appl. Phys. Lett. 27, 595 (1975)

5.2 Che Jen Chen, Phys. Review 163, 1 (1967).

5.3 W. P. West, T. B. Cook, F. B. Dunning, R. D. Rundel, and R. F. Stebbings, J. Chem. Phys. 63, 1237 (1975).

5.4 S. C. Brown, Basic Data of Plasma Physics, (John Wiley & Sons, New York, 1959), pp. 36-45.

5.5 M. Gryzinski, Phys. Rev. 138, A336 (1965).

5.6 D. A. Leonard, IEEE J. Quant. Elect. QE-3, 380 (1967).

PART B

MEASUREMENT OF ELECTRON DENSITY AND DISSOCIATION IN A D.C. CARBON DIOXIDE LASER

CHAPTER VI

INTRODUCTION TO CHARACTERISTICS OF THE CARBON DIOXIDE LASER

In the present chapter a short review of the CO_2 laser and its characteristics is given. Particular attention is paid to influence of additives to the gas mixture in the laser. Also discussed are the plasma characteristics of the glow discharge and dissociation processes occurring in the laser tube.

6.1 The Carbon Dioxide Molecule and the Mechanism of Operation for Carbon Dioxide Lasers

Several types of carbon dioxide lasers exist: glow discharge, transversely excited atmospheric (TEA), waveguide and gas dynamic; in the present study we will be concerned only with the operation of CW carbon dioxide lasers with flowing mixtures and pumped by a DC glow discharge. At the typical operating pressures ($\simeq$ 12 torr) the positive column of the glow discharge comprises most of the lasing volume.

6.1.1 Vibrational States of the CO_2 Molecule

The CO_2 molecule is a linear symmetric triatomic molecule. It has three fundamental modes of vibration. The symmetrical bending $(0,v_2,0)$, the symmetrical stretch $(v_1,0,0)$ and the asymmetrical stretch $(0,0,v_3)$. In the time scale of interest, these modes can be considered uncoupled. Each level is split into fine rotational sublevels of angular momentum J. The interaction among the rotational levels is much stronger than among the vibrational levels, thus rapid "thermalization" of the rotational levels is accomplished within each vibrational level. All the

relevant levels of the CO_2, CO and N_2 molecules are shown in Figure 6.1.

6.1.2 The Carbon Dioxide Laser

Stimulated emission is possible in carbon dioxide molecules with either transition (1) at around 10.6μ or transition (2) at around 9.4μ. The gain coefficient α of such transitions of frequency γ_o has been calculated by Patel (Ref. 6.1) as

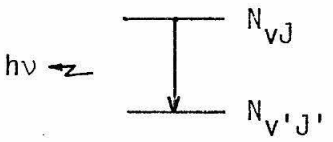

$$\alpha_{\nu_o} = g_J \frac{A_{21}}{8\pi} \left(\frac{c}{\nu_o}\right)^2 \frac{2}{\Delta\nu_D} \sqrt{\frac{\ell n\, 2}{\pi}} \left[\frac{N_{vJ}}{g_J} - \frac{N_{v'J'}}{g_{J'}}\right] \qquad (6.1)$$

where N is the number density of the appropriate level, v and v' denote the upper and lower vibrational, J and J' the upper and lower rotational, g_J and $g_{J'}$ the degeneracy of the respective levels; and $\Delta\nu_D$ the Doppler linewidth, c the speed of light, A_{21} the spontaneous emission coefficient.

If lasing is to occur, the gain given by equation (6.1) must be a positive quantity. With that restriction the following threshold condition may be derived (Ref. 6.2):

$$\frac{T_r}{T_v} < \frac{E_r(J) - E_r(J')}{E(v') - E(v)} \qquad (6.2)$$

T_r and T_v are the rotational and vibrational temperatures respectively.

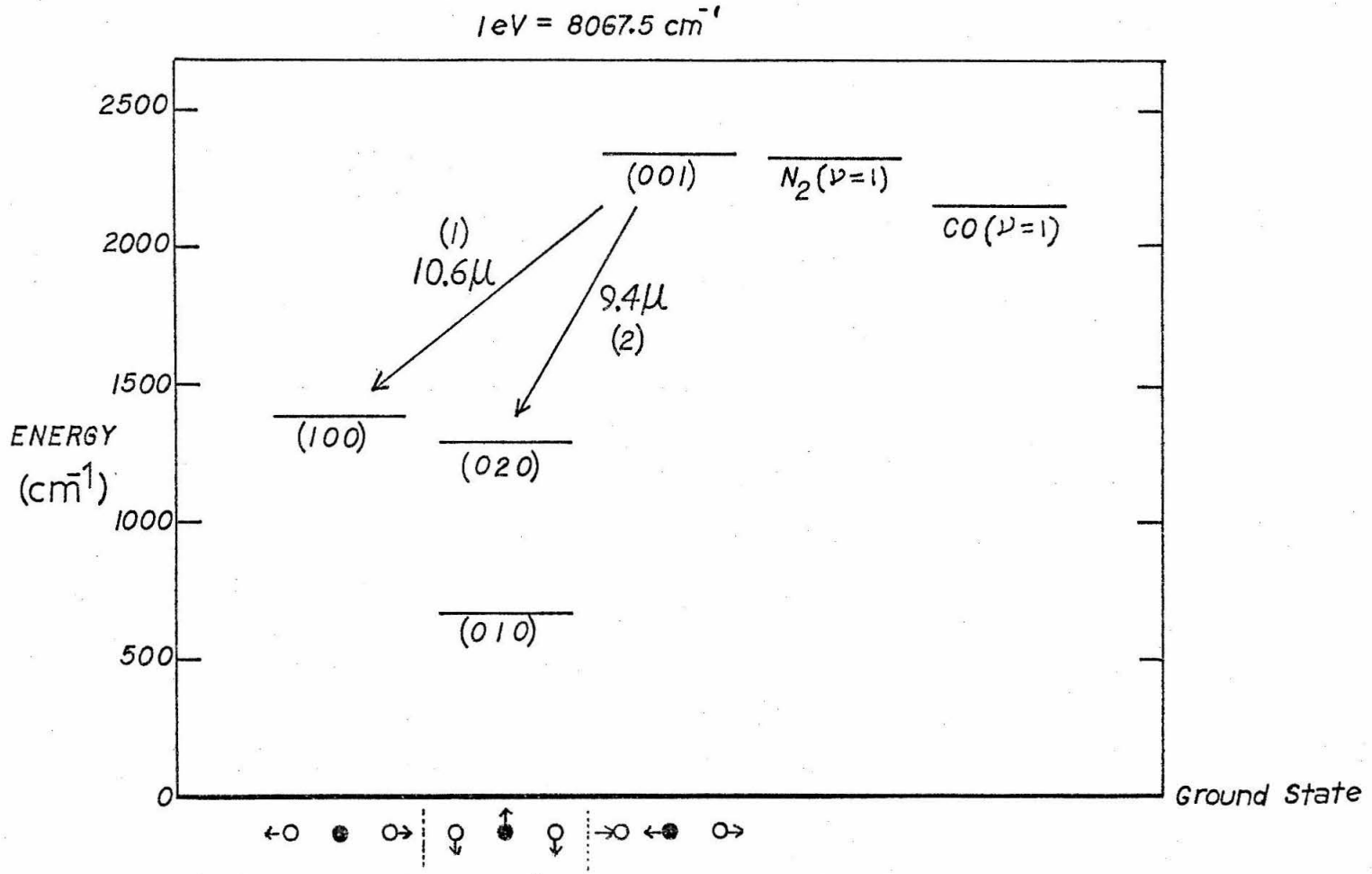

Fig 6.1 *Relevant Vibrational Energy Levels of CO_2, N_2 and CO.*

The transition in terms of the rotational level J may be of three kinds, referred to as P, Q, and R branches (the primed quantities refer to the lower laser level):

P Branch	$J = J' - 1$
Q Branch	$J = J'$ (forbidden in CO_2)
R Branch	$J = J'+1$

For the P branch transition we have $E_r(J') = E_r(J+1) > E_r(J)$, and since $E(v) > E(v')$, both the numerator and the denominator in the right hand side of the relation (6.2) are negative. This implies that it is possible to satisfy the threshold conditions with some positive temperature T_v (T_r is approximately the equal of the gas temperature). Thus it is possible to have amplification without having negative temperatures (i.e., population inversion). This process favors the operation of the CO_2 laser in the P branch, unless some frequency selective element is introduced in the resonator.

The above equations give a criterion to estimate the gain and probable emitting line. They do not give any information as to how the levels actually become populated.

If the energy levels of the CO_2 molecule are to be used for the lasing operation, a likely medium in which CO_2 molecules could be made to lase is an electric discharge. In the discharge the electrons with typical average energies in the order of 1 eV, could excite the CO_2 vibrational levels through several paths: direct excitation collisions; dissociating collisions with subsequent recombination to form an excited

molecule; indirect excitation through a previously excited nitrogen atom. Nitrogen has a near resonant level with the upper laser level. Due to its large electron excitation cross section, N_2 is more easily vibrationally excited than CO_2 by electron impacts.

The first laser to make use of vibrational/rotational transitions was invented by Patel in 1964 (Ref. 6.1), using pure CO_2. With no other gases present, the carbon dioxide laser produces relatively low power. Patel also discovered (Refs. 6.3 and 6.4) that the power is greatly increased with the addition of nitrogen. A further increase of power is achieved by the addition of helium, a fact reported independently by Patel, Tien and McFee (Ref. 6.5) and by Moeller and Rigden (Ref. 6.6). Other additives have been tried, notably water vapor and xenon, but the most dramatic effects occur with nitrogen and helium. Most conventional carbon dioxide lasers operate with $CO_2/N_2/He$, a typical mixture ratio being 1/3/16 moles, so carbon dioxide is the minor constituent. The ideal quantum efficiency for the CO_2 laser, the energy of the transition divided by the energy from ground state to the upper level, is 41 percent. With appropriate gas mixtures, operating efficiencies, defined as power-out divided by electrical power-in, as high as 30 percent have been achieved.

Even though from the initial report (Ref. 6.1) it was evident that significant amounts of CO_2 dissociation took place in the discharge, this fact was often ignored in the calculations and performance analysis. Potentially important effects of CO_2 dissociation were overlooked: (i) depletes the number of CO_2 molecules; (ii) adds new species (CO and O_2, mainly) which may affect the excitation

process. The first vibrational level of CO and N_2 shown in Figure 6.1 are nearly resonant with the upper laser level (100). Therefore the same resonant energy transfer from N_2 to CO_2 can be expected to operate with CO to CO_2. Since all experimental evidence shows that species other than CO_2 are generated in the electrical discharge, the pure CO_2 laser is not so pure. Although the case is not by any means closed, it appears that those other species, particularly carbon monoxide and atomic oxygen, may in fact be necessary to the functioning of a laser which is operated initially with carbon dioxide and no other additives.

Patel (Ref. 6.1) observed sidelight emission from an electronic transition of carbon monoxide, as well as the voltage and current for the discharge, and the output of stimulated emission. He found that while the first three occurred approximately together when the laser was pulsed, the output appeared as much as 300 μsec later. Because it is unlikely that such a long delay would arise if the population inversion were produced directly by collisions of electrons with CO_2 molecules, another mechanism must be found. Patel suggested, and later work by Chen (Ref. 6.7) supported the idea, that the reformation process is dominant.

There has been relatively little interest in the CO_2 laser without additives, mainly because the output is so low compared with those using gas mixtures. However, the mechanism causing the population inversion is an interesting problem which has not yet been satisfactorily resolved. The authors of another work (Ref. 6.8) cite evidence

that direct excitation, by electron impacts, produces the population inversion. The time lag between the current pulse and laser output was found in Ref. 6.8 to be less than 2 μsec, and only weakly dependent on the initial pressure of CO_2; the radiation at 10.6μ occurred later than that at 9.5μ, the delay varying from about 8 sec at 1 torr to 1 μsec at 3 torr. The performance was unusual in that below 2.5 torr the intensity of the radiation at 9.5μ was greater than that at 10.6μ. Owing to the short time delays, the authors conclude that inelastic electron collisions are responsible for the inversion; their description of the operation of the laser is therefore cast in the framework appropriate to a gas discharge.

Water vapor has been used as an additive for CO_2 laser mixtures both sealed and flowing. Witteman,(Refs. 6.9, 6.10) found that by adding a small quantity of water vapor to a sealed off CO_2 laser, its lifetime could be made practically unlimited with also an increase in output power. In flowing systems Smith and Austin (Ref. 6.11) found increased amounts of output power from the laser with the addition of small amounts of water (.4 torr in a 9 torr mixture). They also found reduced dissociation of CO_2 when water was present.

It has been generally supposed that water vapor prevents the dissociation of carbon dioxide molecules, although measurements confirming this are somewhat lacking. A second function of water vapor seems to be to increase the relaxation rate of the lower laser level, thus improving the population inversion. Water and its effects on the CO_2 laser will be discussed more fully in Sections 6.2 and 6.3.

Mixture composition is seen to play an important role in the operation of the laser. The dissociation of CO_2 molecules may drastically change the mixture composition. It deserves a closer study. The addition of H_2O molecules to the mixture seems to change the steady state level of dissociation reached. In the mixtures used in typical lasers, only CO_2 (and H_2O when present) appear to be chemically active. This is probably due to the low dissociation energy of these molecules compared with N_2 which is the only other candidate that could be chemically active. The dissociation energies of CO_2, H_2O and N_2 are, respectively, 5.5 eV, 5.2 eV and 9.8 eV.

6.2 Influence of Additives on the Performance of CO_2 Lasers

The degree of inversion existing in the laser is dependent on the population of the upper and lower lasing level and their pumping rates. Ideally it would be desirable to maximize the pumping of the upper level while at the same time increasing the rate of relaxation of the lower level. One possible way to accomplish this is the addition of molecules other than CO_2 which would favor the effects mentioned above. Not all additives are favorable, and others might be by-products of unavoidable chemical reactions in the laser medium, for instance, the dissociation of CO_2 into CO and O.

Gases present in the CO_2 laser mixtures could have various effects on the operation of the laser. As is the case with N_2 and very likely CO, a gas could act as an intermediary by resonant energy transfer from the electrons to the CO_2 molecule. The low direct excitation cross section of the CO_2 molecule makes almost unavoidable the presence of

such a collision partner if one is to have efficient lasing. In pure CO_2 lasers the creation of CO by dissociation seems to be a major requirement before lasing can be observed (in most cases). An additive could also have the opposite effect; it could introduce a path for increased collisional relaxation of the upper laser level. The energy path would be in direct competition with the lasing transition so its occurrence is to be avoided. Water, hydrogen and carbon dioxide molecules show this effect.

The rate of relaxation of the lower laser level is also strongly influenced by the mixture composition. Helium and water have been shown to have very favorable influences on this relaxation rate. Helium has the additional advantage that its high heat conductivity helps keep the laser operating at lower temperatures and therefore at higher gain (Ref. 6.12).

6.2.1 Nitrogen

Nitrogen was the first additive used (Patel, Ref. 6.3). It has been noted by Sobolev and Sokovikov (Ref. 6.13) that up to the fourth vibrational level the difference between pairs of N_2 and CO_2 (v_i) is less than kT, the typical thermal energy of the molecules in the discharge. Radiative decay of the vibrational levels of N_2 is strictly forbidden, making the transfer of energy from vibrationally excited N_2 to the ground state CO_2 most efficient. Its effect on the relaxation of the lower lasing levels seems to be minor compared with other gases such as helium (Ref. 6.14). Analysis up to a sensitivity of .01 torr by Smith and Austin (Ref. 6.11) failed to reveal any of its oxides.

6.2.2 Helium

The influence of helium is particularly marked in decreasing the kinetic temperatures of the laser. This has been attributed to its high thermal conductivity. In Ref. (6.15) the authors found that for the same current density the temperature rise in mixtures containing helium was considerably lower than without it. Laderman and Byron (Ref. 6.16), in a more detailed analysis, calculated the heat conductivity of a CO_2-N_2-He as a function of helium mole fraction, and found the expected increase.

6.2.3 Carbon Monoxide

Carbon monoxide needs to be considered because it is always present to some degree, due to the dissociation of CO_2 molecules. Its vibrational level structure is similar to N_2 and, as such, it can pump the upper laser level resonantly (Ref. 6.17). It has also been proposed that it increases the relaxation rate of the lower lasing level (Refs. 6.14 and 6.18)

6.2.4 Oxygen

Oxygen is present in the discharge mostly due to dissociation. Its influence on the relaxation of the upper laser level has been studied by fluorescence techniques (Refs. 6.19 and 6.20). A sample of carbon dioxide and other molecules was irradiated with a short pulse of 10.6μ radiation. Then by observing the fluorescent emission at certain wavelengths, information about the relaxation rate of the upper laser level could be monitored. They concluded that oxygen

decreased the population of the upper laser level, although not by dramatic factors.

6.2.5 Xenon

This is another common additive in carbon dioxide lasers. Due to its low ionization energy, xenon distorts the electron energy distribution by decreasing the number of high energy electrons (Ref. 6.21 and 6.22). It reduces the average electron energy and increases the electron density (Ref. 6.15).

6.2.6 Water Vapor

When present in small amounts, water vapor increases the relaxation rate of the lower laser level (Refs. 6.14 and 6.20) and improves the gain of the laser (Ref. 6.11). A reason one would expect H_2O to affect the gain of the laser is the proximity of the (010) level of H_2O (1595.0 cm^{-1}) and the ($10^0$0) and ($01^0$0) levels of CO_2 (1388.3 cm^{-1} and 1285.5 cm^{-1}, respectively). In sealed tubes the lifetime of the tubes is prolonged almost indefinitely (Refs. 6.23, 6.24 and 6.25); the reasons are believed to be chemical, mainly the prevention of carbon dioxide dissociation.

6.3 Characteristics of the Discharge in an Electrically Excited Carbon Dioxide Laser

CW carbon dioxide lasers use glow discharges as active medium. At the pressures and currents normally used, the positive column makes up most of the active lasing region.

The positive column in its steady state provides an environment which is in many respects very close to, and in other respects very far from equilibrium. It is possible to treat the positive column as composed of two almost independent groups of particles: molecular mixture and the electron gas. Each can be characterized by an average energy (temperature) which might be very different. For instance (Ref. 6.21), the mean electron energy in typical CO_2 lasers is about 1.2 eV (approximately 10000°K). The molecular mixture is close to room temperature at about 350°K (Ref. 6.16).

In characterizing the positive column it will be useful to do so by analyzing certain parameters: electron mean energy, electron distribution function (in energy), electron collision frequency, electron density, electric field, current and voltage across the discharge, and pressure of the molecular mixture. The measurement of some of these parameters is difficult and unreliable. Therefore, attempts have been made to determine these quantities theoretically by calculating the electron distribution function.

6.3.1 Electron Energy in the Glow Discharge

The electrons in a glow discharge can be uniquely characterized by an energy distribution function (assuming no space anisotropies). From this function it is in theory possible to calculate most of the excitation rates in the plasma; again, we assume that we know the appropriate cross sections.

Experimentally, the more direct method of measuring the distribution function involves the use of Langmuir probes. At the normal

operating pressures of the CO_2 laser (about 12 torr) simple probe theory does not apply, so it is necessary either to modify the theory or to lower the pressure to the range ($\sim$ 1 torr) where the theory may still be applicable. In practice both tactics have been used (Refs. 6.22, 6.26, 6.27, 6.28, 6.29). In general the distribution function is found to be non-Maxwellian with average energy between 1 and 3 eV. The mixture composition has been found to have a strong influence on the distribution, especially at the higher energies. The authors of Ref. (6.27) obtained different distributions in flowing and non-flowing lasers. In light of the known difference in dissociation characteristics of sealed and flowing lasers, this effect is attributed to the different resulting mixtures. In Refs. (6.22) and (6.30) lasing action has also been observed to have an effect on the distribution function; lasing apparently reduces somewhat the number of high energy electrons. Time resolved measurements using multiple probes have been reported by Chen (6.7).

The mean electron energy is a more easily measured quantity. A microwave radiometer of the type discussed in Section 2.4 was used in Refs. (6.13), (6.21) and (6.32). Their results agree with each other in magnitude (.8 - 1.8 eV).

As previously mentioned, there is evidence (Refs. 6.22, 6.28, 6.30, 6.33, 6.34, 6.35, 6.36, 6.37) indicating that the plasma characteristics (electron distribution, discharge impedance) change when laser radiation is present. This is apparently due to coupling between low energy electrons and the vibrational states of nitrogen, carbon

monoxide and carbon dioxide. It has also been found that the sidelight emission changes (Refs. 6.33, 6.34, 6.35).

A theoretical approach to the plasma analysis is possible by solving the Boltzmann transport equation for the electron distribution. Knowledge of the appropriate cross sections is assumed. In a series of papers (Refs. 6.38, 6.39, 6.40, 6.41, 6.42) Nighan et al solved Boltzmann's equation numerically for the electron distribution in CO_2 laser plasmas under a number of conditions. The distributions thus calculated were used to estimate the different excitation processes in the laser. All the theoretical background necessary for the calculations has been described in Ref. (6.39). Essentially, the same approach was used by Judd (Ref. 6.43) in his kinetic calculations of the CO_2 laser. The qualitative agreement of the calculations with published reports is fairly good, so the model may be taken as the starting point for a number of calculations. The two major drawbacks are: the complicated numerical calculations and manipulations required, and the need for accurate cross sections for the processes involved.

6.3.2 Electron Density and Collision Frequency

The average electron density and collision frequency can be measured simply by a microwave cavity method (Refs. 6.27, 6.44, 6.45). This is the method used in the present study and is described more fully in Chapter VII and Appendix C. Other methods of obtaining the electron density include microwave interferometry and electrical probes. Both microwave methods are conceptually similar, since they are based on the dependence of the plasma index of refraction on the

electron density. The cavity method is more suited for steady state phenomena. Probes have the same limitations (low pressure) discussed in Section 6.3.1; nevertheless, they have been used in CO_2 lasers (Ref. 6.29).

The microwave method of measuring electron density also gives the value of the electron-neutral collision frequency; thus it can be used to calculate drift velocities and thereby the electric field to a first approximation. Although this calculation is not very accurate, in cases in which no other means of measuring the electric field are available it could be of significant value. A further advantage of microwave techniques is the fact that they are independent of the pressure and composition of the plasma.

6.4 Review of Observations of Dissociation and Chemical Composition in CO_2 Lasers

From early reports of CO_2 laser operation, it was found that pure undissociated CO_2 cannot provide appreciable power generation, for in this case the power is limited by the slow rate of direct pumping of the upper laser level, and the slow rate of relaxation of the lower laser level. Brinkschulte (Ref. 6.17) reports that until a certain minimum ratio of CO to CO_2 is formed, no lasing is observed.

In a glow discharge, chemical reactions occur predominantly in the region of the cathode fall and in the positive column. The highest rate of reaction per unit volume is observed in the cathode fall region where there is a high field strength and consequently a greater number of high energy electrons. However, since the cathode

fall region represents only a small fraction of the total reaction volume, the overall reaction rate is controlled by the positive column. Thus it appears justified in the case of flowing systems to analyze the chemical kinetics of the plasma by studying the positive column only. In sealed-off lasers this assumption is no longer valid.

Carbon dioxide laser mixtures commonly used have nitrogen and helium as additives. Also used are xenon and water vapor (in small quantities). Of these only carbon dioxide and water (when present) seem to be chemically active to a significant degree (Ref. 6.11).

6.4.1 Carbon Dioxide Dissociation in Flowing CO_2 Lasers

Published reports in the area of CO_2 dissociation in glow discharges have been similar in nature, for the most part consisting of parametric plots of dissociation versus flow rate with pressure and/or current as parameters. With one exception (Ref. 6.29) none of the reports measured the electron density in the discharge while making the dissociation measurements. Dissociation has been observed to vary from 5 to 85 percent.

Smith and Austin (Ref. 6.46) and Smith (Refs. 6.47 and 6.11) studied flowing mixtures of CO_2-N_2-He (6,12,82), (1,2,0), and pure CO_2. It appears that they took some measurements of dissociation with water present in the mixture; however, they do not quote any numbers and state only that the dissociation is lower when water is present. They presented a simple kinetic model which will be the basis for the analysis in Chapter X of the present work.

Ivanov et al (Ref. 6.29) studied the dissociation in a discharge of pure CO_2 at 2 torr and current densities of .6 to 12 ma/cm^2. With the aid of electrical probes they were able to study the electron density. No other mixture was studied.

In Ref. (6.48) the authors studied flowing mixtures of CO_2-N_2-He having the compositions (1,3,6) and (1,0,9). They displayed their results as dissociation versus flow rate and used current as a parameter. In Ref. (6.49) some of the same authors report on the dissociation of a (2,1,18) mixture.

Limited dissociation results are presented by Wiegand et al (Ref.6.50) with a mixture (1,2,10) in a 3.8 cm diameter tube. With the tube at 10.6 torr and a current density of 11.5 ma/cm^2, they measured the dissociation as a function of flow rate.

In general, published reports show qualitative similar dependences (i.e., with respect to current density, flow rate, pressure and mixture composition). The chemical equation $CO_2 \rightleftarrows CO + \frac{1}{2} O_2$ was satisfied in all cases except in Ref. (6.11). However, the same author, Smith, in a later report (Ref. 6.46), apparently using the same apparatus, used the above equation to analyze the data. We assume that the first report contained a calibration error.

6.4.2 Carbon Dioxide Dissociation in Sealed-Off Tubes

The chemistry of the sealed-off laser is far more complex than that of flowing systems, so in spite of the number of reports on the subject, it is very difficult to make any general statements. Unlike the case of flowing systems, the dissociation is very dependent on the

experimental conditions used (Ref. 6.51). Sometimes even the material of the electrode affects the dissociation behavior (Refs. 6.49 and 6.52); different electrodes gave different results.

Of particular interest is the role of water vapor in the dissociation. It has been established that the presence of water reduces the degree of dissociation of CO_2 molecules (Refs. 6.53 and 6.54) and increases the lifetime of the laser.

6.5 Present Measurements of Electrical Characteristics and Chemical Composition

In the works previously mentioned, the main electrical parameter was the current through the discharge. It is likely that a more appropriate parameter is the electron density and possibly the collision frequency (for electron/neutral collisions) since they are directly tied to the energy transfer mechanism.

The purpose of the present measurements was to measure carefully the dissociation of carbon dioxide as a function of electron density in an operating CO_2 laser (flowing, DC excited). Several initial mixtures were studied: CO_2-N_2-He (1,3,16), (1,2,10) and (2,3,15); CO_2-N_2 (1,3), (1,2) and (2.3); CO_2-He (1,16), (1,2) and (2,3); and pure CO_2. The effect of water was studied with mixture (1,3,16). The parameters varied were total STP flow rate (volume flow rate at standard conditions) and total pressure in the discharge.

The electron density and collision frequency in the laser have been measured with a microwave (3 gHz) cavity. From these values an estimate of the electric field in the tube may be made. A gas chromatograph was used to measure the composition. Only the concentrations

of carbon monoxide, nitrogen and oxygen could be measured and no short-lived species could be detected.

An analysis of the results shows that for all the mixtures and conditions studied, in which no water is present, the degree of dissociation as a function of the electron density depends only on the partial STP flow rate of carbon dioxide regardless of total pressure or mixture composition. It has also been shown that the degree of dissociation decreases significantly (order 50%) when water vapor is present in the discharge.

Two simple models of the dissociation mechanism were developed. In Chapter IX the model is based on the assumption of thermodynamic equilibrium in the discharge. The electrons are replaced by a distributed heat source and the resulting equilibrium composition was calculated. In Chapter X a simple kinetic model is derived.

References

6.1 Patel, C.K.N., "Continuous Wave Action on Vibrational-Rotational Transitions of CO_2", Phys. Rev. 136, A1187 (1964).

6.2 Polanyi, J. C., "Proposal for an Infrared Maser Dependent on Vibrational Excitation", J. Chem. Phys. 34, 347 (1961).

6.3 Patel, C.K.N., "Selective Excitation through Vibrational Energy Transfer and Optical Maser Action in N_2-CO_2", Phys. Rev. Lett. 13, 617 (1964).

6.4 Patel, C.K.N., "CW High Power N_2-CO_2 Laser", Appl. Phys. Lett. 7, 15 (1965).

6.5 Patel, C.K.N., Tien, P. K. and McFee, J. H., "CW High Power CO_2-N_2-He Laser", Appl. Phys. Lett. 7, 290 (1965).

6.6 Moeller, G and Rigden, J. D., "High Power Laser Action in CO-He Mixtures", Appl. Phys. Lett. 7, 274 (1965).

6.7 Chen, C. J., "Pump Mechanism of CO_2 Laser and Formation Rate of CO_2 from CO and O^*", J. Appl. Phys. 42, 1016 (1971).

6.8 Danishevskii, A. M., Fishman, I. M. and Yaroshetskii, I.D., "Investigation of the Laser Effect in CO_2 during Pulsed Excitation", Sov. Phys. JETP 28, 421 (1969).

6.9 Witteman, W. J., "Increasing Continuous Laser Action on CO_2 Rotational Vibrational Transitions through Selective Depopulation of the Lower Laser Level by Means of Water Vapor", Phys. Lett. 18, 125 (1965).

6.10 Witteman, W. J., "Rate Determining Processes for the Production of Radiation in High Power Molecular Lasers", IEEE J. Quant. Elect. QE-2, 375 (1966).

6.11 Smith, A.L.S. and Austin, J.M., "Molecular Composition Changes in a Flowing CO_2, N_2, He, H_2O Laser", Brit. J. Appl. Phys. (J. Phys. D) 2, 1129 (1969).

6.12 Franzen, D. L. and Collins, R. J., "High Gain Small Bore Cooled CO_2 Amplifier", IEEE J. Quant. Elect. QE-6, 63 (1970).

6.13 Sobolev, N. N. and Sokovikov, V. V., "A Mechanism Ensuring Level Population Inversion in a CO_2 Laser", JETP Lett. 4, 204 (1966).

6.14 Sobolev, N. N. and Sokovikov, V. V., "Influence of the Rate of Disintegration of the Lower Laser Level on the Power of a CO_2 Laser", JETP Lett. 5, 122 (1967).

6.15 Bletzinger, P. and Garscadden, A., "Influence of Xe on CO_2 Laser Plasmas", Appl. Phys. Lett. 12, 289 (1968).

6.16 Laderman, A. J. and Byron, A, "Temperature Rise and Radial Profiles in CO_2 Lasers", J. Appl. Phys. 42, 3138 (1971).

6.17 Brinkschulte, H., "The Influence of CO on CO_2 Laser Performance", IEEE J. Quant. Elect. QE-4, 948 (1968).

6.18 Cheo, P. K., "Effects of Gas Flow on Gain of 10.6μ CO_2 Laser Amplifiers", IEEE J. Quant. Elect. QE-3, 683 (1967).

6.19 Deutsch, T. F., "Gain and Fluorescence Characteristics of Flowing CO_2 Laser Systems", IEEE J. Quant. Elect. QE-3, 151 (1967).

6.20 Rosser, W. A. Jr. and Gerry, E. T., "De-Excitation of Vibrationally Excited CO_2^* (^Ve) by Collisions with He, O_2 and H_2O", J. Chem. Phys. 51, 2286 (1969).

6.21 Tyte, D. C., "Mean Electron Energy in a CO_2 Laser Plasma", Elect. Lett. 5, 447 (1969).

6.22 Bletzinger, P., and Garscadden, A., "The CO_2 Laser Plasma", IEEE Proc. 59, 675 (1971).

6.23 Witteman, W. J., "Rate Determining Processes for the Production of Radiation in High Power Molecular Lasers", IEEE J. Quant. Elect. QE-2, 125 (1966).

6.24 Witteman, W. J., "High Output Powers and Long Lifetimes of Sealed Off CO_2 Lasers", Appl. Phys. Lett. 11, 337 (1967).

6.25 Witteman, W. J., "High Power Single Mode CO_2 Laser", IEEE J. Quant. Elect. QE-4, 786 (1968).

6.26 Novgorodov, M. Z., Sviridov, A. G. and Sobolev, N. N., "Electron Energy Distribution in Discharges Used for CO_2 Lasers", JETP Lett. 8, 211 (1968).

6.27 Novgorodov, M. Z., Sviridov, A. G. and Sobolev, N. N., "Electron Energy Distribution in CO_2 Laser Discharges", IEEE J. Quant. Elect. QE-7, 508 (1971).

6.28 Bletzinger, P. and Garscadden, A., "Burning in the Electron Energy Distribution by Lasing Action in the CO_2, N_2 He Discharge", Phys. Lett. 29A, 265 (1969); also, Appl. Phys. Lett. 12, 289 (1968).

6.29 Ivanov, Yu. A., Polak, L. S. and Slovetskii, D. I., "Kinetics of CO_2 Decomposition in the Glow Discharge", High Energy Chem. 5, 344 (1971).

6.30 Aviri, P., Dothan-Deutsch, F. and Keren, H., "Influence of Lasing on Electron Energy Distribution in CO_2 Mixtures", J. Appl. Phys. 42, 5551 (1971).

6.31 Noon, J. H., Blaszuk, P. R. and Holt, E. H., "Electron Radiation Temperature Measurements in a CO_2Laser Amplifier", J.Appl.Phys. 39, 5518 (1968).

6.32 Polman, J. and Witteman, W. J., "Electron Radiation Temperature Measurements in a Sealed-Off CO_2 Laser System", IEEE J. Quant. Elect. QE-6, 154 (1970).

6.33 Weis, K. A., Kershenstein, J. C. and Thaler, W. J., "Visible Sidelight Emission in a CO_2 Laser", J. Quant. Spec. Rad. Transf. 9, 885 (1969).

6.34 Carswell, A. I. and Wood, J. I., "Plasma Properties of a CO_2 Laser Discharge", J. Appl. Phys. 38, 3028 (1967).

6.35 Crane, R. A., "Some Observations of the Widelight and Plasma Impedance Changes Induced by a CO_2 Laser Beam", Can. J. Phys. 47, 2785 (1969).

6.36 Keucman, A. J., Jacobs, H., SoCascio, C., Brand, F. A. and Novick G., "Photon Induced Current Changes in a CO_2 Laser Amplifier", IEEE J. Quant. Elect. QE-5, 474 (1969).

6.37 Kindl, H., Leeb, W. and Schiffner, G., "Dependence of CO_2 Laser Discharge Current on Laser Action", Proc. IEEE (Letters) 56, 781 (1968).

6.38 Nighan, W. and Bennett, J., "Electron Energy Distribution Functions and Vibrational Excitation Rates in CO_2 Laser Mixtures", Appl. Phys. Lett. 14, 240 (1969).

6.39 Nighan, W., "Electron Energy Distributions and Collision Rates in Electrically Excited N_2, CO, CO_2", Phys. Review A 2, 1989 (1970).

6.40 Nighan, W., "Effect of Molecular Dissociation and Vibrational Excitation on Electron Energy Transfer in CO_2 Laser Plasmas" Appl. Phys. Lett. 15, 355 (1969).

6.41 Wiegand, W. J. and Nighan, W., °Plasma Chemistry of CO_2-N_2-He Discharge", Appl. Phys. Lett. 22, 583 (1973).

6.42 Nighan, W. L., Wiegand, W. J. and Haas, R. A., "Ionization Instability in CO_2 Laser Discharges", Appl. Phys. Lett. 22, 579 (1973).

6.43 Judd, O. P., "The Effect of Gas Mixture on the Electron Kinetics in the Electrical CO_2 Gas Laser", Appl. Phys. Lett. 22, 4572 (1974).

6.44 Clark, P. O., and Smith, M., "An Investigation of the Effect of Gas Additives on the Electron Temperature and Density in a CO_2 Laser Discharge", Appl. Phys. Lett. 9, 367 (1966).

6.45 Novgorodov, M. Z., Sviridov, A. G. and Sobolev, N. N., "Electron Density and Collision Frequency inaa CO_2 Laser", Sov. Phys. Tech. Phys. 16, 589 (1971).

6.46 Smith, A.L.S. and Austin, J. H., "Dissociation Mechanism in Pulsed and Continuous CO_2 Lasers", J. Phys. D 7, 314 (1974).

6.47 Smith, A.L.S., "The Effect of Gas Flow on the Composition and Power Output of a CO_2, He, N_2 Laser", Phys. Lett. 27A, 432 (1968).

6.48 Gasilevich, E. S., Ivanov, V. A., et al, "CO_2 Dissociation in a CO_2 Laser", Sov. Phys. Tech. Phys. 14, 86 (1969).

6.49 Lotkova, E. N., Ochkin, V. N. and Sobolev, N. N., "Dissociation of CO_2 and Inversion in CO_2 Laser", IEEE J. Quant. Electr. QE-7, 396 (1971).

6.50 Wiegand, W. J., Fowler, M. C. and Benda, J. A., "Carbon Monoxide Formation in CO_2 Lasers", Appl. Phys. Lett. 16, 237 (1970).

6.51 Brovikova, I. N., Maksimov, A. I. and Svettsov, V. I., "Decomposition and Absorption of Carbon Dioxide during Protracted Out-Gassing of Insulated Discharge Equipment", High Energy Chem. 5, 146 (1971).

6.52 Ochkin, V. N., Lutkava, E. N. and Sobolev, N. N., "Dissociation of CO_2 in Sealed-Off Discharge Tubes of CO_2 Lasers", High Energy Chem. 4, 405 (1970).

6.53 Karube, N., Yamaka, E. and Nakao, F., "Decomposition of CO_2 Molecules in a Sealed CO_2 Laser", J. Appl. Phys. 40, 3883 (1969).

6.54 Witteman, W. J. and Werner, H. W., "The Effect of Water Vapor and Hydrogen on the Gas Composition of a Sealed-Off CO_2 Laser", Phys. Lett. 26A, 454 (1968).

Chapter VII

APPARATUS, INSTRUMENTATION AND MEASUREMENTS

In this chapter we will describe the experimental apparatus. The system consisted of a flowing DC excited low pressure CO_2 laser. This tube was specially built to accommodate a coaxial microwave cavity in order to allow measurements of electron density and collision frequency. The flow system of the laser allowed the working mixture of the laser to be changed. A gas chromatograph was used to analyze the chemical composition of the gases after passing through the discharge.

7.1 Laser Tube, Gas Supply and Power Supply

7.1.1 Laser Tube

The bulk of the measurements reported in the present work was made on a flowing, water cooled carbon dioxide laser. A diagram of the tube is shown in Figure 7.1. The active region was 65 cm long. The tube was made of quartz (in consideration of the low absorption of this material at microwave frequencies) and had an inside diameter of one centimeter with sodium chloride end windows mounted at the Brewster angle. A section of about 20 cm was exposed (no water jacket) in order to accommodate the microwave cavity. This section was forced air cooled. The tube had solid molybdenum electrodes mounted in side branches of the main tube. A limited set of experiments were carried out in a 1.4 cm I.D. tube of similar design. The dependence of the dissociation of carbon dioxide on electron density seemed to be nearly independent of diameter. Difficulties with the microwave cavity (a different one from the one used with

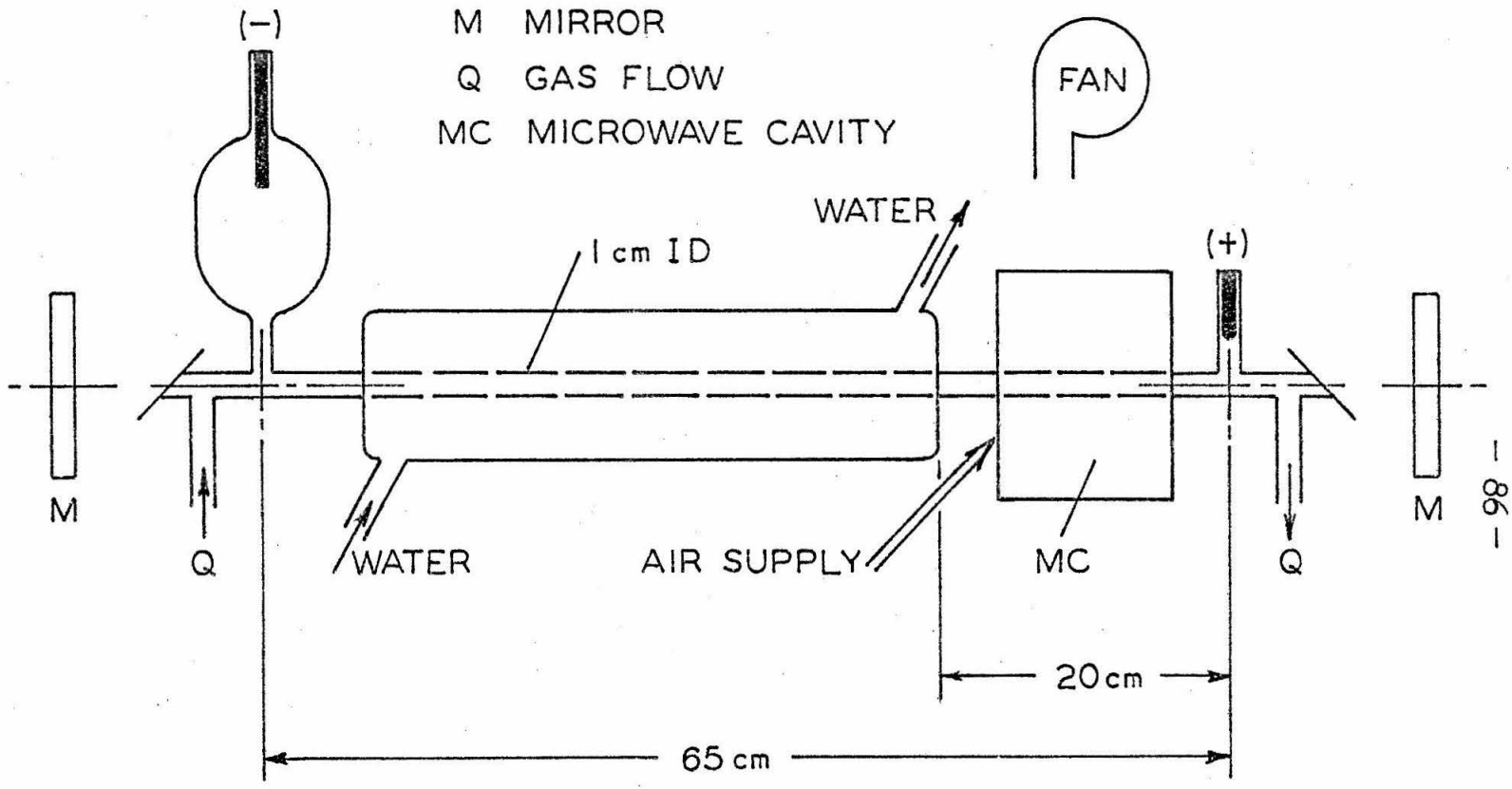

FIG. 7.1 LASER TUBE

the smaller tube) and the air cooling of the larger tube prevented a more complete set of experiments on this tube.

Under optimum conditions, with the current density 10 ma/cm^2, the laser would produce 1.5 watts CW output. However, since stimulated emission caused no change in the dissociation characteristics or the microwave measurements (within the sensitivity of our instruments), no attempt was made to keep the laser oscillating at all times.

7.1.2 Gas Handling and Vacuum System

Figure 7.2 shows a diagram of the flow system used. The working mixture for the laser was prepared by adding the appropriate quantities of gases. To prepare mixtures of three gases, the procedure was to add calibrated amounts of pure carbon dioxide to a ready-made mixture (molar) (1:3:16) of CO_2-N_2-He. In this manner mixtures in the proportion (1:2:10) and (2:3:15) by volume (molar) were prepared. All mixing was done at low pressures ($\doteq$ 54 torr) to prevent any back flow and contamination of the gas supplies. The flowmeters after each gas supply were calibrated but, due to large variations in their accuracy, they were were used as reference only. Gas flow was measured each time a new gas flow was set or a new mixture tried. The flow was measured at the exit of the sampling loop of the gas chromatograph, by measuring the speed of displacement of a soap diaphram along a graduated column. Records of the ambient temperature and pressure were maintained to compensate for any variation in the flow rate measured this way.

The pressure in the laser cavity was constantly monitored with a Wallace and Tiernan vacuum gauge (model FAR 160). This gauge was

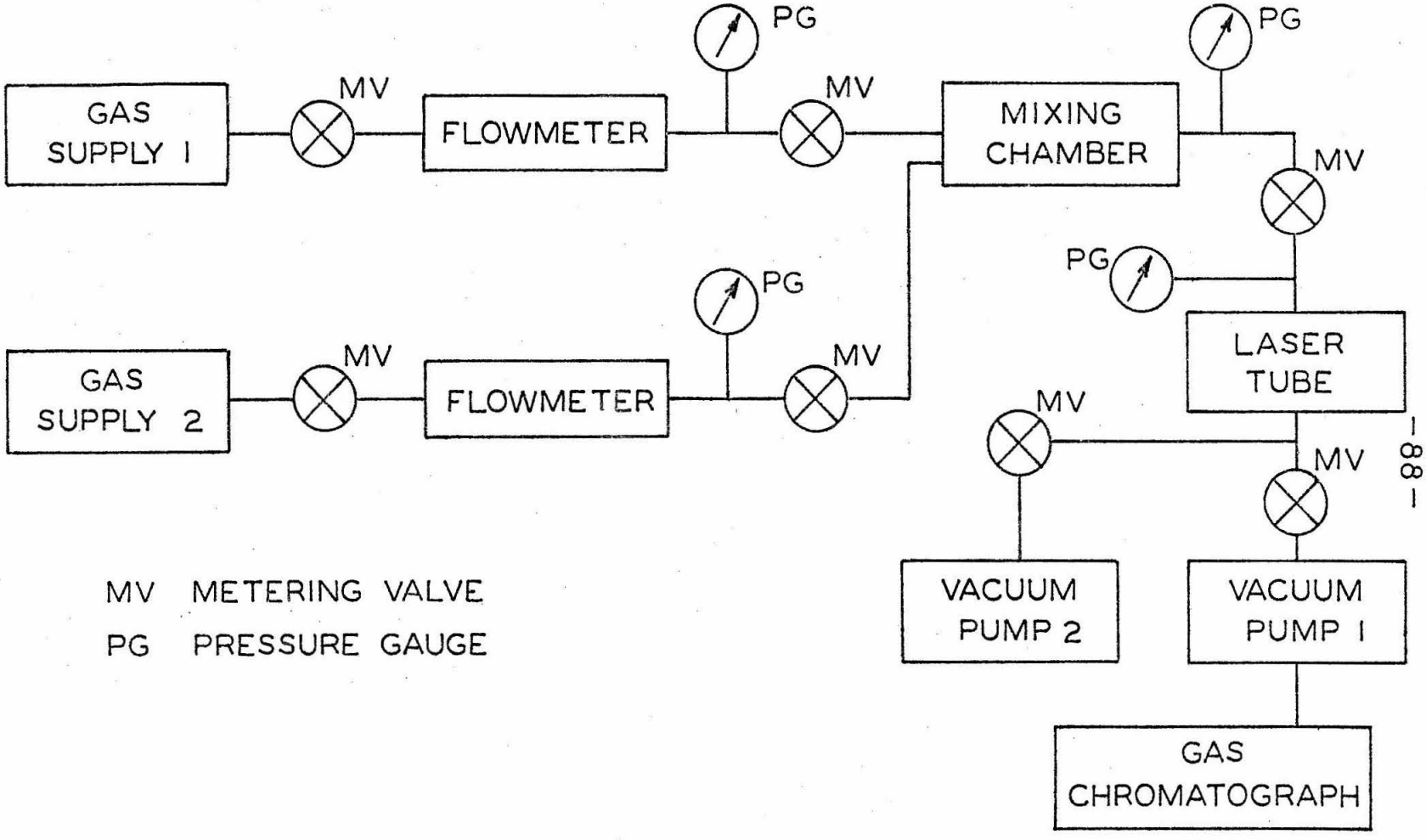

FIG. 7.2 GAS FLOW SYSTEM

calibrated daily with a Todd Scientific Co. McLoud gauge.

A second vacuum pump was connected in parallel with the first in order to be able to reach low operating pressures at high flow rates. The exhaust of the first pump was fed to the gas chromatograph for analysis of the resulting mixture.

7.1.3 Method of Adding Water Vapor to the Mixture

A slight modification of the flow system was made so that calibrated amounts of water vapor could be introduced. The modification is shown in Figure 7.3. Briefly, the gas mixture flow was allowed to "bubble" through distilled water in a closed container before continuing its path to the mixing chamber. Since the pressure and temperature of the water chamber were known, the amount of water vapor present can then be calculated from the known vapor pressure of water at that temperature and the assumption that the gas mixture becomes saturated. The percentage of water (by volume) in a gas mixture flowing through this device as a function of P_{H_2O}, the water vapor pressure, and P_{tank}, the chamber pressure, is given by:

$$\% H_2O = \frac{P_{H_2O}}{P_{tank}} * 100 \qquad (7.1)$$

The validity of the above analysis was checked indirectly by measuring the amount of nitrogen. Since the percentage of an element in a mixture decreases if another element is added, by measuring what percentage of the mixture nitrogen contributes before and after the addition, the amount of water can be found.

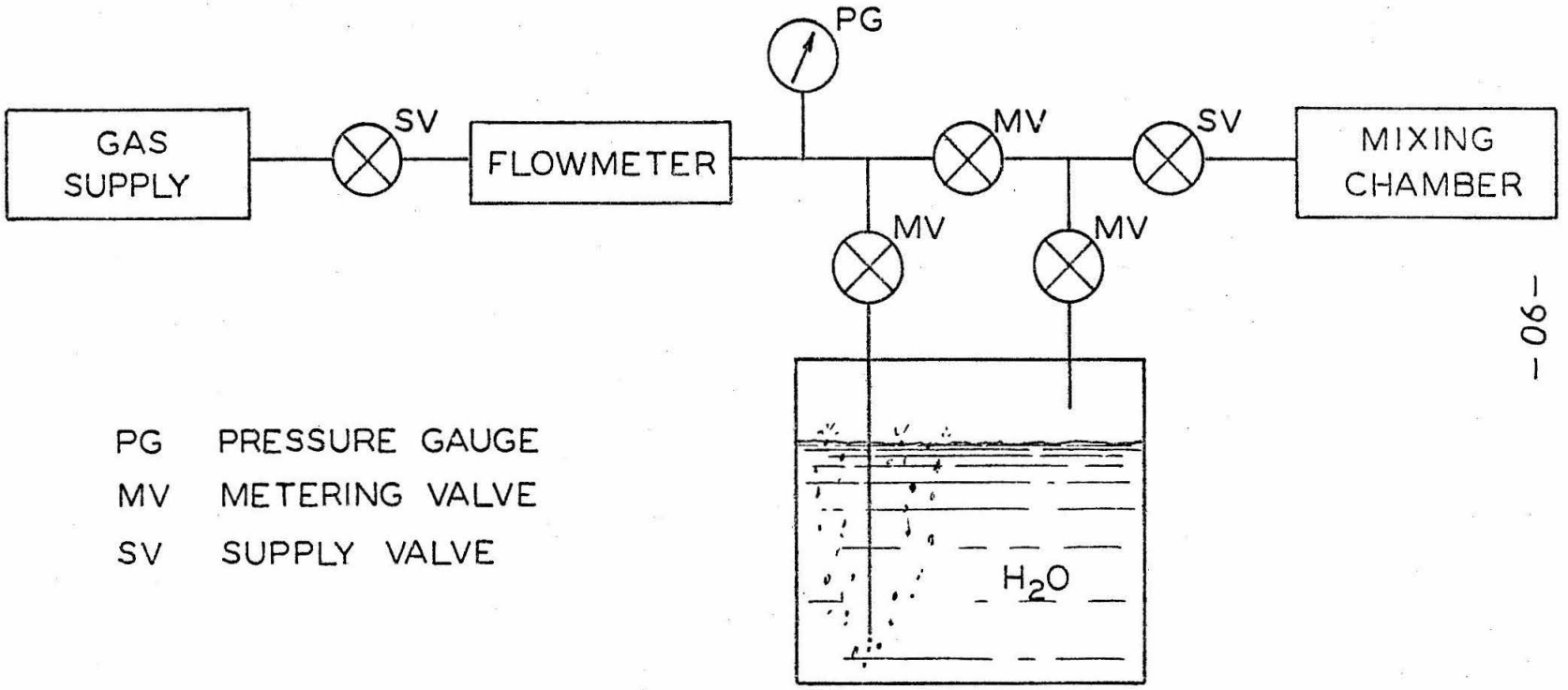

FIG. 7.3 WATER VAPOR SYSTEM

$$\% N_{2(before)} = \frac{\% N_{2(after)}}{100 - \% H_2O} * 100 \qquad (7.2)$$

Thus

$$\% H_2O = \left[1 - \frac{\% N_{2(after)}}{\% N_{2(before)}}\right] * 100 \qquad (7.3)$$

As an example of the agreement between the two methods, the following is a typical case:

$$P_{tank} = 780.9 \text{ torr}$$
$$P_{H_2O} = 19.6 \text{ torr} \quad @ \quad T = 295°K$$

Thus, assuming saturation, the amount of water vapor present is

$$\% H_2O = \frac{19.6}{780.9} * 100 = 2.5\%$$

On the other hand, measurement of the amount of nitrogen present gave:

$$\% N_{2(before)} = 15.3\%$$
$$\% N_{2(after)} = 14.9\%$$

Hence, according to (7.3)

$$\% H_2O = (1 - \frac{14.9}{15.3}) * 100 = 2.6\%$$

The agreement within 4% is satisfactory for the purposes here.

7.1.4 High Voltage D.C. Source

The laser discharge was D.C. excited in the present measurements. A block diagram of the entire system is given in Figure 7.4. A D.C.

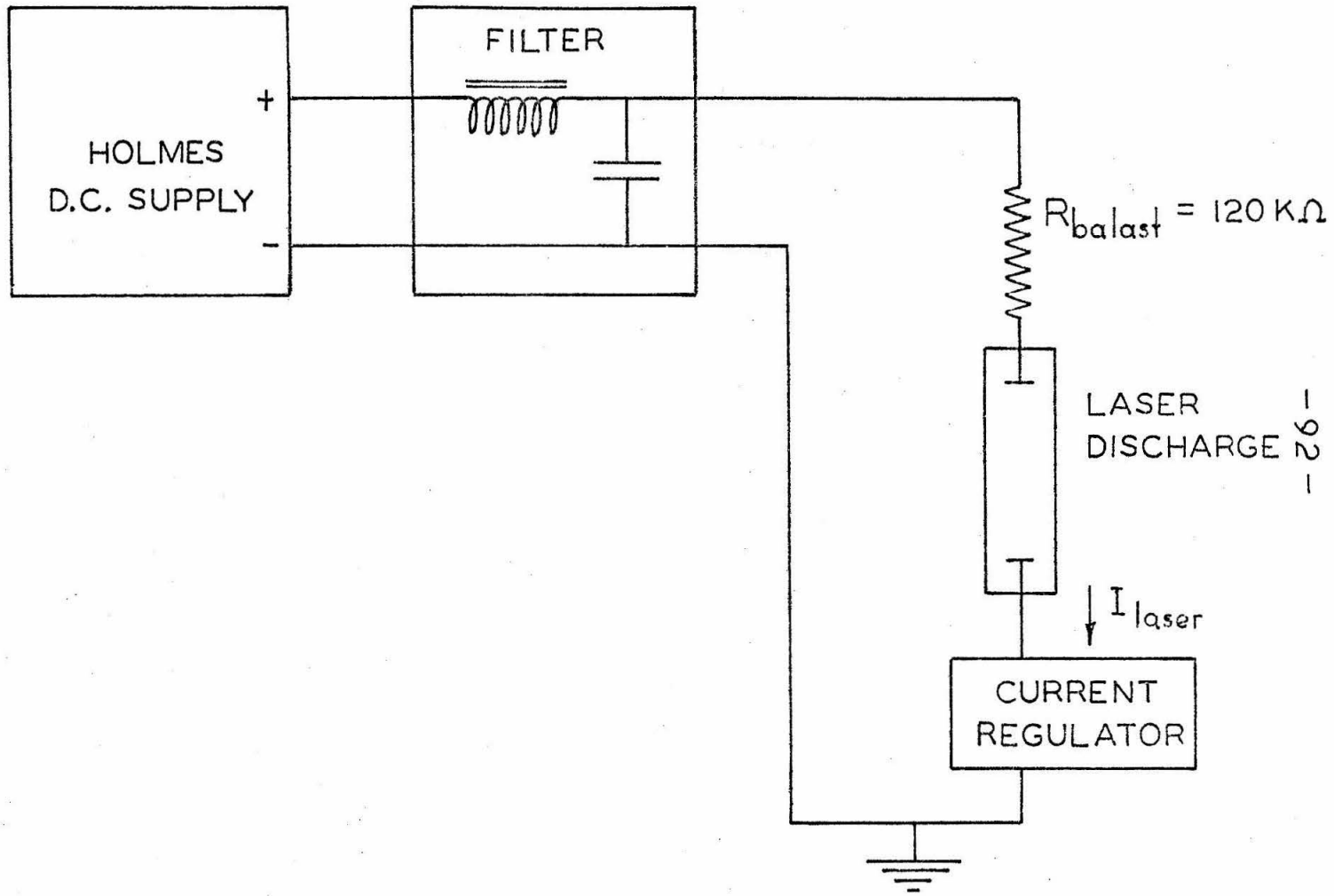

FIG. 7.4 POWER SUPPLY BLOCK DIAGRAM

power supply model 1-1020 made by Carl Holmes Co. capable of up to 500 ma at 200 KVolts was filtered and then connected to the laser tube in series with a 120 K ballast resistor and a current regulator. Most of the regulation of voltage and current was accomplished by the power supply, the filter and the ballast resistor (about 2-3%). Further regulation was obtained with the current regulator (home built). The regulator kept the current constant by dynamically varying its impedance. Referring to Figure 7.5, its operation can be briefly described. If we assume very small leakage currents in the transistor (collector to base) and the amplifiers used, the voltage at point a ($V_a = R_a \cdot I_{laser}$) will be proportional to the current through the laser. A differential amplifier (DA) amplifies the difference between reference voltage V_r and V_a. The difference signal (appropriately biased) is applied to the base of the transistor (T) making it conduct more if $V_a < V_r$ or less if $V_a > V_r$. Thus the system will maintain $V_a = V_r$ (i.e., keep I_{laser} constant). By varying the reference voltage the current could be set to any fixed value (in our case 3-25 ma). The complete system had less than .5% variation in current.

7.2 Microwave Measurements for Electron Density and Collision Frequency

The use of a microwave cavity to measure the electron density and collision frequency in a glow discharge has been established for many years (Ref. 7.1) and used by many authors (Refs. 7.2, 7.3, 7.4, 7.5, for example). A good review of the subject is given by Ingraham and Brown (Ref. 7.6).

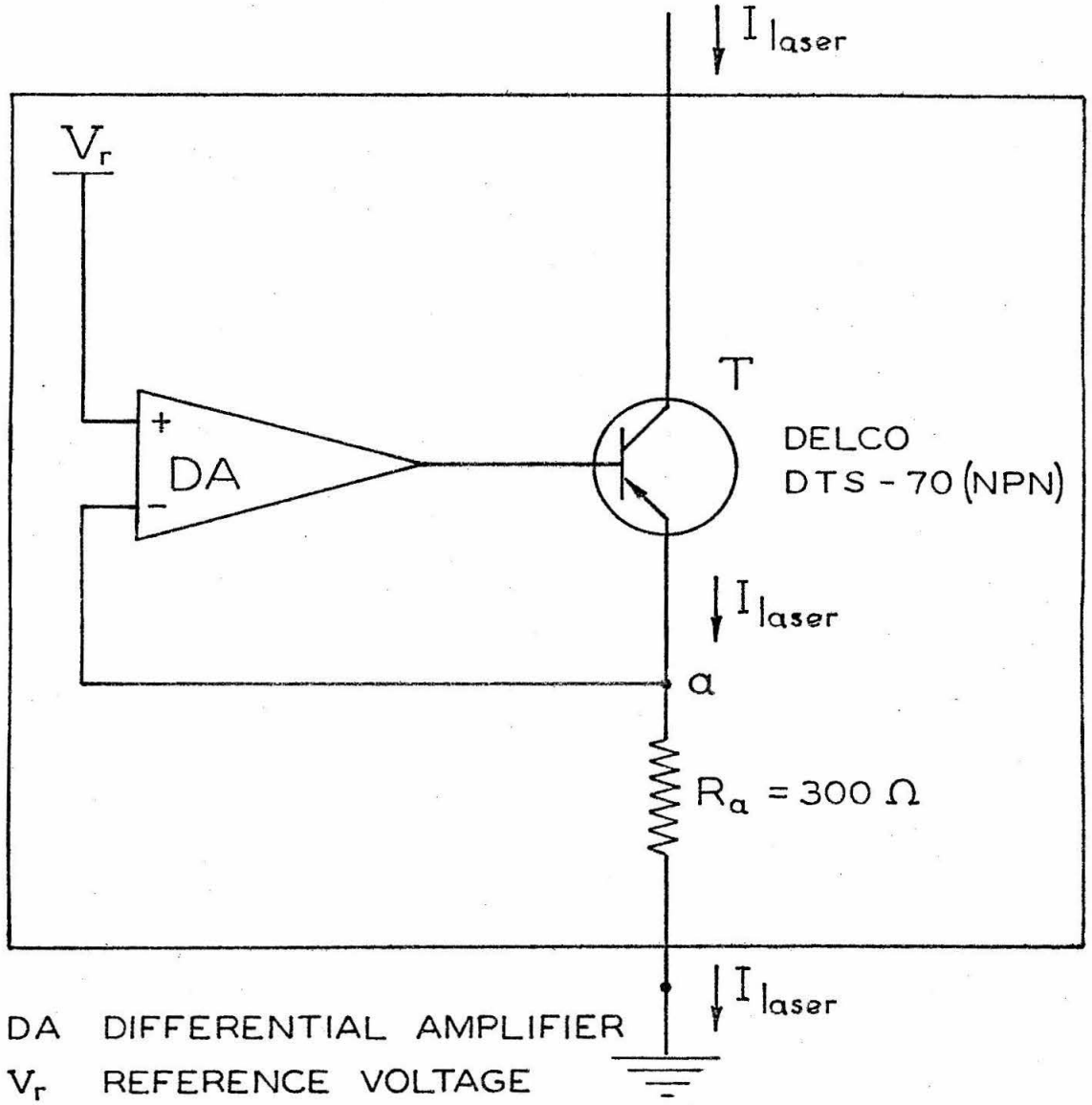

FIG. 7.5 CURRENT REGULATOR BLOCK DIAGRAM

7.2.1 Relationship between the Microwave Cavity Characteristics and the Plasma Parameters

A microwave cavity can be characterized by an infinite set of electromagnetic resonant modes. Each mode has a center frequency f and a quality factor Q. Any arbitrary field inside the cavity can be then described as a linear combination of those modes.

If a material of index of refraction μ^2 is placed inside such a cavity, the cavity's modes change both in frequency and in Q. The change is given to a first order perturbation (Ref. 7.6 and Appendix C),

$$\Delta\left(\frac{1}{Q}\right) = \frac{1}{Q} - \frac{1}{Q_o} = \frac{\int (\mu^2)_I \; E_o \cdot E_o \; dV}{\int E_o \cdot E_o \; dV} \tag{7.3}$$

$$\frac{\Delta f}{f_o} = \frac{f - f_o}{f_o} = \frac{-\int [(\mu^2)_R - 1] \; E_o \cdot E_o \; dV}{\int E_o \cdot E_o \; dV} \tag{7.4}$$

Subscripts "o" refer to the empty (no plasma) cavity values. The index of refraction of an electron plasma is given by (Ref. 7.6 and Appendix C):

$$\mu^2 = 1 - \frac{\omega_p^2}{\nu_m^2 + \omega^2}\left(1 + i\,\frac{\nu_m}{\omega}\right) \tag{7.5}$$

ν_m is the electron collision frequency, ω_p is the plasma frequency, ω is the microwave frequency in radians per second. The electron density in the discharge is assumed to follow a Bessel function distribution radially (Ref. 7.7):

$$n_e = n_e^o \, J_o(2.4 \, r/R_{tube})$$

Solving for ν_m and n_e^o

$$\nu_m = \frac{\omega \, \Delta(1/Q)}{2(\Delta f/f_o)} \tag{7.6}$$

$$n_e^o = \frac{2\omega^2 m_e \varepsilon_o}{\eta \, e^2} \left(\frac{\Delta f}{f_o}\right)\left[1 + \left\{\frac{\Delta(1/Q)}{2(\Delta f/f_o)}\right\}^2\right] \tag{7.7}$$

η is a dimensionless form factor dependent on the cavity dimensions and the resonant frequency used. For the TM_{011} cylindrical mode and the cavity used in this study, the value of η was measured (Ref. 7.8) to be $\eta = .0096$. This was verified by the numerical calculation described in Appendix C.

7.2.2 Instruments Used in the Microwave Measurements

The microwave system used in the present work was developed originally by Dr. A. Ravimohan and Dr. Fred Shair (Ref. 7.8) and was used without change. Figure 7.6 shows the components of the system, and Figure 7.7 shows details of the microwave cavity. The TM_{011} mode of the cavity was used exclusively (3043 MHz).

The main function of the microwave system was to obtain resonance curves (RF output vs frequency) of the cavity under different plasma conditions. Figure 7.8 shows a typical resonance curve. Since the resonant frequency and Q of the empty cavity were known, any shift due to the plasma could be easily measured. In order to reduce errors, a reference curve was traced for each set of conditions studied (for example, a set

COAXIAL CIRCUIT FOR AUTOMATIC PLOTTING OF TRANSMISSION CHARACTERISTIC OF MICROWAVE CAVITY WITH GLOW DISCHARGE PLASMA

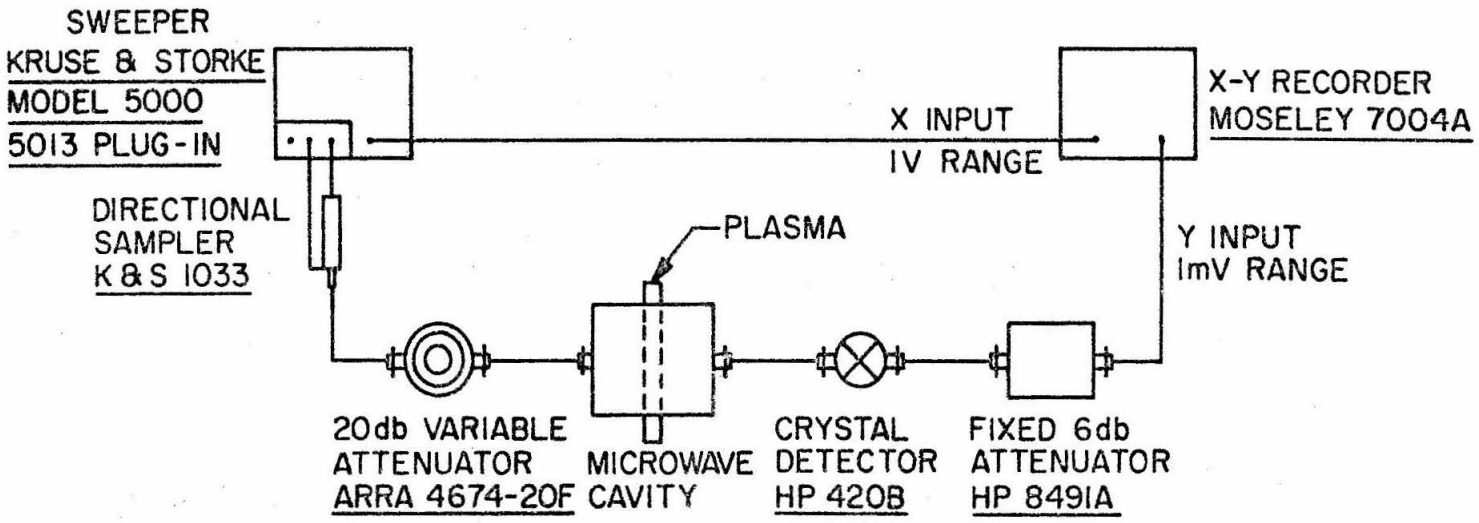

Fig. 7.6 Coaxial circuit for automatic plotting of transmission characteristic of microwave cavity with glow discharge plasma

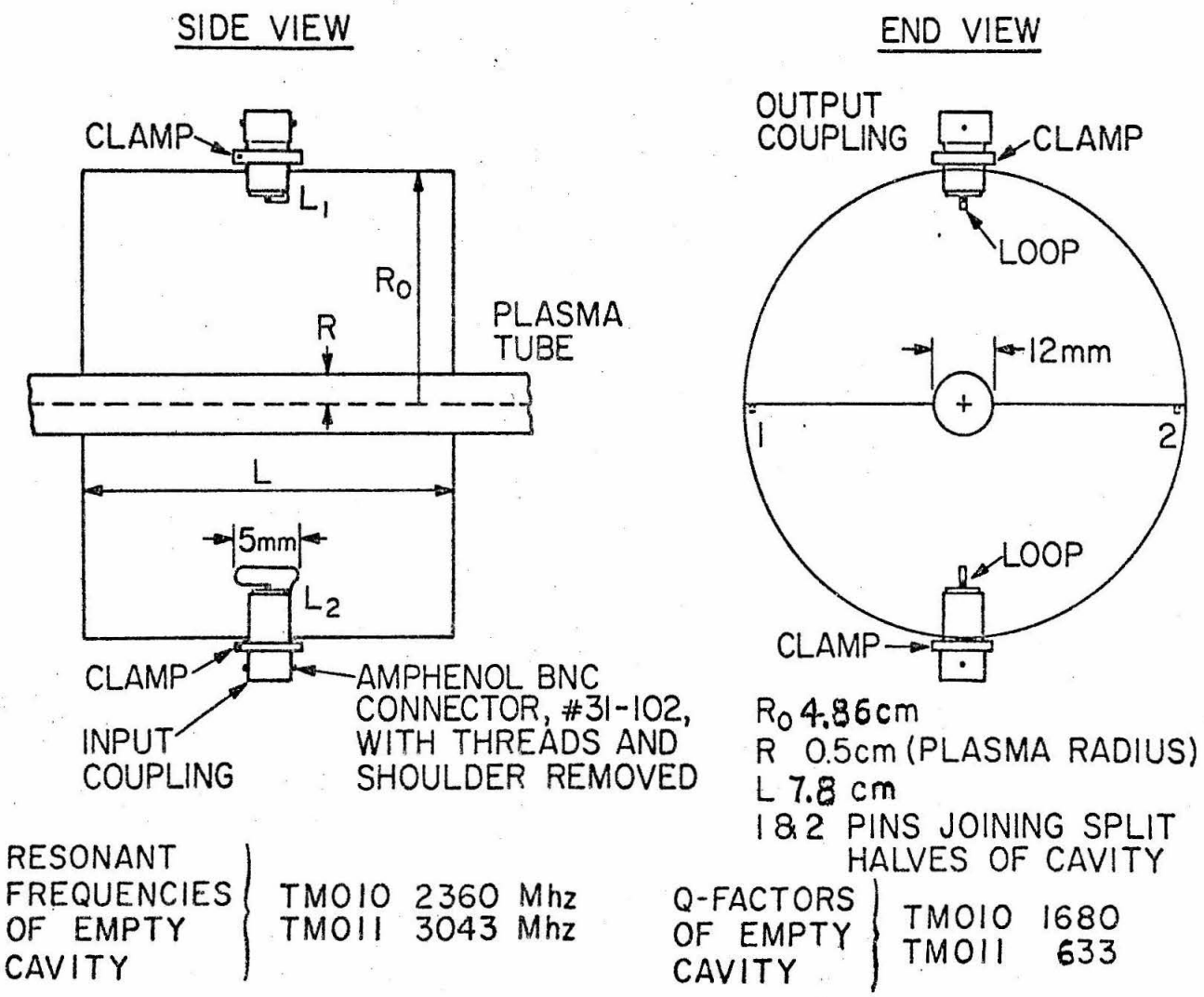

Fig.7.7 The microwave cavity

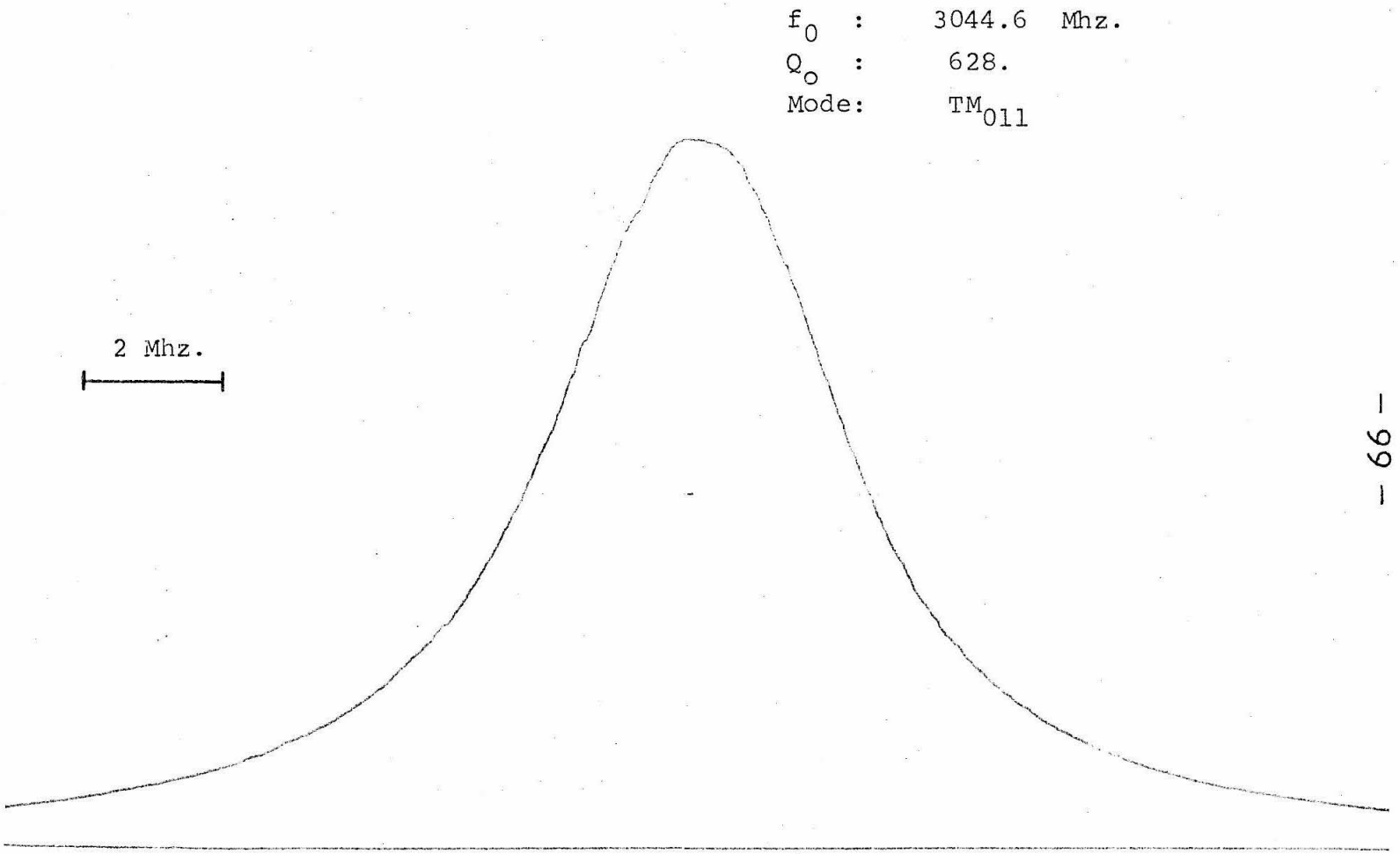

FIGURE 7.8 .- Resonance Curve; vertical scale proportional to power .

of six different current values) for the same initial composition, flow rate and pressure.

7.3 Estimates of the Electron Energy and Average Electric Field

The microwave measurements do not give a direct measure of either the electric field or the average energy of the electrons. By making some simplifying assumptions, it is possible to obtain both. The resulting accuracy is estimated to be low, and only information as to order of magnitude and trends can be expected. The electric field calculated in this manner was used later as a parameter in the thermodynamic equilibrium calculations described in Chapter IX.

7.3.1 Estimate of the Electric Field in the Discharge

The time between collisions for an electron is given by $(1/\nu_n)$, the inverse of the collision frequency. If we further assume that during this time the electron is acted upon by the electric field E, then the velocity of this electron at the end of the period between collisions will be given by

$$v = \left(\frac{E \cdot e}{m_e}\right) \cdot (1/\nu_n) \text{ (acceleration)} \cdot \text{(time)} \qquad (7.8)$$

or

$$E = \left(\frac{m_e \nu_m}{e}\right) v \qquad (7.9)$$

The current through the laser can be written as

$$I_{laser} = n_e \cdot v_d \cdot A \cdot e \qquad (7.10)$$

$$v_d = \frac{I_{laser}}{n_e \cdot A \cdot e} \tag{7.11}$$

where n_e is the mean electron density, v_d is the drift velocity of electrons, A is the cross sectional area of the tube, and e is the charge of an electron.

Averaging over all directions (Ref. 7.9, p. 36)

$$v_d = \frac{2}{3} v = \frac{2}{3} \frac{E \cdot e}{m_e \cdot \nu_n} \tag{7.12}$$

and combining (7.11) and (7.12) gives

$$E = \left(\frac{2}{3} \frac{m_e}{e^2 A}\right) \frac{I_{laser} \cdot \nu_n}{n_e} \tag{7.13}$$

7.3.2 Average Electron Energy

If λ is the fraction of energy each electron loses per collision, the following equation for conservation of energy can be written:

$$eEv_d = \lambda \nu_n \langle \varepsilon \rangle \tag{7.14}$$

where $\langle \varepsilon \rangle$ is the electron average energy; use of (7.12) and (7.13) leads to

$$\langle \varepsilon \rangle = \frac{3m_e}{2e^2 \lambda} \left(\frac{I_{laser}}{A \cdot n_e}\right)^2 \tag{7.15}$$

Unfortunately, the value of λ in (7.15) is not easily calculated or measured. In the case of purely elastic collisions, λ would be equal to twice the mass ratio of electrons to heavy particles in the plasma.

For example, a pure carbon dioxide plasma would give a value of λ (elastic collision only) $\doteq 2 \times 10^{-5}$. If we take the results of Ref. 7.10 ($\langle\varepsilon\rangle \doteq 1$ eV), then $\lambda \simeq 10^{-2}$ to account for the observed average energy.

7.4 Measurements of Chemical Composition

The composition of the laser mixture was calculated entirely from the oxygen concentration, assuming the process $CO_2 \leftrightarrows CO + \frac{1}{2} O_2$. This assumption was deemed valid within the sensitivity of the chromatograph and was later confirmed by analysis with a mass spectrometer on two occasions.

7.4.1 Description of the Gas Chromatograph

A gas chromatograph based on measurement of thermal conductivity consists of three basic elements: a supply of reference or carrier gas (helium in our case); a column which has different diffusion characteristics with different gases; and a thermal conductivity detector. A slow flow of the reference gas is established through the column and detector. The detector constantly monitors the thermal conductivity of the flowing gas. If a small sample of gases is inserted into the reference flow before it enters the column, each of the gases will come out of the column at different times due to the different diffusivity of the various gases. The detector senses the presence of a gas other than the carrier by noting the change in thermal conductivity of the gases flowing through it.

The gas chromatograph used in the present experiment was a CARLE BASIC (c). Its column was packed with 13X molecular sieve, allowing detection of carbon monoxide, nitrogen and helium. It was baked and purged with helium and checked for linearity every three months. The error in the oxygen concentration measurements is estimated to be .2%; error in the carbon monoxide measurement is about 1%.

Since the chromatograph could only detect the three aforementioned gases, it was felt necessary to check for any other gases not detected, such as oxides of nitrogen or any other undetermined substance. The chemical analysis was made at the Jet Propulsion Laboratory with a Consolidated Electrodynamics Corp. model 21-103C mass spectrometer, having a sensitivity of .01%. In addition to the dissociation products of carbon dioxide (CO and O_2) no contaminants were found nor oxides of nitrogen.

References

7.1 M. A. Biondi and S. C. Brown, "Measurements of Ambipolar Diffusion in Helium", Phys. Rev. 75, 1700 (1949).

7.2 J. H. Harris and D. Balfour, "A Microwave Cavity Method for Recording Rapid Variations of Electron Density and for Observing Electron Collision Effects", in Phenomena in Ionized Gases Vol. III (1965), pp.79-83.

7.3 P. O. Clark and M. R. Smith, "An Investigation of the Effect of Gas Additives on the Electron Temperature and Density in a CO_2 Laser Discharge", Appl. Phys. Lett. 9, 367 (1966).

7.4 L. D. Pleasance and E. V. George, "Electron Density in Ion-Laser Discharges", Appl. Phys. Lett. 18, 557 (1971).

7.5 M. Z. Novgorodov, A. G. Sviridov, and N. N. Sobolev, "Electron Density and Collision Frequency in a CO_2 Laser", Sov. Phys. Tech. Phys. 16, 589 (1971).

7.6 J. C. Ingraham and S. C. Brown, "Plasma Diagnostics", R.L.E. Technical Report #454, MIT (1966).

7.7 A. von Engel, Ionized Gases, 2nd edition, (Oxford, 1965), p. 241.

7.8 A. Ravimohan, Ph.D. thesis, California Institute of Technology, 1971.

7.9 F. Llewellyn-Jones, The Glow Discharge and an Introduction to Plasma Physics (Methuen and Co., Ltd., London, 1966).

7.10 J. Polman and W. J. Witteman, "Electron-Radiation Temperature Measurements in a Sealed-Off CO_2 Laser System", IEEE J. Quantum Electr. QE-6, 154 (1970).

Chapter VIII

EXPERIMENTAL RESULTS

In this chapter we describe the experimental procedures and results of the present experiment. Results for the dissociation of carbon dioxide and the plasma parameters were obtained for twelve different initial gas compositions. If the dissociation was measured for a constant STP flow rate, we found no dependence on the pressure. The electron density was found to vary somewhat with composition.

By describing the experimental results in terms of a rate constant K it was possible to represent all the experimental points for compositions not containing water vapor in a single graph of K vs CO_2 partial flow rate (at STP). The presence of small amounts of water vapor causes a marked reduction of K.

Inasmuch as they can be compared, the results agree with previously published results.

8.1 Experimental Procedures and Ranges of Independent Variables

8.1.1 Gas Mixtures Used

In the present experiment three basic mixtures of CO_2-N_2-H_e were studied; other mixtures of either CO_2-N_2 or CO_2He were derived from the original three. They were in molar or volume proportions:

SET A: (1,3,16); (1,3,0); (1,0,16)

SET B: (1,2,10); (1,2,0); (1,0,10)

SET C: (2,3,15); (2.3,0); (2,0,15)

Also, pure CO_2 was studied, and the volume proportion (1,3,16) with .5 H_2O or 1.1 H_2O added. The mixtures were selected because they are

typical for flowing low pressure lasers (Ref. 8.1) or (Ref. 8.2), for example.

The pressure of the discharge was set at values typical of similar mixtures (Ref. 8.2), with usually additional data taken at pressures above and below that point. For example, mixtures of three gases (CO_2-N_2-He) with or without water added were usually run at points between 8 and 16 torr. Mixtures of CO_2-N_2 at 2 to 4 torr, CO_2-He at 6 to 11 torr, and pure CO_2 at .9 to 2.0 torr.

8.1.2 Gas Flow Rate: STP Flow

There is no unique way of specifying a gas flow rate. Reports on CO_2 lasers have mostly used either STP flow rates (Ref. 8.1) or volume flow rate in the discharge tube (Ref. 8.3), for example. Both measurements are related and it is possible to obtain one from the other, but the latter is the most widely used.

STP flow rate is the volume flow rate at atmospheric pressure and 300°K. In the present work all flow rates are reported as STP flow rates. Conversion formulas to obtain different parameters, volume flow rate, Q_{laser}, flow speed, v_{laser}, and mass flow rate $\dot{m}$, are given below:

$$Q_{laser} = Q_{STP}/P_{laser} \ (atm) \tag{8.1}$$

$$v_{laser} \left(\frac{cm}{sec}\right) = \frac{Q_{STP}(cm^3/sec)}{P_{laser}(atm) + A \ (cm^2)} \tag{8.2}$$

$$\dot{m} \ (cm/sec) = \frac{Q_{STP}(cm^3/sec)}{22.4 \times 10^3} \cdot MW \tag{8.3}$$

P_{laser} is the pressure in the laser expressed in atmospheres (1 torr = .001316 atm), A is the cross sectional area of the laser tube, MW is the molecular weight of the gas. In the case of mixtures of n gases, the molecular weight (MW) is computed from the concentration of each of the components by volume (C_i) and their respective molecular weights (MW_i) as follows:

$$1 = \sum_{i=1}^{n} C_i \tag{8.4}$$

$$MW = \sum_{i=1}^{n} C_i \cdot (MW_i) \tag{8.5}$$

8.1.3 Summary of Conditions Studied

Table 8.1 lists all the conditions studied in the present work. The entries are listed by data set ID number and each corresponds to a specific initial composition, a given STP flow rate $Q_{STP}(cm^3/sec)$, a total laser pressure, and the calculated average electric field E. The field was calculated using equation (7.13).

Table 8.2 shows the information collected in a typical data set (#147). The results were generated as tables of average electron density, electron collision frequency, voltage drop across the discharge tube, calculated electric field in the positive column, dissociation percentage, all as functions of the current. As already mentioned, the initial gas composition, the STP volume flow rate, and the total pressure were kept constant while taking these measurements.

In general, flow rates for all mixtures (and pure CO_2) were chosen in such a way that the partial STP flow rate of CO_2 would be in the

range from .1 to 1.0 cc/sec.

The usual laboratory procedure consisted of selecting a mixture and STP flow rate (Q_{STP}); then by varying the pressure different data sets corresponding to these different pressures would be generated.

8.2 Dependence of Electron Density on Experimental Variables

From simple calculations, assuming that the electrons carry all the current in the discharge, the following equation for the average electron density $\bar{n}_e$ can be written

$$\bar{n}_e = \frac{j}{v_d e} \simeq (\text{constant})\ j \qquad (8.6)$$

In the above equation, j is the average current density (current/cross sectional area), v_d is the drift velocity, and e is the charge of an electron.

For most of the experimental conditions studied in the present work, the average electron density $\bar{n}_e$ could be closely approximated by a linear function of j. The flow rate and pressure seemed to have only a small influence on the plots of n_e vs j, as can be seen in Figure 8.1. Measurements of electron density plotted against current density for the different CO_2-N_2-He compositions studied, are shown in the following:

Figure 8.2: (1,3,16); (1,0,16); (1,3,0); 100% CO_2

Figure 8.3: (1,2,10); (1,0,10); (1,2,0); 100% CO_2

Figure 8.4: (2,3,15); (2,0,15); (2,3,0); 100% CO_2

Figure 8.5: (1,3,16) + $\frac{1}{2}$ H_2O; (1,3,16) + 1.1 H_2O

In general terms, the behavior of the electron density shows a direct dependence on current density. The proportionality factor is, however, dependent on the composition. At the same current density, mixtures of CO_2-He have higher electron densities than CO_2-N_2-He mixtures, the latter are higher than CO_2-N_2, and they in turn are higher than pure CO_2.

8.3 Dissociation of Carbon Dioxide as a Function of Average Electron Density

In this section the main results of the experiments are presented. It was found that for a given mixture only the STP flow rate and electron density is required to determine the dissociation.

Figures 8.6 through 8.17 show plots of dissociation vs electron density for various STP flow rates and different pressures. The initial mixtures were CO_2-N_2-He:

Figure 8.6:	(1,3,16)	SET A
8.7:	(1,3,0)	
8.8:	(1,0,16)	
Figure 8.9:	(1,3,16) + .5 H_2O	
Figure 8.10:	(1,3,16) + 1.1 H_2O	
Figure 8.11:	(1,2,10)	SET B
8.12:	(1,2,0)	
8.13:	(1,0,10)	
Figure 8.14:	(2,3,15)	SET C
8.15	(2,3,0)	
8.16	(2,0,15)	
Figure 8.17:	100% CO_2	

In general, dissociation vs $\bar{n}_e$ was found to be a function of both the STP flow rate and the mixture composition. It was almost independent of pressure. The addition of water vapor decreased dissociation markedly.

8.3.1 Effect of Pressure and STP Flow

In the experiments for a given initial mixture composition and STP flow rate data were taken at several pressure levels. Within the accuracy of the instruments no dependence on pressure was found for variations of pressure up to a factor of 2. In Figures 8.6 through 8.17, except Figure 8.12, the data points for dissociation are identified according to the pressure at which they were taken. Theories of the type used by (Ref. 8.4) predict as strong a dependence on pressure as on flow rate, contrary to the behavior found here. For example, if we refer specifically to Figure 8.6, we observe that the dissociation curve at 3.2 cm^3/sec is almost 50% higher than at 7.1 cm^3/sec. On the other hand, in the same figure, variations in pressure 8 to 16 torr do not seem to change the dissociation very much. Similar behavior was encountered throughout the experimental data.

8.3.2 The Effect of the Initial Mixture Composition

Although it is a bit more difficult to visualize from the figures presented, the following statement holds true: For a given total STP flow rate the dissociation (% D) as a function of electron density $\bar{n}_e$:

% D (1,3,16) > % D (1,2,10) > % D (2,3,15)

% D (1,3,0) > % D (1,2,0) > % D (2,3,0)

% D (1,0,16) > % D (1,0,10) > % D (2,0,15)

It will be shown later that an even more significant parameter in specifying dissociation is the CO_2 partial flow rate at STP conditions. Dissociation will be described as a single valued function of the CO_2 partial flow rate.

8.3.3 Effect of Water Vapor

Limited experiments were conducted with the mixture (1,3,16) with and without water added. It was found that the dissociation of CO_2 was significantly reduced when the water was added to the system. The reduction was greater when more water was added up to the largest amount used here.

Figure 8.9 shows plots of dissociation vs electron density for a mixture of CO_2-N_2-He-H_2O of (1,3,16,.5). As previously discussed (Sec. 8.3.1) in regard to dissociation in mixtures without water vapor, the dissociation was independent of the total pressure in the tube; and it was inversely dependent on the STP flow rate.

Figure 8.10 shows dissociation vs n_e for a mixture CO_2-N_2-He-H_2O (1,3,16,1.1). The degree of dissociation is even lower than for the similar flow rate shown in Figure 8.9.

8.3.4 Characterizing the Dissociation: Dissociation Constant K

To facilitate analysis of the information collected, it is convenient to define a constant K given by the equation:

$$D = 1 - e^{-K\bar{n}_e} \tag{8.7}$$

where D is the dissociation fraction of carbon dioxide molecules

$$D = \frac{n_{CO}}{n_{CO} + n_{CO_2}} \tag{8.8}$$

$$\frac{dn_{CO_2}}{dt} = -k_1 n_{CO_2} \bar{n}_e \tag{8.9}$$

$$K = k_1 \tau \tag{8.10}$$

k_1 is the rate constant to first order in $\bar{n}_e$ for dissociation by electron collision, τ is the residence time of the gases in the discharge. Equation 8.10 does not take into consideration any recombination reaction or higher order rate constants. Equation 8.7 is discussed more fully in Chapter X.

In order to make a more quantitative analysis of the dissociation information collected, the experimental data points (for a given initial mixture and STP flow rate) were fitted (least squares fit) to equation (8.7). The results are tabulated in Table 8.3. The table is organized under initial composition heading with listings of STP flow rates and corresponding calculated K's. The partial flow rate of CO_2 is also listed (Q_{CO_2}). The values of K thus calculated give a more direct measure of the relative degree of dissociation.

Figures 8.18 to 8.21 show a plot of K as a function of carbon dioxide partial flow rate ($Q_{CO_2}^{STP}$) for the following mixtures:

Figure 8.18 SET A: (1,3,16), (1,3,0), (1,0,16)
(1,3,16) + .5 H_2O, (1,3,16) + 1.1 H_2O

Figure 8.19 SET B: (1,2,10), (1,2,0), (1,0,10)

Figure 8.20 SET C: (2,3,15), (2.3,0), (2,0,15)

Figure 8.21: Pure CO_2

In reference to the above figures the following observations can be readily made:

1) Except when water is present, the dissociation constant K as a function of the STP partial flow rate of CO_2 and defined by equation (8.7) appears to be independent of the initial mixture composition.
2) The general form of the dependence is close to $K \propto 1/Q_{CO_2}$. As a guide, a line with such a dependence was drawn in each of the graphs (8.18 to 8.21).
3) When water is added the degree of dissociation decreases substantially (Fig. 8.18).

8.4 Summary of Observed Behavior

8.4.1 Electron Density

In most cases studied, the electron density was found to have a linear dependence on the current density (I_{laser}/tube area). The proportionality constant was dependent on the gas mixture and to a far lesser degree on the gas pressure. The flow rate did not appear to affect it. These measurements support our conclusion that the current density is not a consistent parameter with which to describe the dissociation in the laser.

Comparison with previously published reports is somewhat difficult due to the different methods of measurement and varying parameters. Clark and Smith (Ref. 8.5), using a microwave cavity method, measured $\bar{n}_e \doteq .4 \cdot 10^{10} cm^{-3}$. If we use Figure 8.4 at their current densities we

get $\bar{n}_e \doteq .38 \cdot 10^{10} cm^{-3}$. In the work of Ref. 8.6 for pure CO_2 at 2 torr, the electron density was inferred by two methods (using probes): by integrating a measured distribution function of electrons; and by measuring the ion current. Our results for similar conditions lie between their two measurements. For ecample, for $j = 2.76$ ma/cm^2 they measured $.1 < \bar{n}_e \cdot 10^{-10}(cm^{-3}) < .45$; in our case $n_e \doteq .2 \cdot 10^{10} cm^{-3}$. A more complete measurement of electron densities was done by Novgorodov et al. (Ref. 8.7). They used the microwave cavity technique used presently (they used TM_{0n0}). Their results of $\bar{n}_e$ vs current density, although agreeing qualitatively with ours, differ in absolute magnitude. For the same current density, their results are about 1/3 below ours. Since no details of the measurement were given in the paper, it is very hard to establish the reason for the discrepancy.

8.4.2 Results for the Dissociation of CO_2

The most significant results found were:

1) There is no pressure dependence in the dissociation vs electron density ($\bar{n}_e$) if the data are taken at constant STP flow rate. This appears to hold for all the mixtures studied.
2) Under similar conditions the presence of water vapor (2.5% to 5%) reduces the dissociation by as much as 50%.
3) The dissociation constant K, defined by equation (8.7) and discussed in Chapter X, showed a unique dependence on the partial flow rate of CO_2. This dependence was not affected by the presence or absence of other gases (He and/or N_2).

Direct comparison of our results for dissociation with those of others authors is indirect and therefore approximate. With one exception (Ref. 8.6) the results for dissociation quoted in the literature are not accompanied by measurements of the electron density. The current is assumed to give an indication of the behavior of the electron density. In light of the variations encountered here in the values of the electron density in the laser discharge, the published results of dissociation with current as a parameter have to be corrected.

The present author is aware of only one instance in which the dissociation in a CO_2 glow discharge was studied as a function of the electron density. Ivanov et al. (Ref. 8.6) studied the dissociation in a discharge of pure CO_2 at 2 torr and current densities of .6 to 12 ma/cm^2. Agreement with our measured values is satisfactory: for a residence time of .1 sec and $\bar{n}_e = .48 \cdot 10^{10} cm^{-3}$, they measured 16% dissociation. In our experiment for a residence time (τ) = .12 sec, p = 1.8 torr, and $n_e = .48 \times 10^{10} cm^{-3}$, we measure 10% dissociation. The electron densities calculated by Ivanov were obtained from probe measurements.

More extensive analysis of the dissociation in CO_2 has been reported by Soviet (Refs. 8.8 and 8.9) and British (Ref. 8.3 and 8.4) authors. The authors of Ref. 8.8 report the dissociation as a function of flow rate through the laser; they used current as a parameter and studied two compositions CO_2-N_2-He (1,3,6) and (1,0,9). They used a water cooled laser tube 60 cm x 2.2 cm dia. In order to compare their

results with the present experiments, it is necessary to transform their current values (current densities) into electron densities. Figure 8.4 is used for that purpose. The following table compares results obtained in that way:

(1,3,6), Q_{STP}= 7.3(cm^3/sec) (Fig. 3, Ref. 8.8)		(2,3,15), Q_{STP}= 7.0(cm^3/sec) (Fig. 8.14, Present work)	
j(ma/cm^2)	% D	$n_e^*(j)$	% D
2.6	11%	.24	8%
5.3	20%	.53	15%
7.9	28%	.79	20%

n_e is calculated from the current density (Fig. 8.4).

Our results are somewhat lower than their measured values, but the general behavior seems to be the same. The differences may be attributed to the different experimental conditions. Qualitatively the agreement is fairly close. In Ref. 8.9 some of the same workers analyzed a flowing CO_2-N_2-He (2,1,18) mixture. Their results for dissociation are presented in terms of a reaction constant related to the K we defined in equation (8.7). Again, they use the current through the laser as the main parameter so direct comparison is difficult. For example, they measure $(K\,\bar{n}_e/\tau) \doteq .3\ sec^{-1}$ at 8 torr and j = 5.25 (ma/cm^2); comparing this to our experimental results we estimate $\bar{n}_e = .5 \cdot 10^{10} cm^{-3}$, $Q_{CO_2} \doteq .3$ (cm^3/sec) gives τ = .33 sec, and K = .4. Therefore in our case for similar conditions we obtain $(K\,\bar{n}_e/\tau)$ = .6. Discrepancies may again be attributed to the different experimental conditions and models used.

Smith and Austin (Refs. 8.3 and 8.4) report on various parametric dependences of dissociation in CO_2 lasers. The mixtures they studied were CO_2-N_2-He (6,12,82), (1,2,0) and pure CO_2. Although it appears that they took some measurements of dissociation as a function of water vapor pressure, unfortunately they only reported qualitative results. Their results agree with ours in general behavior and order of magnitude. For example, they obtain 52% dissociation for a (6,12,82) mixture at 9 torr, j = 14 ma/cm^2, and 5 (cm^3/sec) STP flow. Our experiments for conditions close to those give 42% dissociation. In Ref. 8.4 the same authors report similar results; in addition they construct a kinetic model for the dissociation process based on the electric current through the laser.

Limited dissociation results are reported in Ref. 8.10 using a CO_2-N_2-He (1,2,10) mixture in a 3.8 cm diameter tube. With the mixture at 10.6 torr, STP flow of 5 (cm^3/sec) and j = 11.5 (ma/cm^2), they measured approximately 65% dissociation. Our results yield about 40%. The wide difference in diameters (ours is 1 cm) might be the cause of the discrepancy in this case.

In conclusion it is felt that the results for the dissociation of carbon dioxide reported here may be taken as typical of operating CO_2 lasers and as such the model to be derived from them would be a fair representation of the laser.

References

8.1 P. K. Cheo, "Effects of Gas Flow on Gain of 10.6 CO_2 Laser Amplifiers", IEEE J. Quant. Elect. QE-3, 683 (1967).

8.2 D. C. Tyte, "Carbon Dioxide Lasers" in Advances in Quantum Electronics, V1, D. W. Goodwin, ed. (Academic Press, 1970), p. 129.

8.3 A.L.S. Smith, "Molecular Composition Changes in a Flowing CO_2, N_2, He, H_2O Laser", Brit. J. Appl. Phys. D 2, 1129 (1969).

8.4 A.L.S. Smith and J. M. Austin, "Dissociation Mechanism in Pulsed and Continuous CO_2 Lasers", J. Phys. D: Appl. Phys. 7, 314 (1974).

8.5 P. O. Clark and M. Smith, "An Investigation of the Effect of Gas Additives on the Electron Temperature and Density in a CO_2 Laser Discharge", Appl. Phys. Lett. 9, 367 (1966).

8.6 Yu. A. Ivanov, L. S. Polak, and D. I. Slovetskii, "Kinetics of CO_2 Decomposition in the Glow Discharge", High Ener. Chem. 5, 344 (1971).

8.7 M. Z. Novgorodov, A. G. Sviridov, and N. N. Sobolev, "Electron Density and Collision Frequency in a CO_2 Laser", Soviet Physics, Tech. Physics 16, 589 (1971).

8.8 E. S. Gasilevich, V. A. Ivanov, E. N. Lotkova, V. N. Ochkin, N. N. Sobolev, and N. G. Yaroslavskii, "Carbon Dioxide Dissociation in a CO_2 Laser", Soviet Physics, Tech. Phys. 14, 86 (1969).

8.9 E. N. Lotkova, V. N. Ochkin, and N. N. Sobolev, "Dissociation of Carbon Dioxide and Inversion in CO_2 Laser", IEEE J. Quant. Elect. QE-7, 396 (1971).

8.10 W. J. Wiegand, M. C. Fowler, and J. A. Benda, "Carbon Monoxide Formation in CO_2 Lasers", Appl. Phys. Lett. 16, 237 (1970).

Table 8.1 SUMMARY OF CONDITIONS STUDIED

Data Set ID No.	% CO_2	% N_2	% He	STP Flow Rate (cc/sec)	P torr	(CO_2,N_2,He) Ideal	<E> volts/cm
4	100	-	-	.163	1.0	100%	11.07
5	100	-	-	.163	2.0	100%	15.4
6	10.3	13.5	76.2	3.73	10.0	(2:3:15)	33.2
7	10.3	13.5	76.2	3.67	11.0	(2:3:15)	32.7
8	10.3	13.5	76.2	3.67	12.0	(2:3:15)	31.7
9	11.4	13.3	75.3	3.21	13.0	(2:3:15)	44.1
11	10.1	13.6	76.3	3.70	15.0	(2:3:15)	30.1
12	10.1	13.6	76.3	3.68	16.0	(2:3:15)	46.8
13	9.9	13.6	76.5	3.68	17.0	(2:3:15)	44.3
15	100	-	-	.18	1.0	100%	27.7
16	100	-	-	.18	2.0	100%	21.6
17	10.6	13.4	76.0	3.13	16.0	(2:3:15)	43.3
18	10.3	13.5	76.2	3.30	10.0	(2:3:15)	32.85
19	10.3	13.5	76.2	3.17	14.0	(2:3:15)	33.4
20	10.5	13.5	76.0	3.15	9.0	(2:3:15)	34.1
21	9.3	13.6	77.1	3.05	9.0	(2:3:15)	34.5
22	7.6	13.9	78.5	3.19	10.0	(1:2:10)	37.2
23	7.6	13.9	78.5	3.19	11.0	(1:2:10)	34.97
24	7.6	13.9	78.5	3.19	12.0	(1:2:10)	38.5
25	7.6	13.9	78.5	3.19	13.0	(1:2:10)	40.8
26	7.6	13.9	78.5	3.19	15.0	(1:2:10)	41.1
27	7.6	13.9	78.5	3.19	17.0	(1:2:10)	48.1
28	5.2	14.3	80.5	3.21	9.1	(1:3:16)	33.1
29	5.2	14.3	80.5	3.21	11.0	(1:3:16)	33.45
30	5.2	14.3	80.5	3.21	13.0	(1:3:16)	37.7
32	5.2	14.3	80.5	3.21	15.0	(1:3:16)	40.6
33	5.2	14.3	80.5	3.21	17.0	(1:3:16)	43.8
34	5.2	14.3	80.5	4.47	12.0	(1:3:16)	42.0
35	5.2	14.3	80.5	4.17	9.0	(1:3:16)	33.4

Table 8.1 (continued)

Data Set ID No.	% CO_2	% N_2	% He	STP Flow Rate (cc/sec)	P torr	(CO_2,N_2,He) Ideal	<E> volts/cm
36	5.2	14.3	80.5	4.17	14.0	(1:3:16)	47.3
37	5.2	14.3	80.5	5.0	8.0	(1:3:16)	33.1
38	5.2	14.3	80.5	5.0	12.0	(1:3:16)	37.4
39	5.2	14.3	80.5	5.0	16.0	(1:3:16)	45.9
40	5.2	14.3	80.5	6.25	8.0	(1:3:16)	30.7
41	5.2	14.3	80.5	6.25	12.0	(1:3:16)	38.9
42	5.2	14.3	80.5	6.25	16.0	(1:3:16)	41.0
43	7.7	14.9	77.4	4.92	8.0	(1:2:10)	39.5
44	7.7	14.9	77.4	4.92	12.0	(1:2:10)	38.2
45	7.7	14.9	77.4	4.92	16.0	(1:2:10)	47.5
46	8.1	14.8	77.0	5.02	8.0	(1:2:10)	38.4
47	7.6	14.9	77.4	6.00	8.0	(1:2:10)	35.5
48	7.6	14.9	77.4	6.00	12.0	(1:2:10)	36.8
49	7.6	14.9	77.4	6.00	16.0	(1:2:10)	44.4
50	7.6	14.9	77.5	7.0	8.0	(1:2:10)	35.1
51	7.6	14.9	77.5	7.0	12.0	(1:2:10)	42.3
52	7.6	14.9	77.5	7.0	16.0	(1:2:10)	46.3
53	10.6	14.4	74.9	5.0	8.0	(2:3:15)	34.2
54	10.6	14.4	74.9	5.0	12.0	(2:3:15)	41.2
55	10.6	14.4	74.9	5.0	16.0	(2:3:15)	47.5
56	10.4	14.5	75.1	6.1	8.0	(2:3:15)	31.9
57	10.4	14.5	75.1	6.1	12.0	(2:3:15)	35.5
58	10.4	14.5	75.1	6.1	16.0	(2:3:15)	44.3
59	10.5	14.5	75.0	7.04	8.0	(2:3:15)	37.0
60	10.5	14.5	75.0	7.04	12.0	(2:3:15)	38.9
61	10.5	14.5	75.0	7.04	16.0	(2:3:15)	45.2
62	5.3	15.3	79.4	7.10	8.0	(1:3:16)	39.0
63	5.3	15.3	79.4	7.04	12.0	(1:3:16)	38.19
64	5.3	15.3	79.4	7.1	16.0	(1:3:16)	39.0

Table 8.1 (continued)

Data Set ID No.	% CO_2	% N_2	% He	STP Flow Rate (cc/sec)	P torr	(CO_2,N_2,He) Ideal	<E> volts/cm
66	10.6	14.5	75.0	5.0	12.0	(2:3:15)	36.4
67	10.6	14.5	75.0	5.0	14.0	(2:3:15)	45.8
68	10.6	14.5	75.0	5.0	16.0	(2:3:15)	54.6
69	10.6	14.5	75.0	5.0	8.0	(2:3:15)	47.6
70	7.5	15.0	77.5	5.0	8.0	(1:2:10)	28.6
71	7.5	15.0	77.5	5.0	12.0	(1:2:10)	46.8
72	7.5	15.0	77.5	5.0	16.0	(1:2:10)	56.8
73	7.5	15.0	77.5	5.0	8.0	(1:2:10)	34.2
74	5.3	15.3	79.4	5.0	8.0	(1:3:16)	50.8
75	5.3	15.3	79.4	5.0	12.0	(1:3:16)	54.2
76	5.3	15.3	79.4	5.0	16.0	(1:3:16)	62.0
82	5.6	-	94.4	10.10	10.1	(1:-:16)	26.25
83	100	-	-	1.05	1.8	100%	22.37
84	100	-	-	.75	1.4	100%	37.6
85	100	-	-	.529	1.3	100%	20.2
86	100	-	-	.529	3.0	100%	22.35
87	100	-	-	.373	0.9	100%	18.45
89	100	-	-	.262	0.8	100%	14.9
90	26.0	74.0	-	2.05	2.8	(1:3:0)	35.4
91	25.6	74.4	-	1.404	2.5	(1:3:0)	27.26
92	25.6	74.4	-	1.462	2.3	(1:3:0)	29.07
93	34.0	66.0	-	2.2	2.2	(1:2:0)	32.8
94	33.7	66.3	-	2.2	2.7	(1:2:0)	29.7
95	42.0	58.0	-	2.4	2.3	(2:3:0)	31.1
96	33.6	66.4	-	2.4	3.0	(1:2:0)	35.33
97	33.6	66.4	-	1.2	2.0	(1:2:0)	22.6
98	42.0	58.0	-	1.2	3.0	(2:3:0)	25.0
99	34.0	66.0	-	1.1	1.8	(1:2:0)	27.1
100	33.3	66.7	-	1.1	2.7	(1:2:0)	27.9

Table 8.1 (continued)

Data Set ID No.	% CO_2	% N_2	% He	STP Flow Rate (cc/sec)	P torr	(CO_2,N_2,He) Ideal	<E> volts/cm
101	25.0	75.0	-	1.0	1.6	(1:3:0)	29.0
102	25.0	75.0	-	1.0	2.5	(1:3:0)	31.4
103	42.2	57.8	-	1.7	2.8	(2:3:0)	36.2
104	33.3	66.7	-	1.5	2.7	(1:2:0)	36.73
105	33.3	66.7	-	1.5	3.6	(1:2:0)	33.85
110	12.0	-	88.0	8.6	7.3	(2:0:15)	29.15
111	12.0	-	88.0	8.6	10.3	(2:0:15)	30.22
112	9.0	-	91.0	8.3	7.2	(1:0:10)	27.74
113	9.0	-	91.0	8.3	10.2	(1:0:10)	30.89
116	6.0	-	94.0	8.3	7.3	(1:0:16)	26.3
117	6.0	-	94.0	8.3	10.2	(1:0:16)	29.7
118	9.0	-	91.0	6.0	6.8	(1:0:10)	28.9
119	9.0	-	91.0	6.0	10.2	(1:0:10)	33.2
120	12.0	-	88.0	4.4	6.8	(2:0:15)	21.0
121	12.0	-	88.0	4.4	10.3	(2:0:15)	27.1
122	9.0	-	91.0	4.2	6.8	(1:0:10)	24.3
123	9.0	-	91.0	4.2	10.2	(1:0:10)	29.6
124	6.2	-	93.8	4.2	6.8	(1:0:16)	22.0
125	6.2	-	93.8	4.2	10.2	(1:0:16)	22.7
131	5.3	15.3	79.4	13.2	10.0	(1:3:16)	55.6
132	5.3	15.3	79.4	13.2	12.0	(1:3:16)	39.9
133	5.3	15.3	79.4	8.3	8.1	(1:3:16)	45.2
134	5.3	15.3	79.4	8.3	12.0	(1:3:16)	48.9
135	5.2	14.9	77.2	5.0	8.0	(1:3:16)	29.0
136	5.2	14.9	77.2	5.0	12.0	(1:3:16)	44.0
137	5.2	14.9	77.2	5.0	16.0	(1:3:16)	68.0
138	5.2	14.9	77.5	10.0	8.0	(1:3:16)	49.25
139	5.2	14.9	77.5	10.0	12.0	(1:3:16)	52.0
140	5.2	14.9	77.5	10.0	16.0	(1:3:16)	62.0

Table 8.1 (continued)

Data Set ID No.	% CO_2	% N_2	% He	STP Flow Rate (cc/sec)	P torr	(CO_2,N_2,He) Ideal	<E> volts/cm
141	5.2	14.9	77.3	7.14	8.0	(1:3:16)	42.0
142	5.2	14.9	77.3	7.14	12.0	(1:3:16)	57.0
143	5.2	14.9	77.3	7.14	16.0	(1:3:16)	61.0
144	5.3	15.3	79.4	7.14	16.0	(1:3:16)	50.8
145	5.3	15.3	79.4	7.14	12.0	(1:3:16)	42.0
146	5.3	15.3	79.4	7.14	8.0	(1:3:16)	38.5
147	5.3	15.3	79.4	10.0	16.0	(1:3:16)	53.8
148	5.3	15.3	79.4	10.0	12.0	(1:3:16)	51.0
149	5.3	15.3	79.4	10.0	8.0	(1:3:16)	44.2
150	5.3	15.3	79.4	5.0	16.0	(1:3:16)	43.1
151	5.3	15.3	79.4	5.0	12.0	(1:3:16)	46.1
152	5.3	15.3	79.4	5.0	8.0	(1:3:16)	37.2
153	5.0	14.5	75.1	4.9	16.0	(1:3:16)	61.6
154	5.0	14.5	75.1	4.9	12.0	(1:3:16)	54.4
155	5.0	14.5	75.1	4.9	8.0	(1:3:16)	46.6

DATA SET ID NUMBER : 147

FLOW RATE : 10.0 cm^3/sec (@ STP)

Total Pressure : 16. torr

(CO_2:N_2:He) : (5.3:15.3:79.4)

Current (ma.)	Electron Density ($10^{-10}cm^{-3}$)	Electron Coll.Freq. ($10^{-10}sec^{-1}$)	Volt drop (KV)	E field (V/cm)	%CO	$\%O_2$	$\%N_2$	$\%\frac{(CO)}{(CO)+(CO_2)}$
6.0	.75	4.15	11.4	64.7	1.6	.67	15.3	25.5
8.0	.89	3.49	10.8	61.5	1.9	.80	15.3	30.4
10.0	1.14	3.04	10.5	52.3	2.1	.91	15.3	34.8
12.0	1.30	2.68	10.2	48.3	2.4	1.0	15.3	39.0
16.0	1.66	2.23	9.45	42.0	2.8	1.2	15.3	45.9

TABLE 8-2 .- Typical data collected .

TABLE 8.3.- Least square fit of experimental results to equation 8.7 . All compositions are given in molar fractions(volume) CO_2-N_2-He .Q_{tot} is the total flow rate and Q_{CO2} is the partial flow rate of CO_2. Both flow rates are volume flow rates measured at STP conditions and are given in (cm^3/sec) . K is in units of ($10^{-10} cm^3$).

(figure 8.18)

○(1,3,16)			□(1,3,0)			△(1,0,16)		
Q_{tot}	Q_{CO2}	K	Q_{tot}	Q_{CO2}	K	Q_{tot}	Q_{CO2}	K
3.2	.16	.72	1.0	.25	.46	4.2	.25	.69
4.2	.21	.51	1.5	.38	.35	8.3	.49	.21
5.0	.25	.50	2.1	.53	.22	10.0	.59	.12
6.3	.31	.43						
7.1	.36	.40						
8.3	.42	.38						
10.0	.50	.32						
13.2	.66	.33						

●(1,3,16) + ½ H_2O			⊕(1,3,16) + 1.1 H_2O		
Q_{tot}	Q_{CO2}	K	Q_{tot}	Q_{CO2}	K
5.0	.24	.20	5.0	.24	.14
7.1	.35	.15			
10.0	.49	.13			

(figure 8.19)

○(1,2,10)			□(1,2,0)			△(1,0,10)		
Q_{tot}	Q_{CO2}	K	Q_{tot}	Q_{CO2}	K	Q_{tot}	Q_{CO2}	K
3.2	.25	.57	1.1	.37	.35	4.2	.38	.32
4.9	.38	.37	1.5	.50	.32	6.0	.55	.24
5.0	.38	.38	2.3	.77	.21	8.3	.75	.14
6.0	.46	.33						
7.0	.54	.28						

(figure 8.20)

○(2,3,15)			□(2,3,0)			△(2,0,15)		
Q_{tot}	Q_{CO2}	K	Q_{tot}	Q_{CO2}	K	Q_{tot}	Q_{CO2}	K
3.2	.32	.47	1.2	.48	.29	4.4	.52	.24
3.6	.36	.43	1.7	.68	.26	8.6	1.01	.10
5.0	.50	.25	2.4	.96	.19			
6.1	.61	.23						
7.0	.70	.23						

TABLE 8.3.- (cont.)

(figure 8.21)

Pure Q_{CO_2}	CO_2 K ($Q_{tot}=Q_{CO_2}$)
.16	.86
.18	1.08
.38	.35
.53	.31
.56	.25
.75	.23
1.05	.15

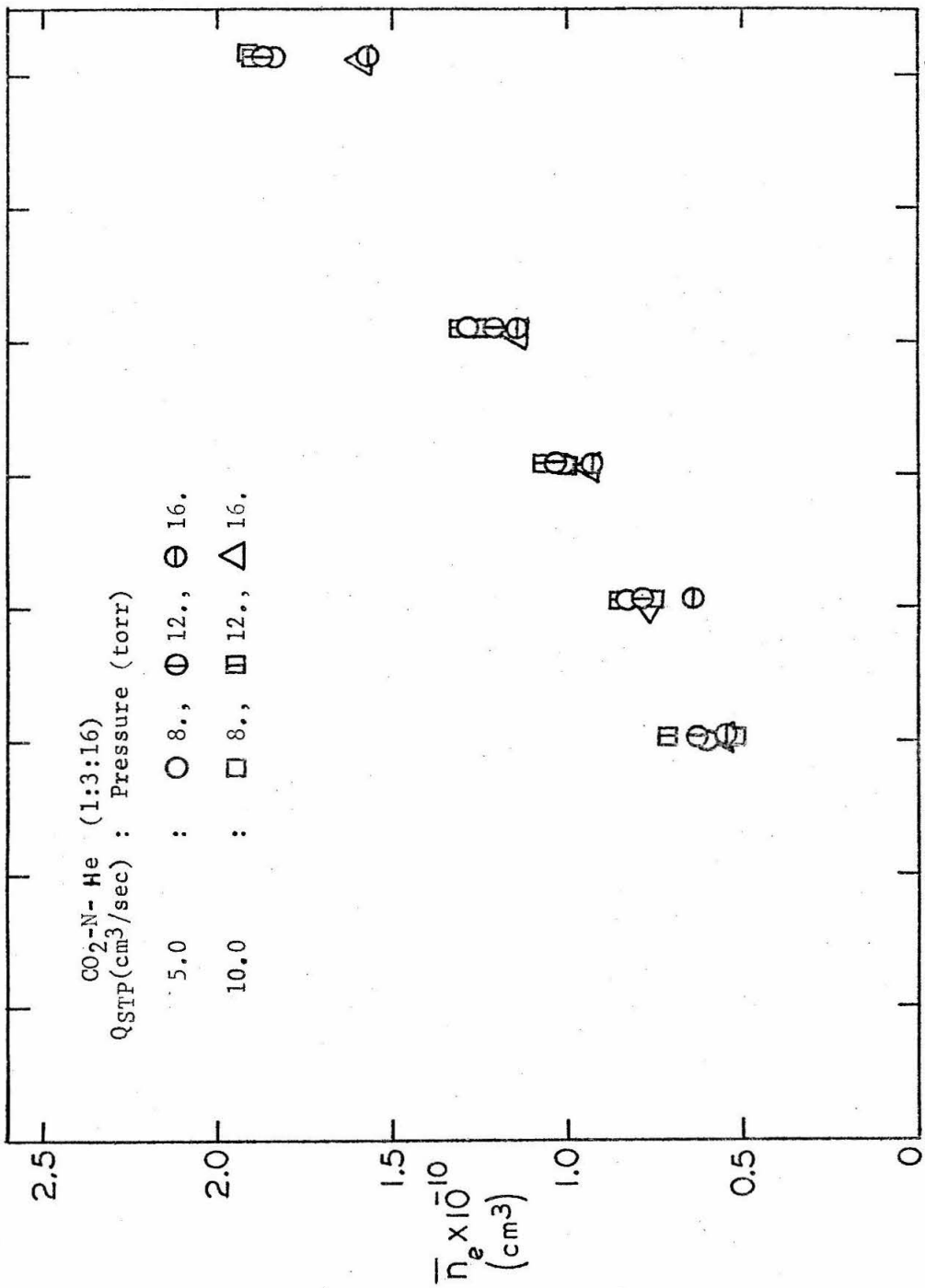

Fig. 8.1 Average electron density as function of current density

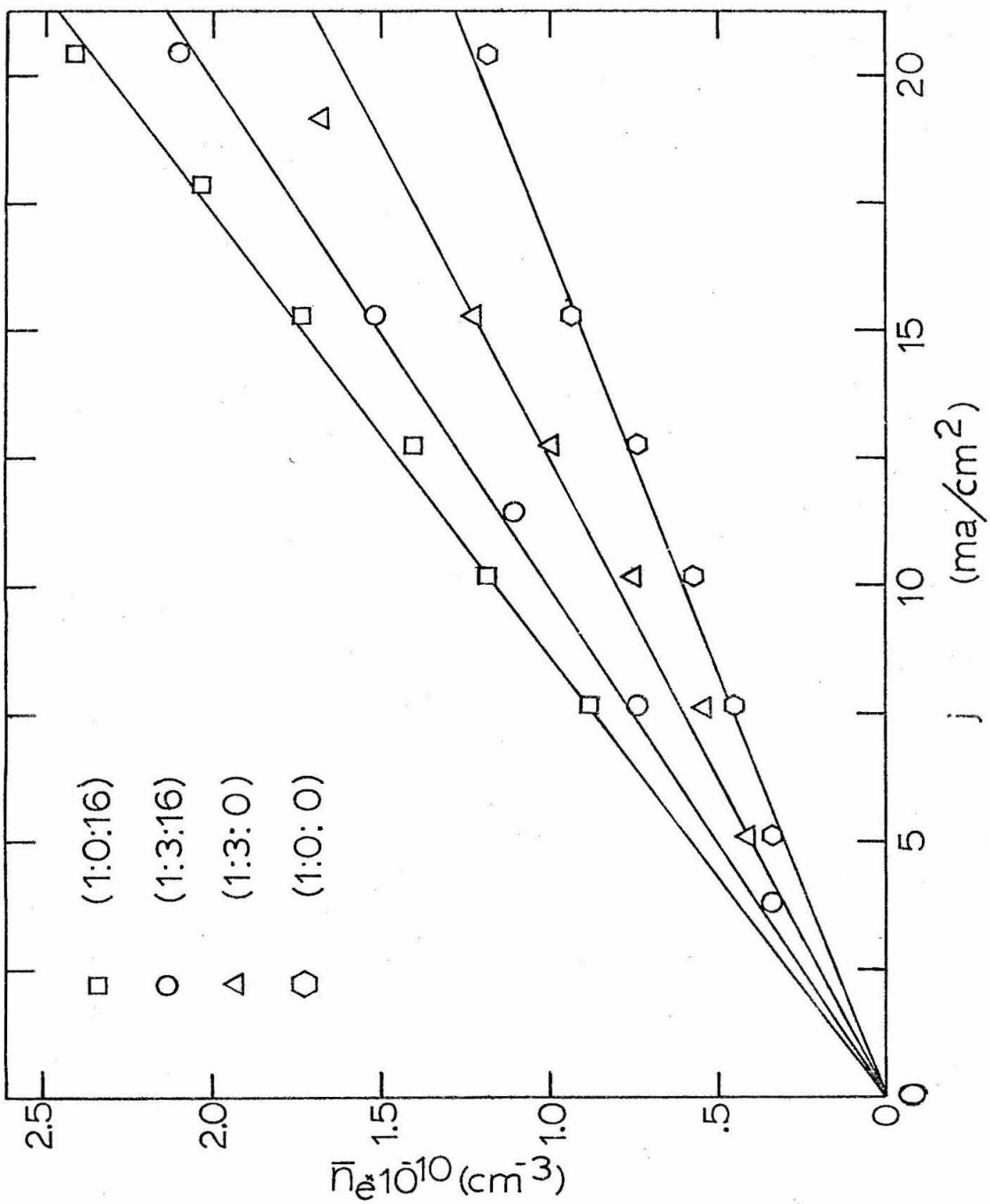

Fig. 8.2 - Electron vs. Current Density.

($A = .79\ cm^2$)

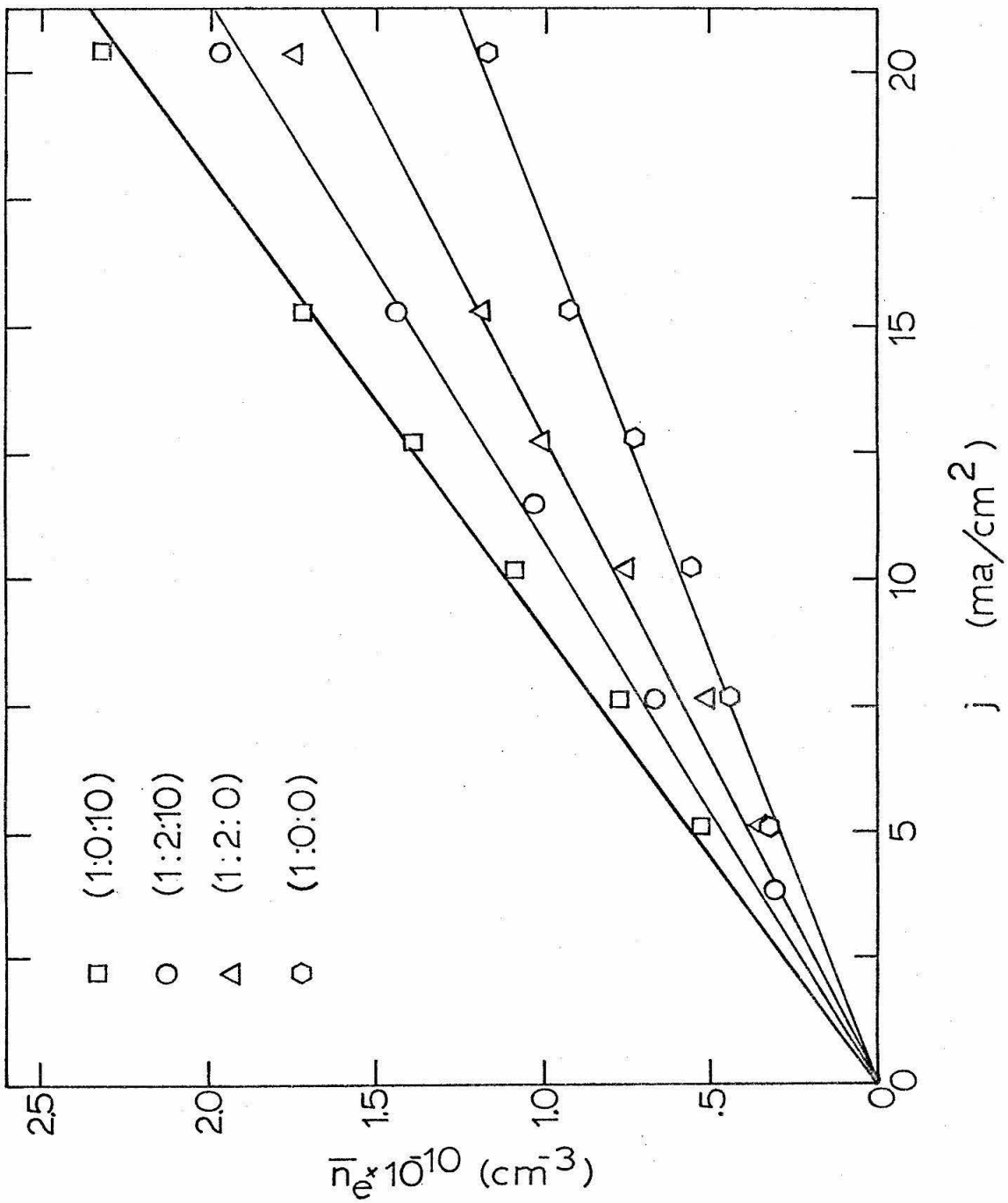

Fig 83 Electron vs. Current Density.

(A = .79 cm^{-2})

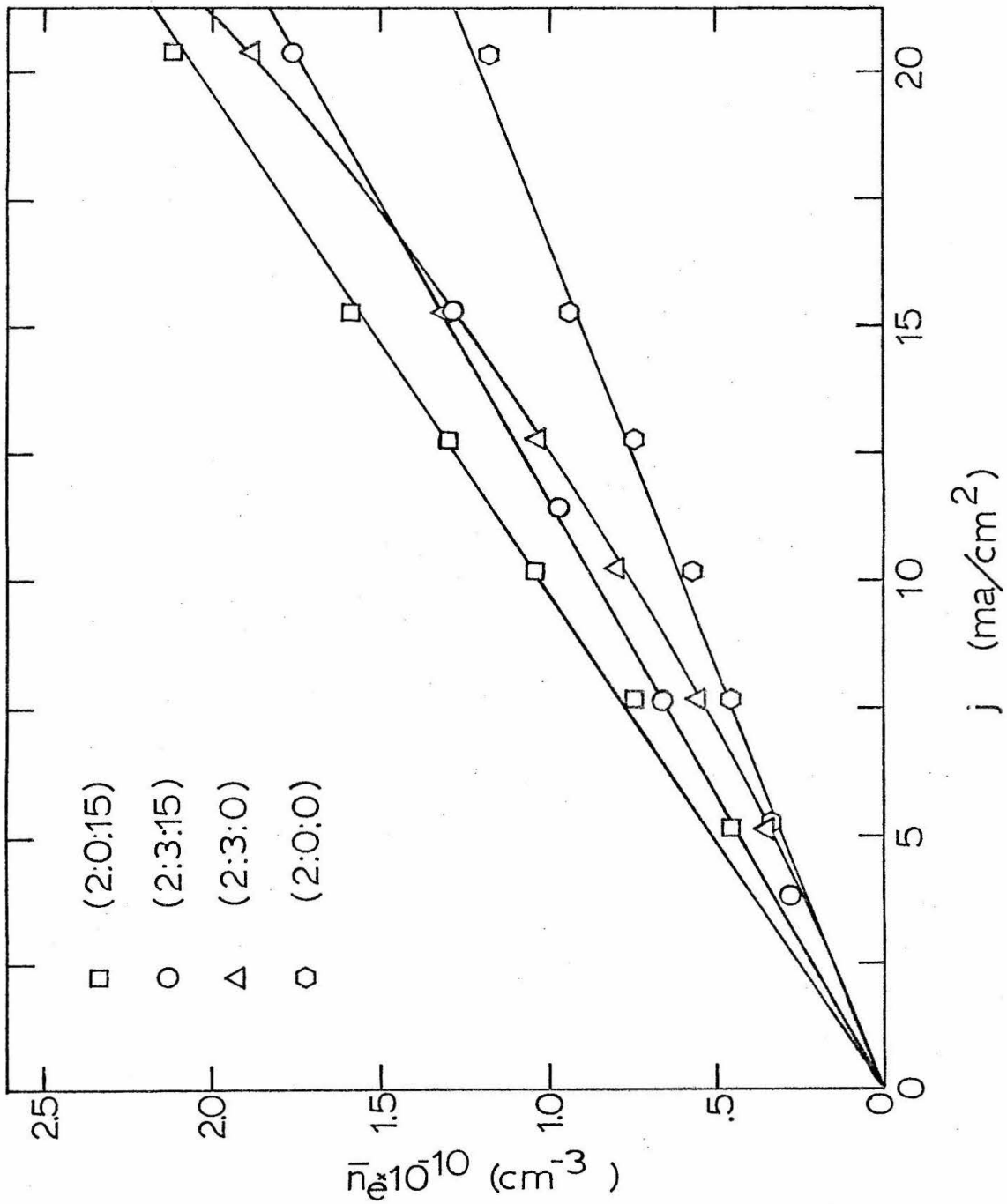

Fig 8.4-Electron vs. Current Density.
(A =.79 cm^2)

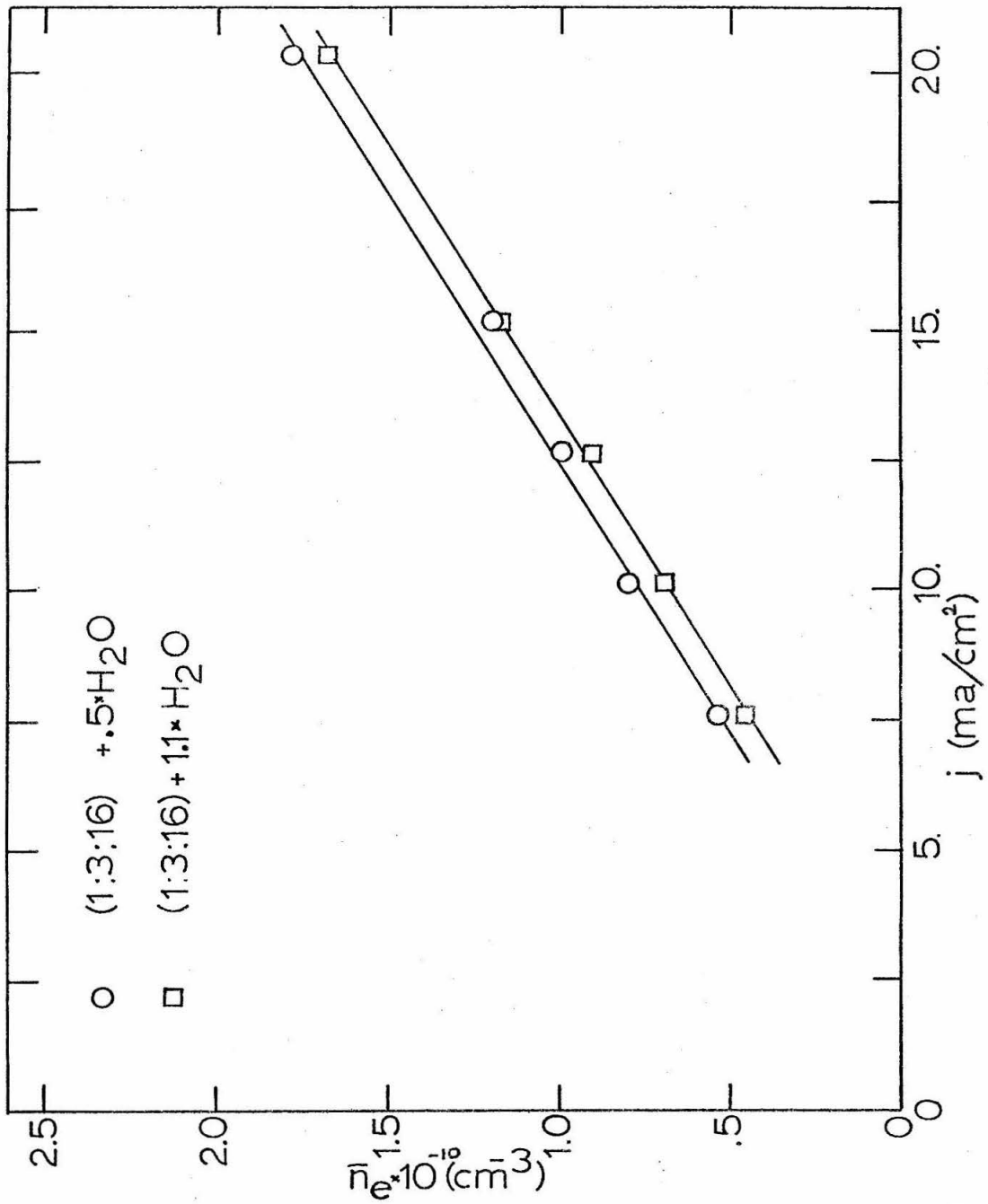

Fig 8.5 Electron vs. Current Density (A=.79cm^2).

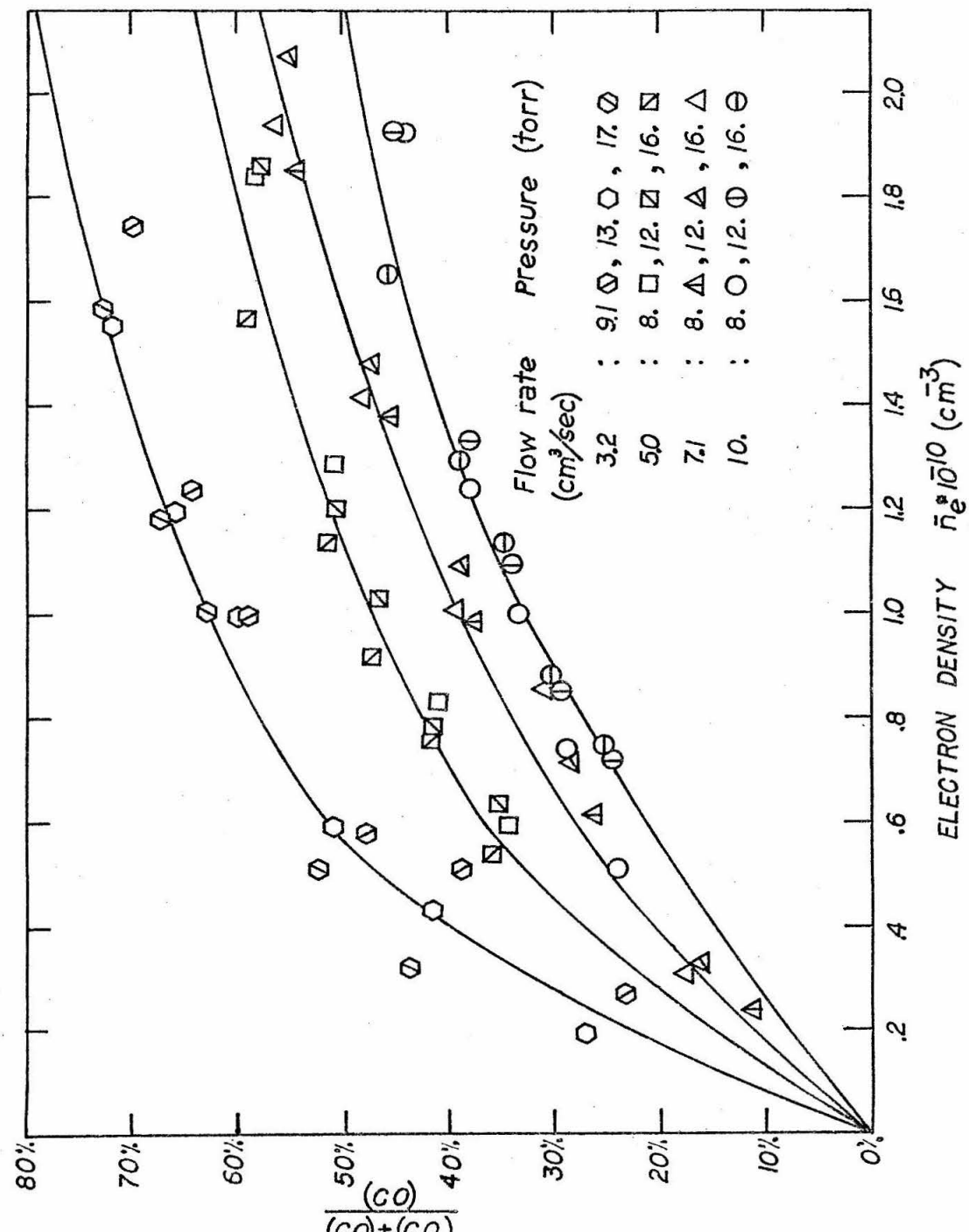

FIG. 8.6 Carbon Dioxide Dissociation vs Electron Density
CO_2 - N_2 - He (1:3:16)

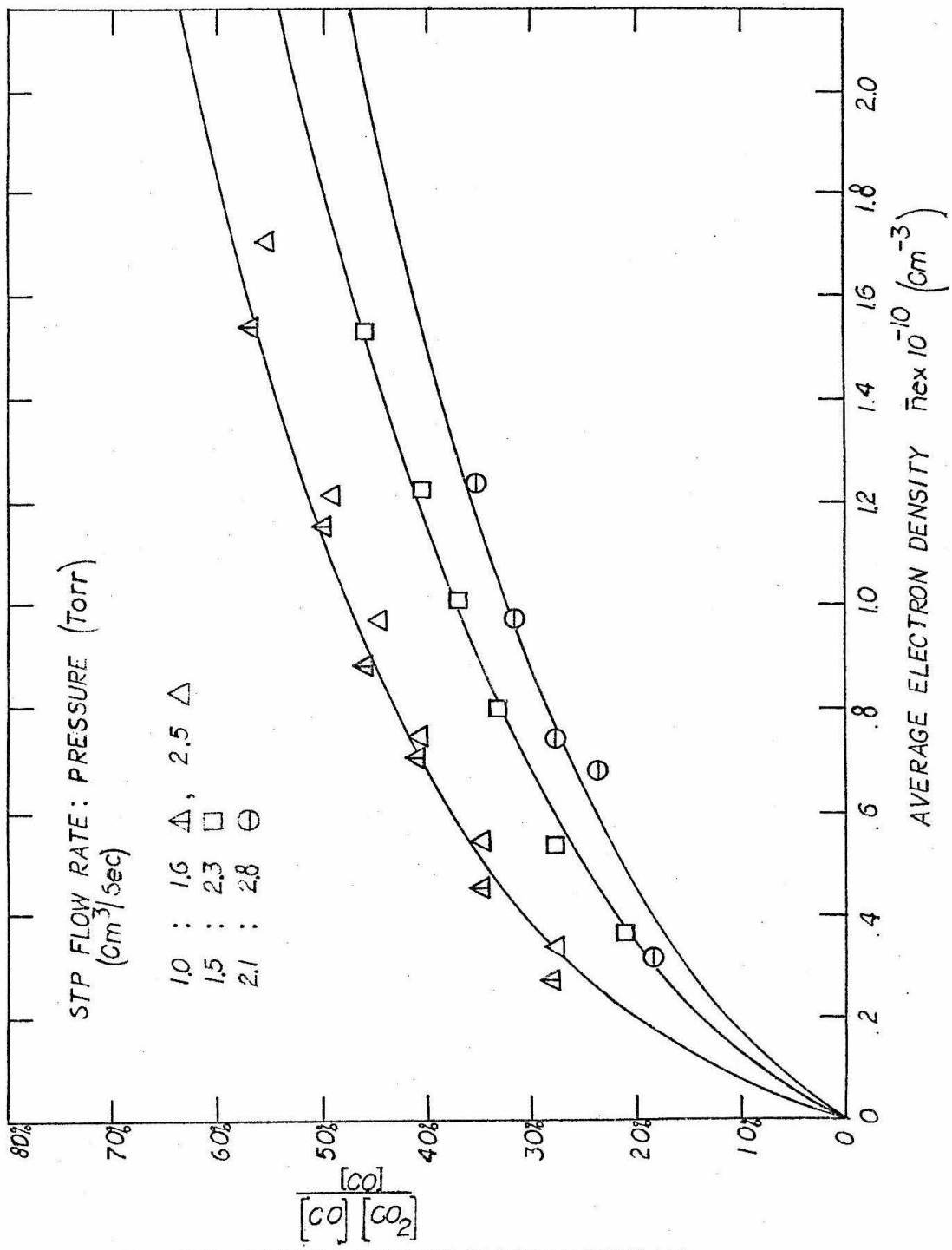

FIG. 8.7 CARBON DIOXIDE DISSOCIATION VS. ELECTRON DENSITY
CO_2-N_2 (1:3)

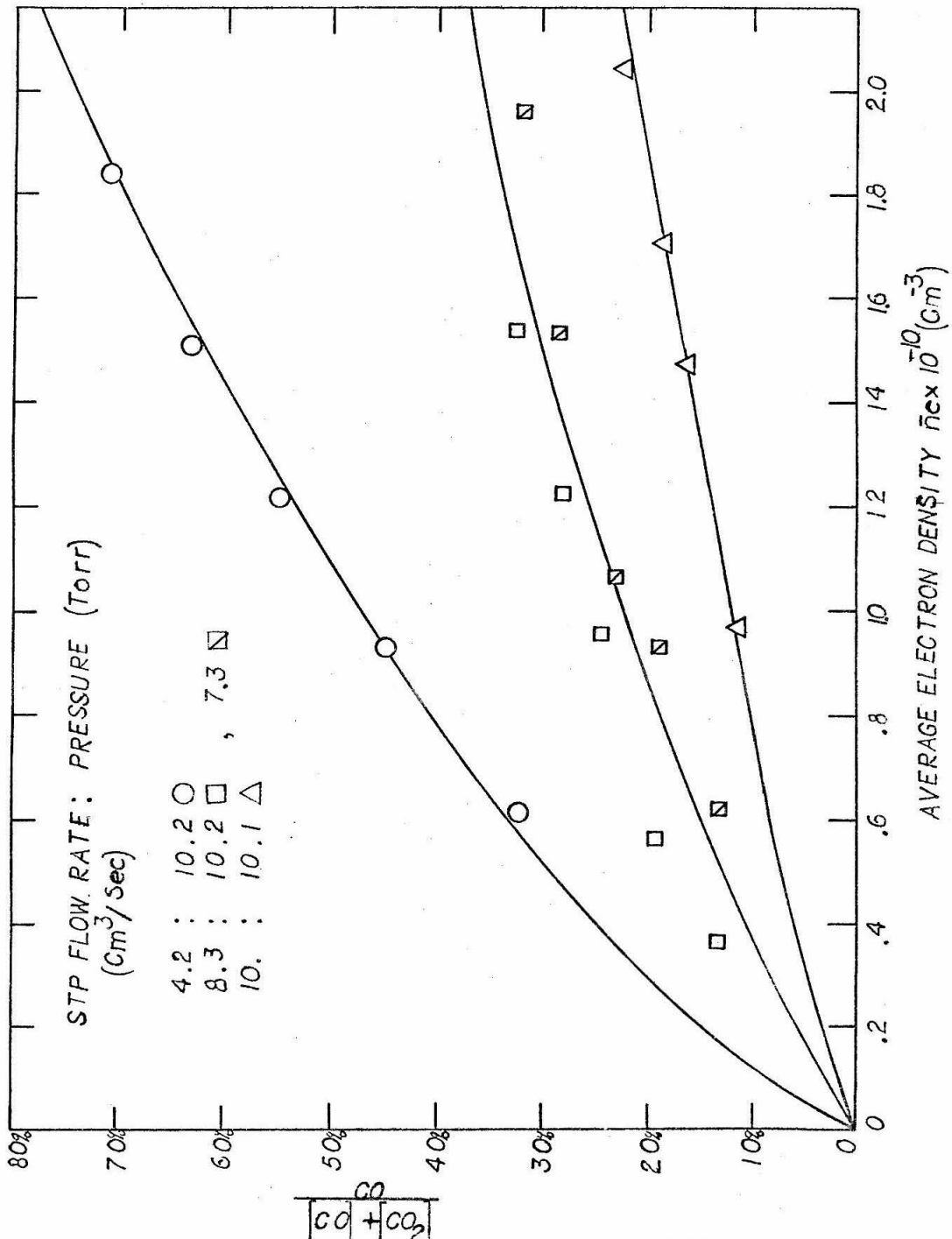

FIG 8.8 CARBON DIOXIDE DISSOCIATION VS. ELECTRON DENSITY
CO_2–HE (1:16)

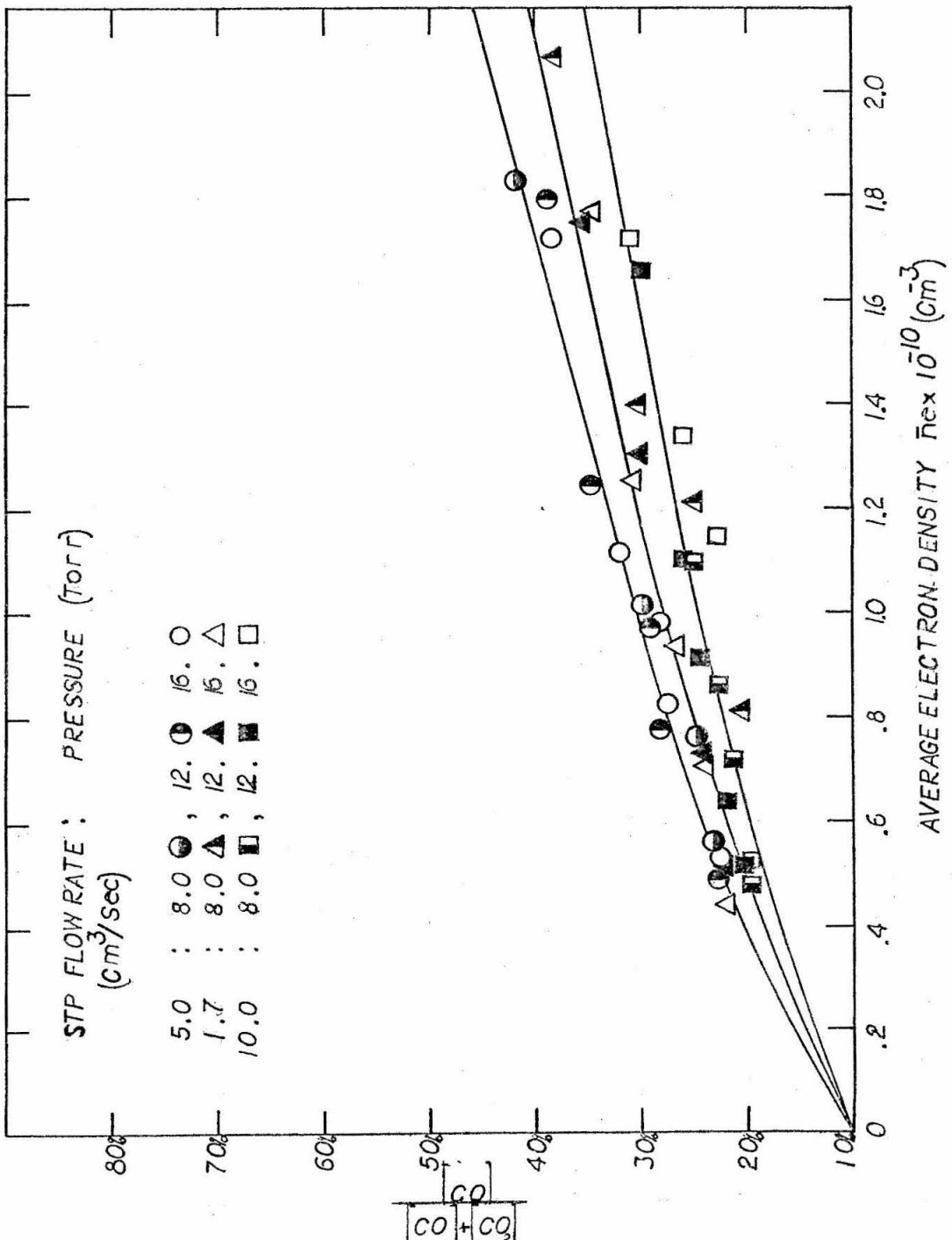

FIG. 8.9 CARBON DIOXIDE DISSOCIATION VS. ELECTRON DENSITY $(CO_2, N_2, HE, H_2O) = (1:3:16:.5)$

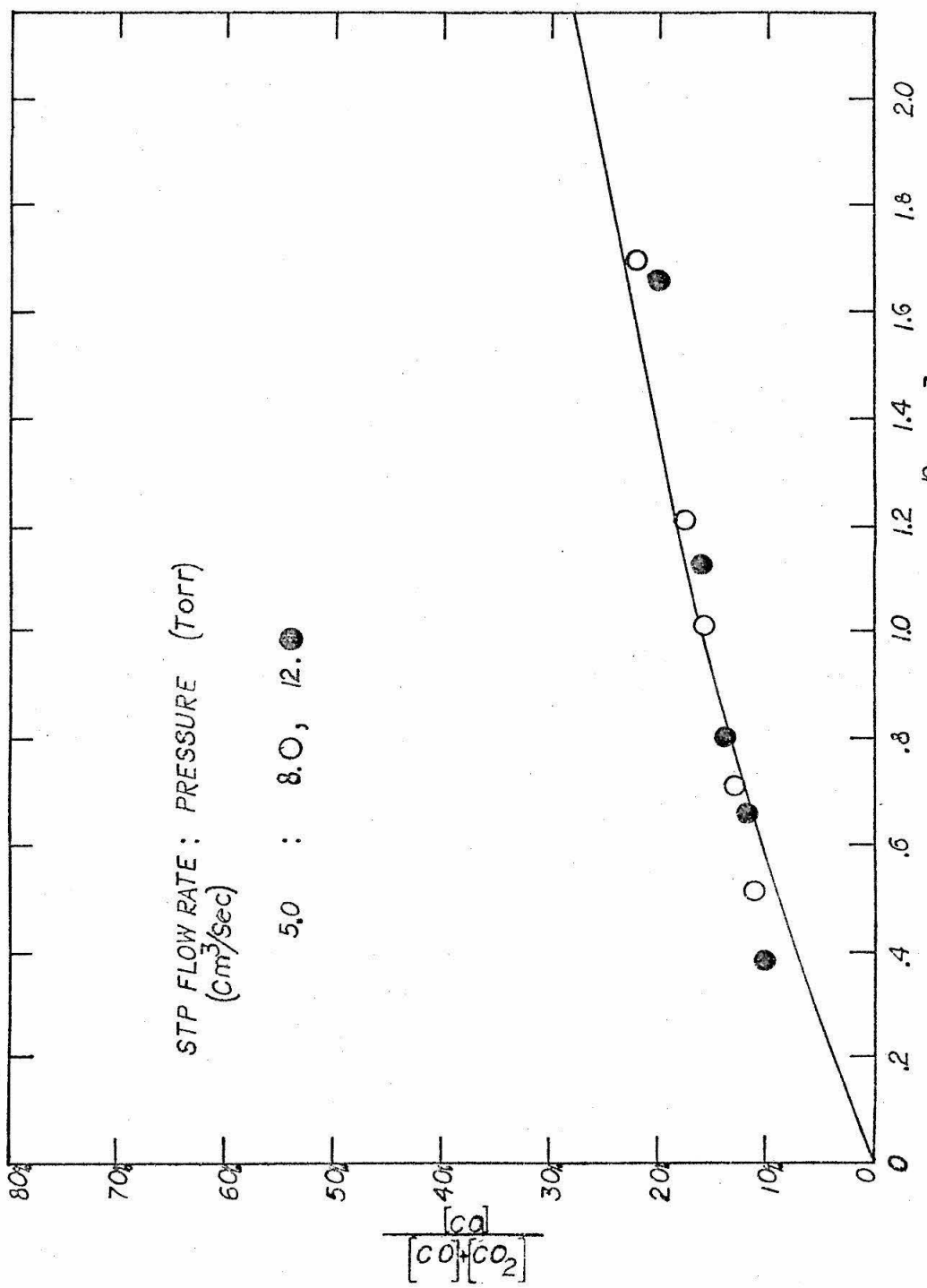

FIG. 8.10-CARBON DIOXIDE DISSOCIATION VS. ELECTRON DENSITY $(CO_2 ; N_2 : He : H_2O) = (1:3:16:1.1)$

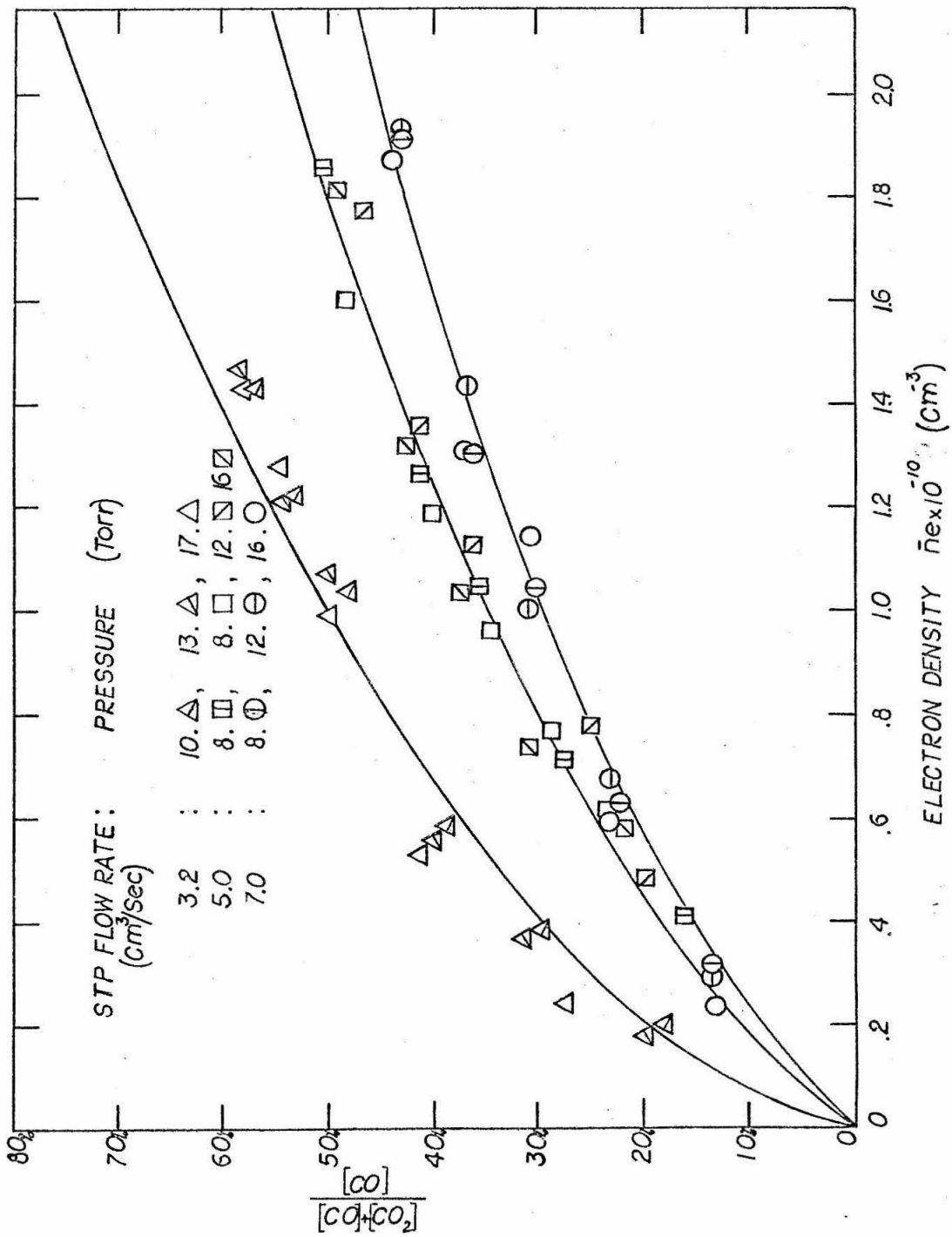

FIG 8.11 CARBON DIOXIDE DISSOCIATION VS. ELECTRON DENSITY $(CO_2:N_2:He) = (1:2:10)$

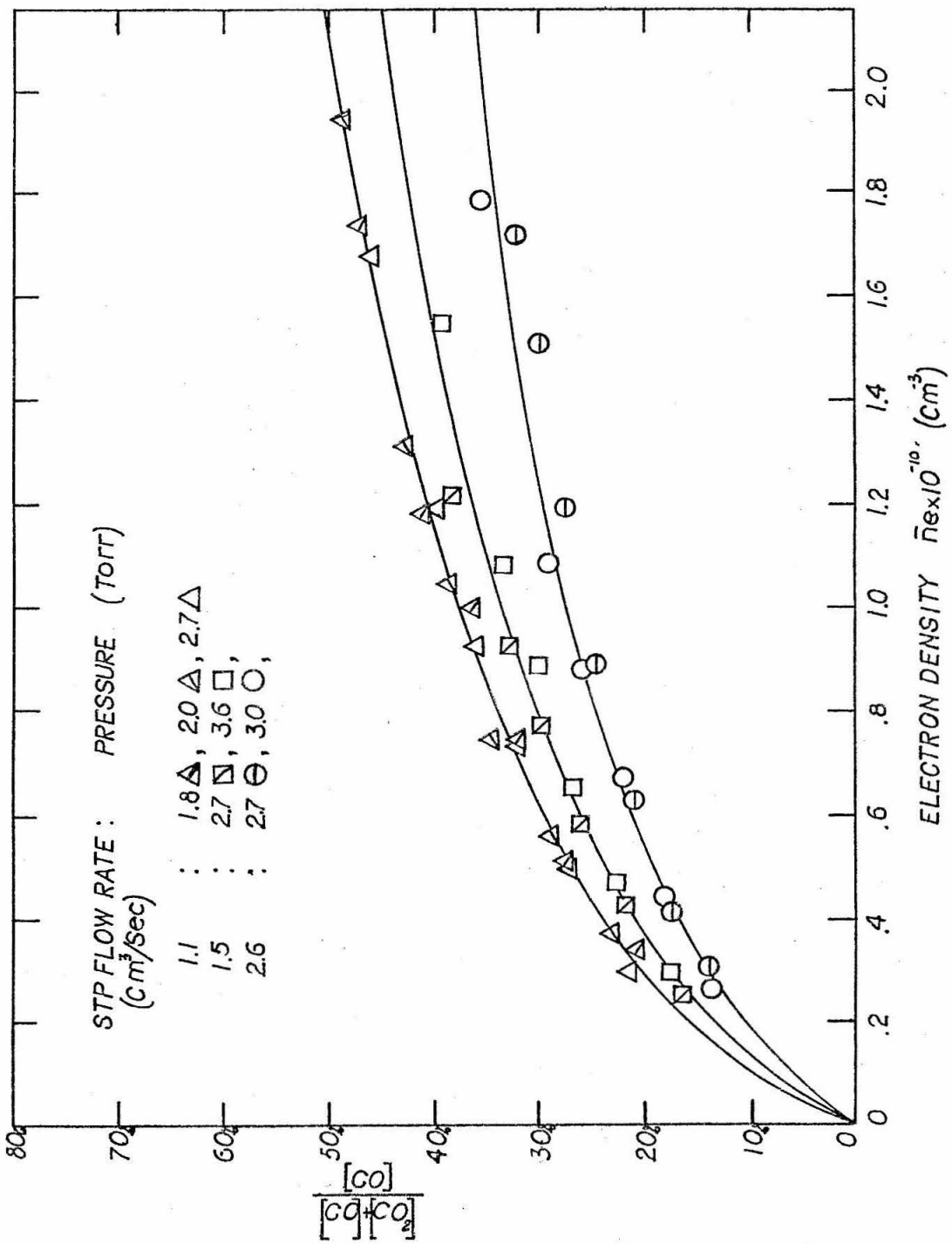

FIG. 8.12 - CARBON DIOXIDE DISSOCIATION VS. ELECTRON DENSITY. CO_2-N_2-He (1:2:0)

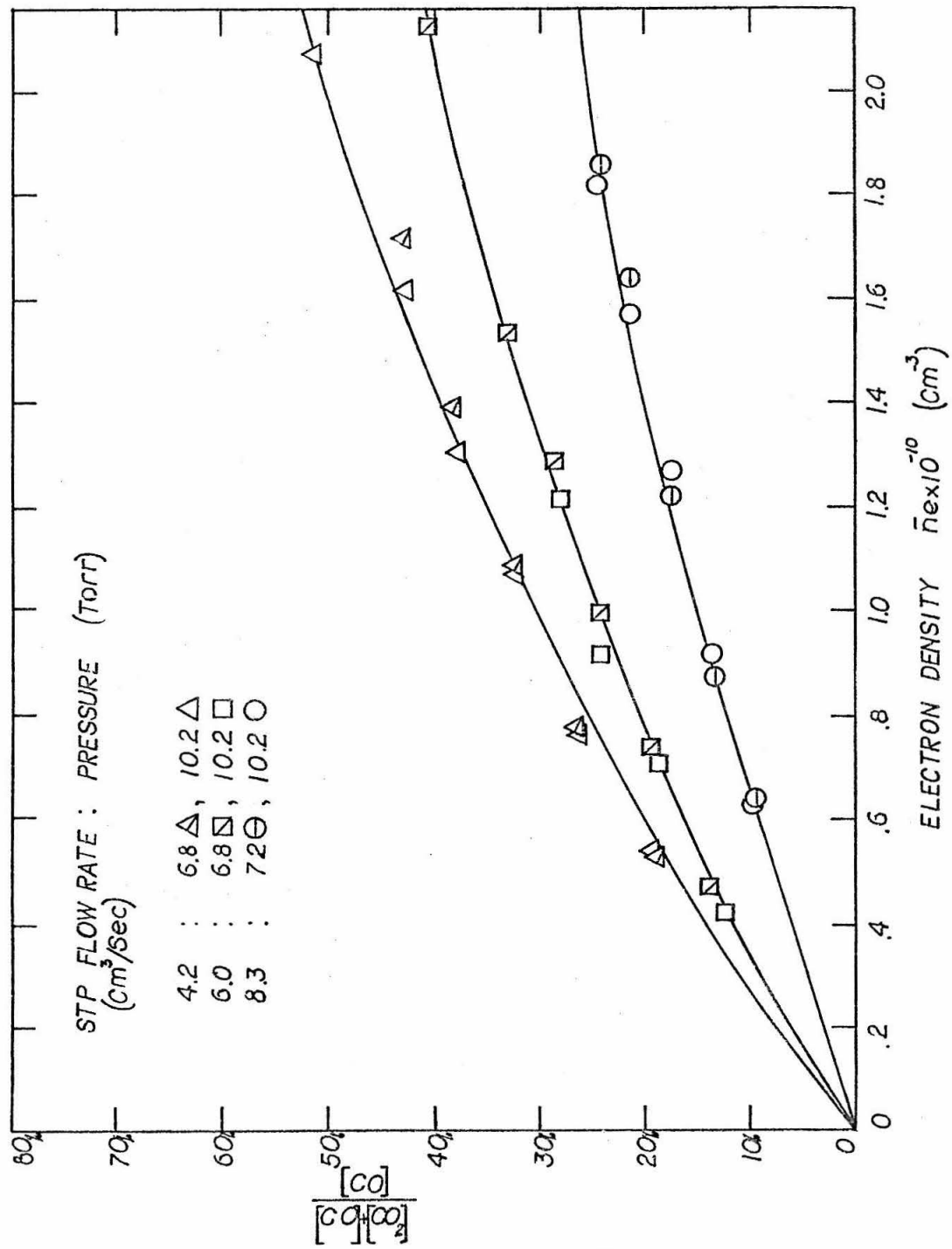

FIG 8.13 CARBON DIOXIDE DISSOCIATION VS. ELECTRON DENSITY (CO_2:He)=(1:10)

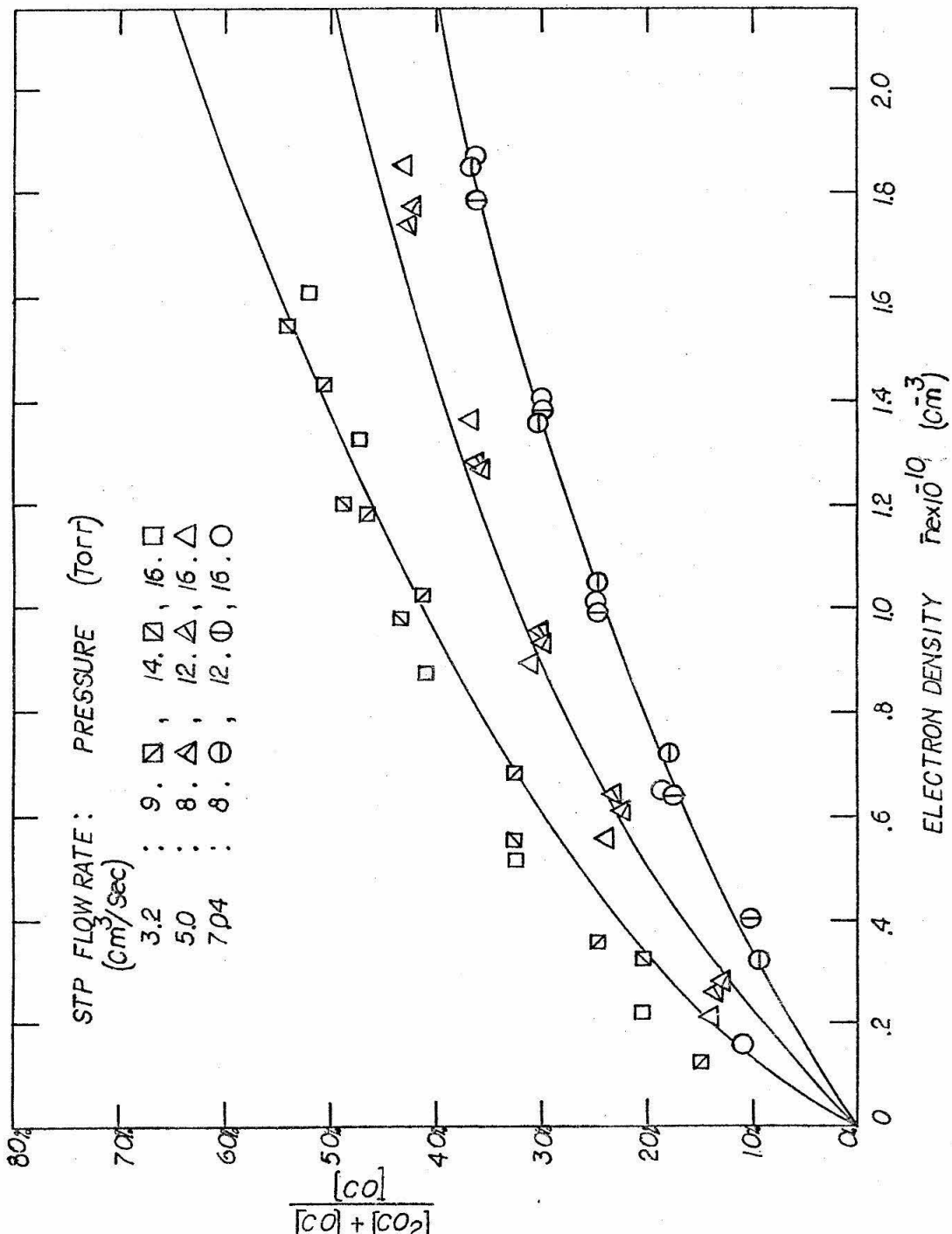

FIG 8.14 CARBON DIOXIDE DISSOCIATION VS. ELECTRON DENSITY $(CO_2 : N_2 : He) = (2:3:15)$

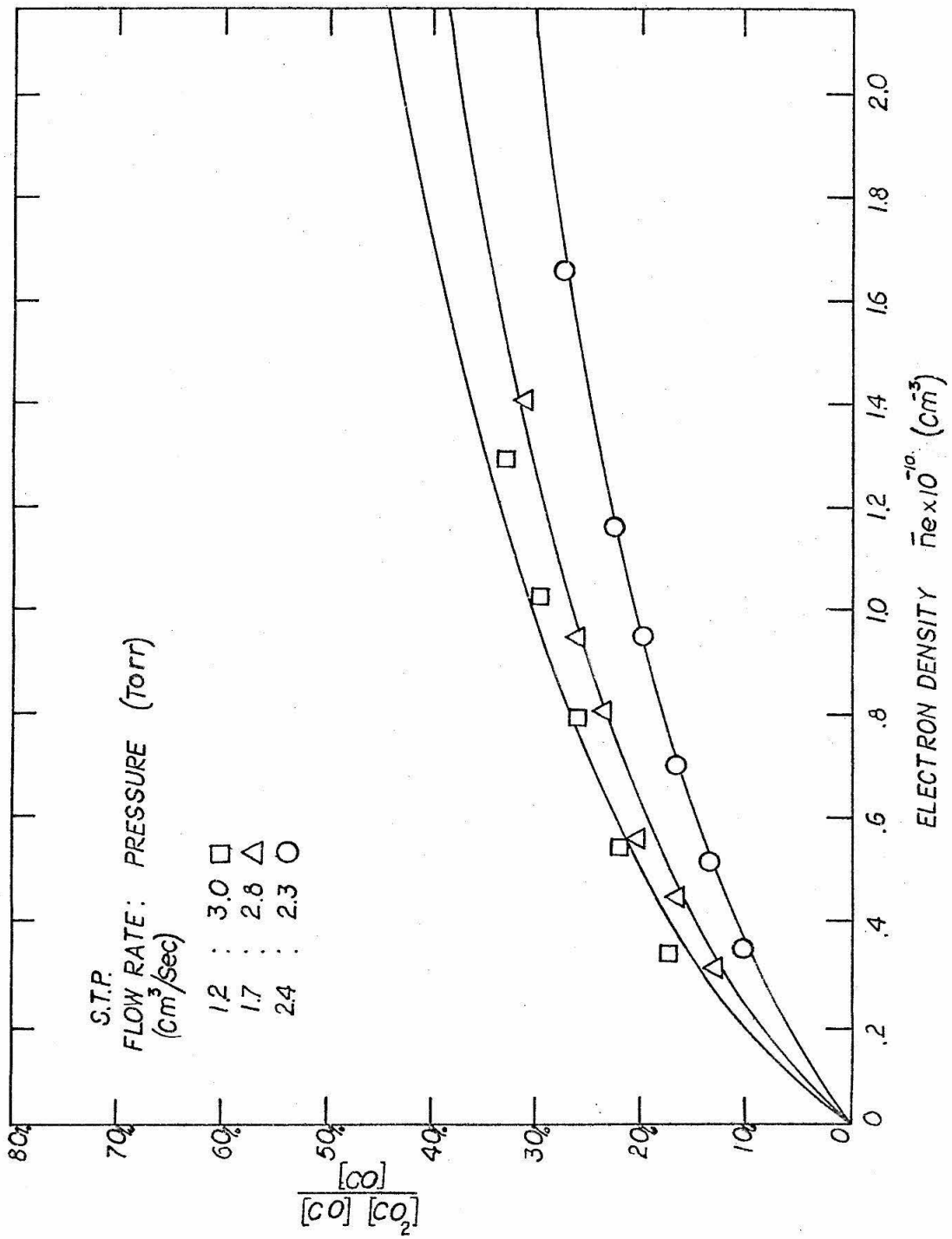

FIG.8.15 CARBON DIOXIDE DISSOCIATION VS. ELECTRON DENSITY $(CO_2 : N) = (2:3)$

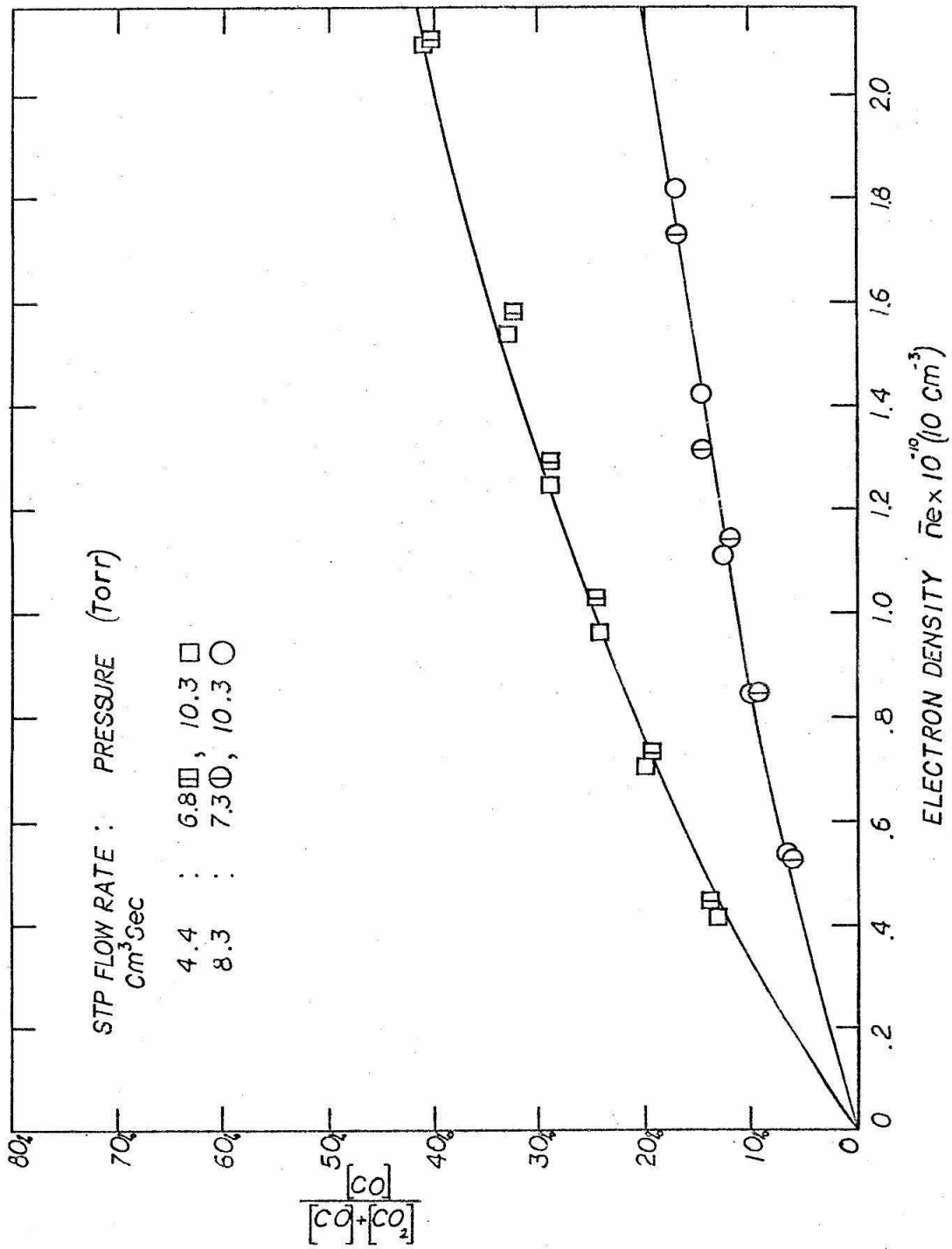

FIG. 8.16 CARBON DIOXIDE DISSOCIATION VS. ELECTRON DENSITY (CO_2:HE) = (2:15)

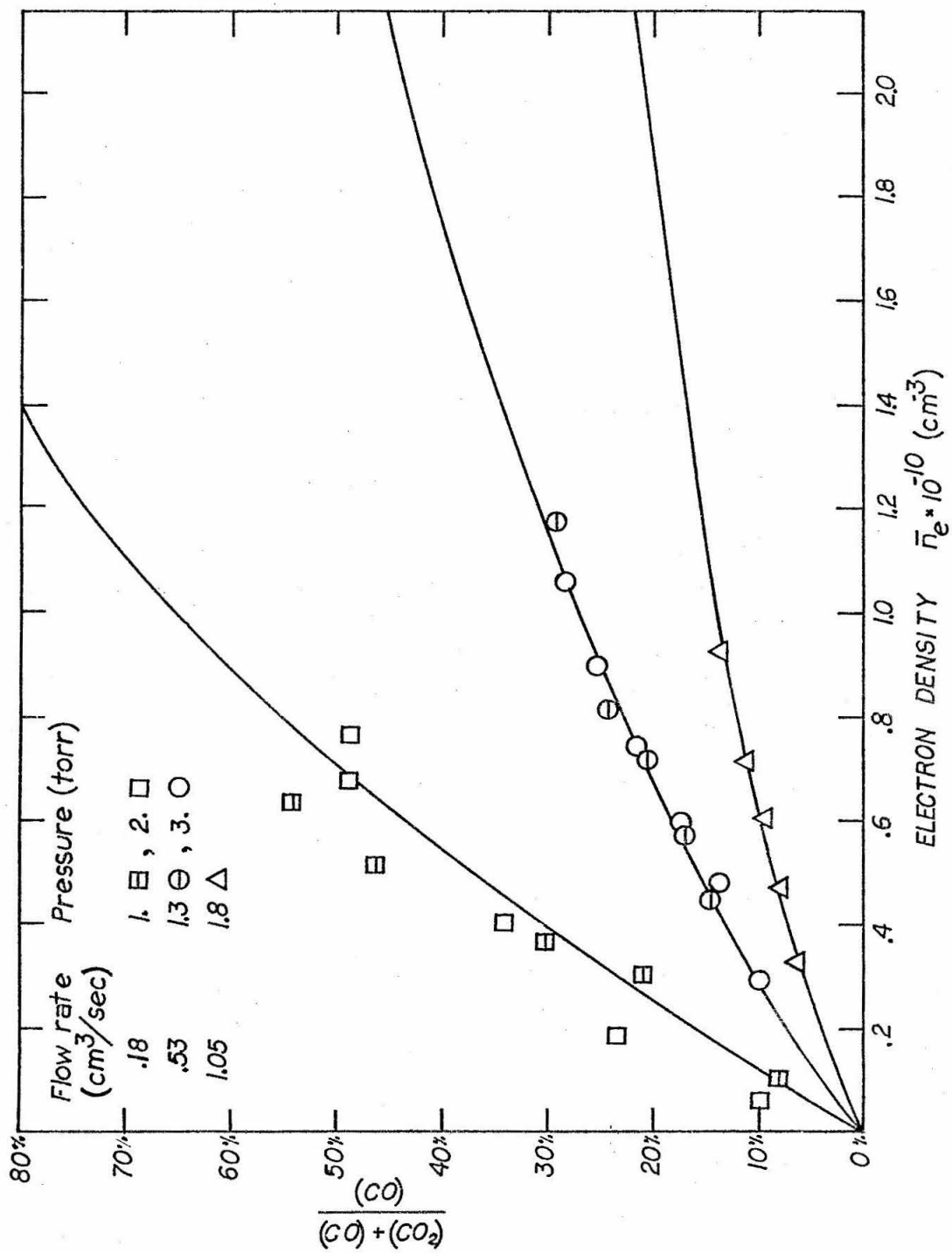

FIG 8.17 CARBON DIOXIDE DISSOCIATION VS. ELECTRON DENSITY. PURE CO_2.

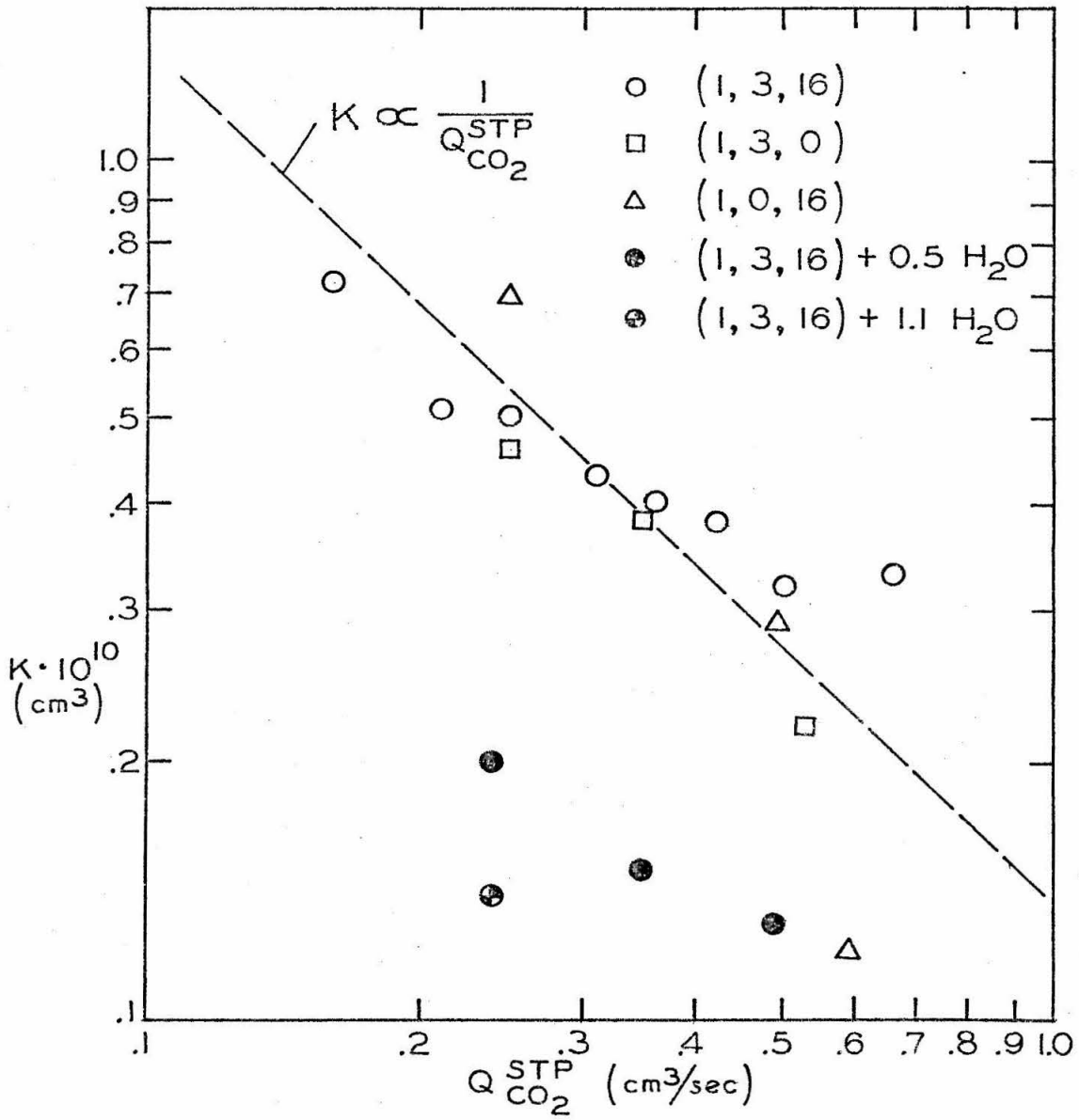

Fig. 8.18 K as function of CO_2 partial flow rate

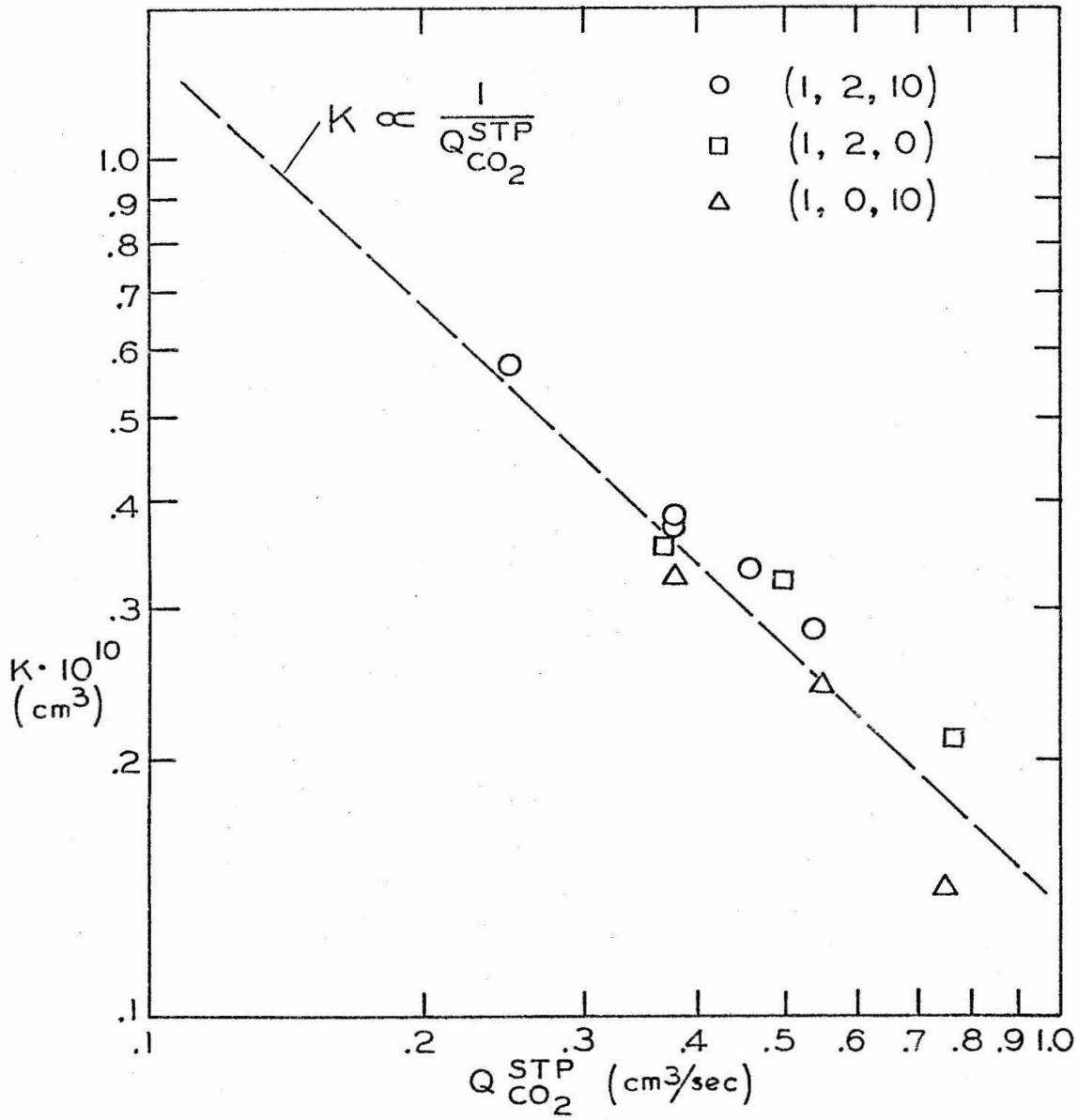

Fig. 8.19 K as function of CO_2 partial flow rate

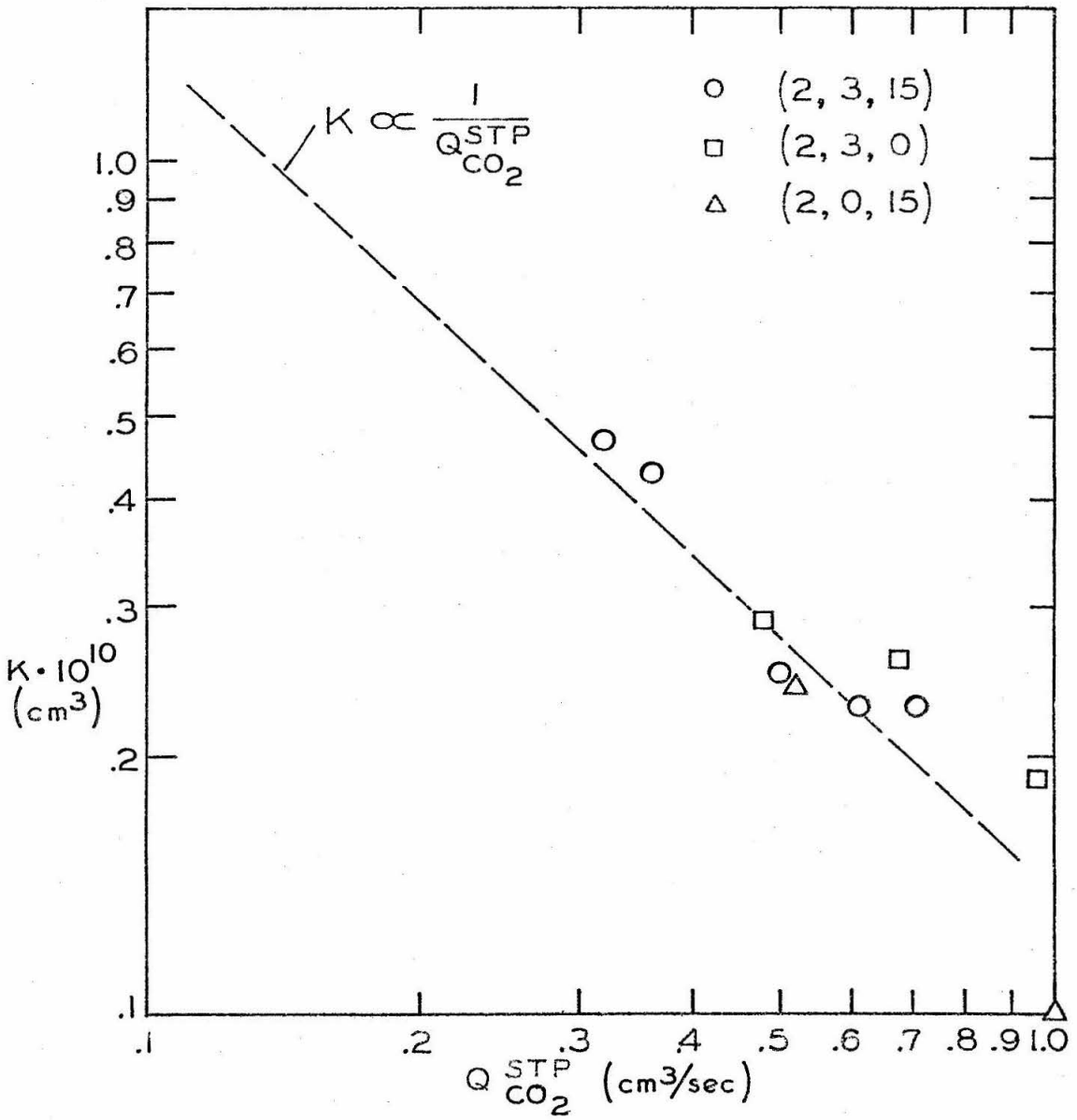

Fig. 8.20 K as function of CO_2 partial flow rate

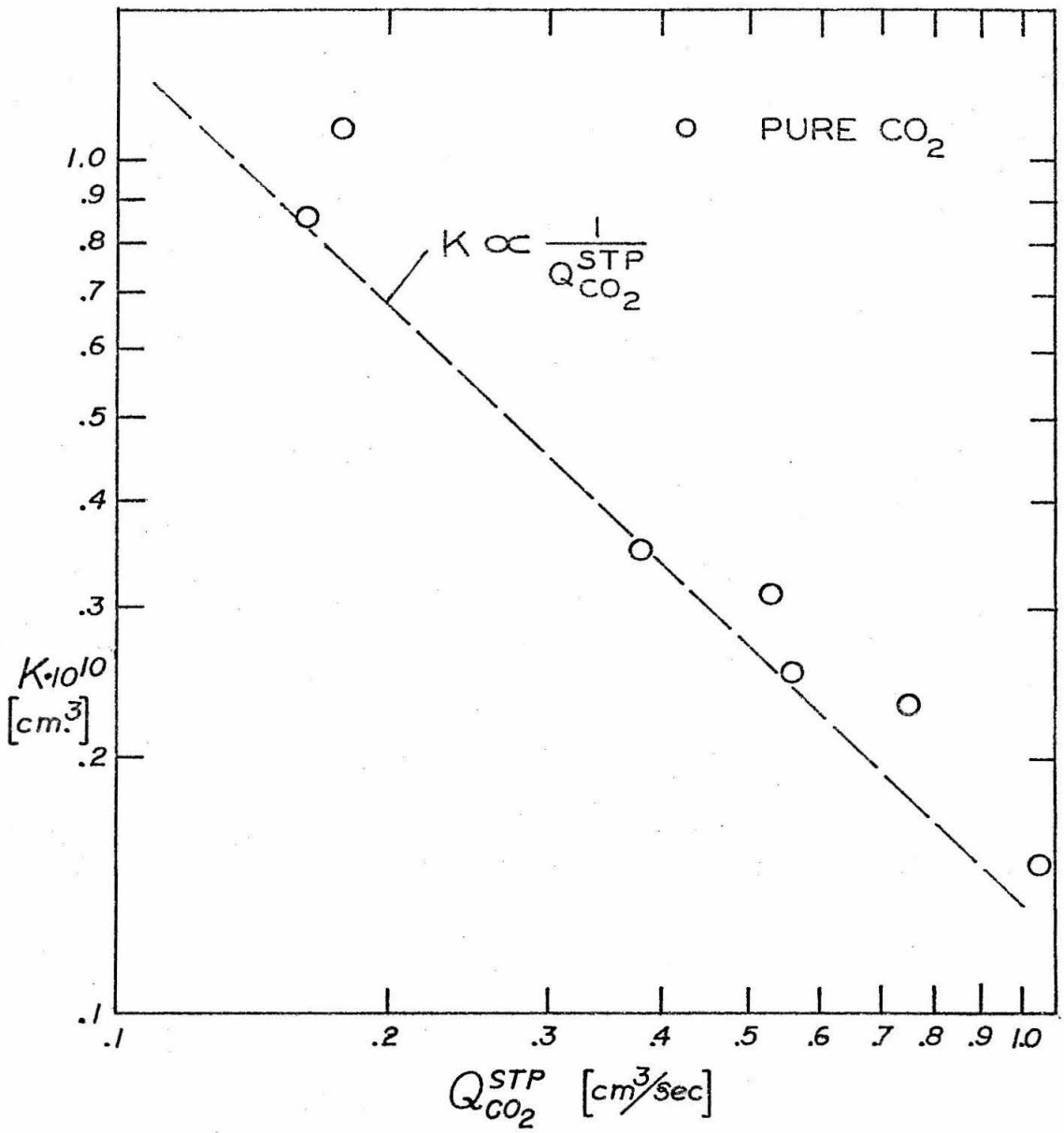

Fig. 8.21 K as function of CO_2 partial flow rate

Chapter IX

CALCULATIONS OF THE DISSOCIATION OF CARBON DIOXIDE BASED ON THERMODYNAMIC EQUILIBRIUM

Calculations of the degree of dissociation in the CO_2 laser discharge are discussed. The model used is constructed to make use of an existing computer program, based on the minimization of free energy to define chemical equilibrium calculations. No allowance is made for nonequilibrium conditions other than to account for the influence of the electric field on the electrons. This is represented as an initial energy (heat) input to the system. The energy input is calculated from the electrical power dissipated by the discharge.

As a first approximation this calculation yields reasonable results. In particular the weak dependence of dissociation on the pressure of the mixture observed in the experiments is predicted. No information on the vibrational level population of the molecules is obtained.

9.1 Calculations for Chemical Equilibrium

Chemical reactions occurring in mixtures of reacting substances lead ultimately to the establishment of a state of equilibrium in which the quantity of each substance taking part in the reaction remains constant. This case of thermodynamic equilibrium is called chemical equilibrium. The subject of thermodynamics, as applied to a chemical reaction, is the study of chemical equilibrium only and not to the reactions leading to it.

It is essential to note that the state of chemical equilibrium does not depend upon the way (i.e., under what conditions) the reaction occurred; it depends only on the condition of the mixture of the reagents in the actual state of chemical equilibrium. Hence to deduce conditions for chemical equilibrium, one can make any assumptions at all as to the way the reaction took place.

The condition of chemical equilibrium, given an initial mixture, may be stated in terms of any of several thermodynamic functions such as the minimizations of the Gibbs or Helmholtz free energy or the maximization of entropy. If one wishes to use temperature and pressure to characterize a thermodynamic state, the Gibbs free energy is most easily minimized, inasmuch as temperature and pressure are its natural variables. Similarly, the Helmholtz free energy is most easily minimized if the thermodynamic state is characterized by temperature and volume or density.

9.1.1 Minimization of the Gibbs Free Energy. Enthalpy and Pressure Fixed

For a mixture of n species the Gibbs free energy per unit mass of mixture is given by

$$g = \sum_{j=1}^{n} \mu_j n_j \tag{9.1}$$

where the chemical potential per mole of species j is defined to be

$$\mu_j = \mu_j\left(\frac{n_j}{n}, P, T\right) = \left(\frac{\partial g}{\partial n_j}\right)_{T,P,n_{i\neq j}} \tag{9.2}$$

and n_j is the molar concentration of compound j.

The minimization of the free energy g, equation (9.1), will determine the equilibrium composition of the mixture. This minimization is subject to the following constraints:

a) Conservation of mass

$$\sum_{j=1}^{n} a_{ij} n_j = b_i^o \qquad i=1,\cdots,\ell \tag{9.3}$$

where a_{ij} is the number of i atoms in the j molecule, and b_i^o is the initial number of i atoms in the reactants mixture (ℓ different atoms).

b) Pressure

The pressure is specified and constant.

c) Enthalpy of the system

The total enthalpy of the system is conserved:

$$h_o = \sum_{j=1}^{n} n_j h_j \tag{9.4}$$

With the above information, it is possible in theory to calculate the composition, the values of the n_j, when equilibrium is reached.

A complete review of this type of problem can be found in Ref. 9.1.

9.1.2 Chemical Equilibrium Calculations (CEC72) Program

Considerable numerical calculations are necessary to obtain equilibrium compositions for complex chemical systems. This has resulted in a number of digital computer programs to do the calculations. References 9.2 and 9.3 contain discussions of the mathematical

procedures and give references to programs.

One such program has been used to carry out the calculations discussed in this section. It was written at NASA Lewis Research Center and is designated CEC72. A complete description of the program and its background can be found in Ref. 9.4.

The program calculates the equilibrium compositions by minimizing the appropriate thermodynamic potential. It assumes all gases to be ideal and that interaction among phases may be neglected. Condensed species are assumed to occupy a negligible volume and exert negligible pressure compared with the gaseous species.

The program (CEC72) is capable of obtaining equilibrium compositions for assigned thermodynamic states. The thermodynamic states may be specified by assigning of two thermodynamic state functions:

a) Temperature and pressure (TP);

b) Enthalpy and pressure (HP);

c) Entropy and pressure (SP);

d) Temperature and volume or density (TV);

e) Internal energy and volume or density (UV);

f) Entropy and volume or density (SV).

9.2 A Model for Calculations of Chemical Equilibrium in the CO_2 Laser

In order to make meaningful estimates of the equilibrium composition in the CO_2 laser discharge, it is necessary to take into consideration the effect the electrons will have on the final equilibrium composition. Although the concentration of electrons is very small compared with the other constituents of the plasma ($n_e \doteq 10^{-10} cm^{-3}$),

their average energy is fairly high (of the order of 1.5 eV).

The laser discharge temperature, T_g, is of the order of 300°K (Ref. 9.5) under conditions similar to those used here. Clearly the wide difference in the temperature of electrons and gases ($T_e/T_g \doteq 40$) prevents the consideration of the electrons as just another component of the mixture, as could be done in the problem of equilibrium ionization. Since the electrons are the main path of energy transfer in the discharge, the model used here replaces the electrons by a distributed heat source supplying the power P_{in} to the discharge:

$$P_{in} = I \cdot V = I \cdot E \cdot L \quad \text{(watts)} \tag{9.5}$$

Here I is the total current through the discharge tube, V is the voltage drop across the active region (volume where reactions take place), E(V/cm) is the electric field, and L is the length of the active region (65 cm).

The computer program CEC72 can calculate the equilibrium composition of a mixture if the following are given: initial mixture, temperature, pressure and enthalpy of the system. The last two items are kept fixed as constraints in the minimization of the Gibbs free energy (Sec. 9.1.2(f)).

The calculations carried out by the CEC72 program are equivalent to analyzing the composition of a mixture in a closed reaction box after an initial mixture and initial enthalpy (or energy input) are given and the pressure of the system is kept constant.

In the carbon dioxide laser it is necessary to calculate the enthalpy input from the electrical parameters and the flow rate of

gases. If the volume flow rate under STP conditions is known, $\dot{Q}_{STP}$, the molar flow rate can be easily calculated:

$$\dot{M} = \frac{\dot{Q}_{STP}(cm^3/sec)}{22400(cm^3/mole)} \text{ (moles/sec)} \qquad (9.6)$$

The enthalpy input per unit mole (energy/mole) is:

$$H_{in} = \frac{P_{in} \text{ (watts)}}{\dot{M} \text{ (moles/sec)}} \text{ (Joules/mole)} \qquad (9.7)$$

or using (9.5):

$$H_{in} = \frac{I(ma)\cdot E(V/cm)\cdot L(cm)\cdot 22.4}{\dot{Q}_{STP}\ (cm^3/sec)} \text{ (Joules/mole)} \qquad (9.8)$$

As an example, for I = 10 am, E = 35 V/cm, L = 65 cm and $\dot{Q}_{STP}$ = 3 cm^3/sec, equation (9.8) gives:

$$H_{in} = 1.7 \cdot 10^5 \text{(Joules/mole)} = 4\cdot 10^4 \text{ (calories/mole)}$$

The initial temperature of the mixture was taken to be 300°K in all cases. A comparison of our experimental conditions and results published by Laderman and Byron (Ref. 9.5) indicate that the temperature rise (from inlet to outlet port of discharge) is 40°K at most.

To facilitate comparison with the experimental results, it is convenient to rewrite equation (9.8) as

$$H_{in} = \left(\frac{E \times L \times 22.4}{Q}\right) \times I \qquad (9.9)$$

The calculation carried out by the program computes the fractional dissociation of carbon dioxide as a function of enthalpy input

(H_{in}) or, as expressed by equation (9.9), as a function of the current I. For a given composition and a given flow rate, the electric field does not vary much, therefore the quantity in parentheses in (9.9) has a constant value. In this case H_{in} becomes a linear function of the current I.

Of course this simple analysis does not take into consideration the fact that not all the energy being dissipated in the discharge goes into the dissociation process. Some of it is obviously lost to the walls of the tube, some more lost as sidelight emission and lasing. If all the losses are taken into consideration, the true dependence of H_{in} with current might look something like that sketched below:

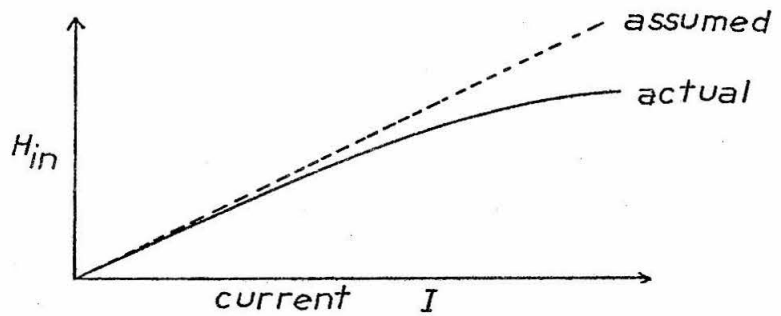

It is possible to modify equation (9.9) further to compensate for many of these effects, but since their exact nature is not well understood, it appeared that to do so would mean losing the basic simplicity of the model without gaining a better understanding of the problem.

9.3 Results of Calculations for Equilibrium

The initial mixtures examined were chosen to correspond to conditions studied in the dissociation experiments (Chapter VIII). All the mixtures were generated from three basic mixtures of CO_2-N_2-He:

	(1,3,16)	Fig. 9.1
(a)	(1,3,0)	Fig. 9.2
	(1,0,16)	Fig. 9.3
	(2,3,15)	Fig. 9.5
(b)	(2,3,0)	Fig. 9.6
	(2,0,15)	Fig. 9.7
	(1,2,10)	Fig. 9.8
(c)	(1,2,0)	Fig. 9.9
	(1,0,10)	Fig. 9.10

The results for pure CO_2 are shown in Fig. 9.11. The effect of water in a mixture is shown in Fig. 9.4. In each case a set of initial enthalpies were assigned. The C.E.C. program would then compute the resulting equilibrium composition, in particular the dissociation of carbon dioxide. Thus, for each initial mixture a curve, dissociation of carbon dioxide vs enthalpy input, could be constructed.

In order to make a prediction or a comparison with experimental results, it is necessary to transform the variable enthalpy input (H_{in}) into a more easily measurable quantity. With the aid of equation (9.9) and selection of the appropriate experimental conditions, the curve of dissociation vs enthalpy can be transformed into curves of dissociation vs current.

It was our purpose to compare the experimentally measured values of dissociation vs those calculated for equilibrium. Thus, the electric field E, needed in equation (9.9), was calculated from experimental data using equation (7.13) for similar initial conditions. The values of the field, according to these estimates, varied from 21 to 44 volts/cm. The length of the tube L was 65 cm, in all cases.

Figures 9.1 to 9.11 show the results of the calculations. Also plotted are the experimentally measured dissociation for the same initial conditions. Both curves are plotted as functions of the current through the laser tube. In one case, Figure 9.4, two initial conditions are plotted: the mixture (1,3,16) with and without water added. In all cases the enthalpy input to the mixture (needed by the CEC72 program) was calculated as a function of the current, according to equation (9.9).

As previously mentioned, the chemical equilibrium model is only an approximation to the real system, and as such it can obviously give only approximate results. In general they agree qualitatively with the experiments in the following respects:

(1) For a given mass (S.T.P. volume) flow rate the dissociation is very weakly dependent on the pressure of the mixture. For example, for the mixture (1,3,16) and $7 \times 10^4 K_{joule}/K_g$-mole enthalpy input the following results are calculated:

P (torr)	8	10	12	16
% dissociation	50.9	49.6	48.5	46.8

(2) As observed experimentally, the results of the calculations indicate that very small amounts of species other than carbon monoxide and oxygen are formed (less than .05% in most instances).

(3) Qualitatively, the curves calculated with the equilibrium model compared fairly well with curves obtained experimentally. The

calculated curves show a higher degree of dissociation in Figure 9.1 than in Figure 9.2. The same relationship holds true for the measured curves. Figure 9.3, however, which completes the set of mixtures (a) listed above, shows a lower calculated dissociation curve than the other gases of the set, contrary to measured results The curves for the mixture set (b) shown in Figures 9.5, 9.6 and 9.7, agree qualitatively in their degree of dissociation both calculated and measured. The degree of dissociation is higher in Figure 9.5 than in Figure 9.7, and Figure 9.7 shows higher dissociation than Figure 9.6. A similar pattern is found with the third set of curves for the set of mixtures (c), shown in Figures 9.8, 9.9 and 9.10. The degree of dissociation, calculated and measured, is higher in Figure 9.8 than in Figure 9.10, and this in turn is higher than that shown in Figure 9.9.

In conclusion, in the calculations the mixtures of three elements $CO_2/N_2/He$ showed a higher degree of dissociation than the same mixture with either helium or nitrogen removed. Mixtures containing only CO_2/He had a higher degree of dissociation than those containing CO_2/N_2, with the exception of the mixtures (1,3,0), (1,0,16) which showed the opposite.

(4) As can be seen in Figure 9.4, the role of water vapor in inhibiting the dissociation of carbon dioxide molecules is qualitatively predicted. The calculation predicts a 25% less dissociation when water is present. The experimental results indicate roughly a 50% reduction.

9.3.1 Some Comments on the Discrepancies with the Experiments

The results of the equilibrium calculations show marked departures from the experimental results at both high and low currents (enthalpy input).

At high current values, it is believed that less and less energy goes into the system as the current is increased further. The fact that the actual laser is not a closed system and can exchange energy with the exterior, gives a different dependence of the enthalpy input with current than that shown in equation (9.9). The consequence of this effect would be to expand the dissociation curve calculated in the higher current region (see Fig. 9.1, for example), moving it closer to the measured curve. The curve would remain unchanged in the lower current region (left half). For example, if at 8 ma only half of the energy dissipated goes into the dissociation process, then the real enthalpy input is approximately $.65 \times 10^5$ (K_{joule}/K_g-mole) and not the 1.3×10^5 shown. The corresponding calculated dissociation would also be smaller (40% instead of the almost 100% shown).

At the low current region the departure from the experiments is hard to account for within the equilibrium model. The microscopic nature of the dissociation, the electrons with their high energies and collision cross-sections, evidently dominate the purely thermal effects assumed under thermodynamic equilibrium. That is, the energy dissipated in the discharge is not distributed according to the principle of equipartition of energy. Rather, a significantly greater proportion is consumed in dissociation of the carbon dioxide molecules. It has

been found in all cases that the experimentally observed dissociation is enormously greater than that calculated with the model of thermodynamic equilibrium.

References

9.1 K. Denbigh, The Principles of Chemical Equilibrium, 3rd Edition (Cambridge University Press, 1971).

9.2 F. J. Zeleznik and S. Gordon, "Calculation of Complex Chemical Equilibria", Ind. Eng. Chem. 60, 27 (1968).

9.3 F. van Zeggeren, and S. H. Storey, The Computation of Chemical Equilibria (Cambridge University Press, 1970).

9.4 S. Gordon and B. J. McBride, "Computer Program for Calculation of Complex Chemical Equilibrium Compositions, Rocket Performance, Incident and Reflected Shocks, and Chapman-Jouguet Detonations", NASA SP-273 (1971).

9.5 A. J. Laderman and S. R. Byron, "Temperature Rise and Radial Profiles in CO_2 Lasers", J. Appl. Phys. 42, 3138 (1971).

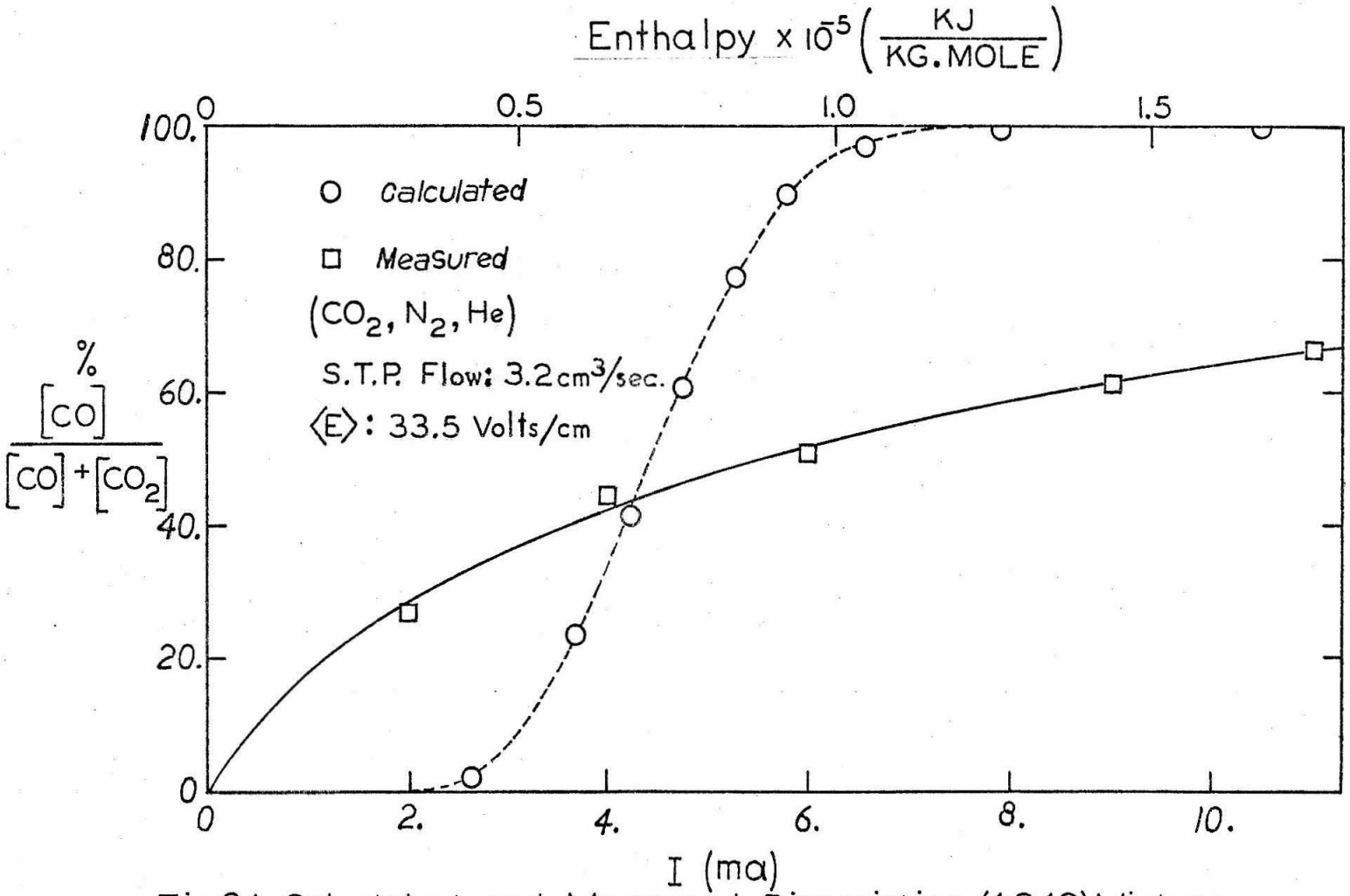

Fig.9.1- Calculated and Measured Dissociation.(1:3:16) Mixture.

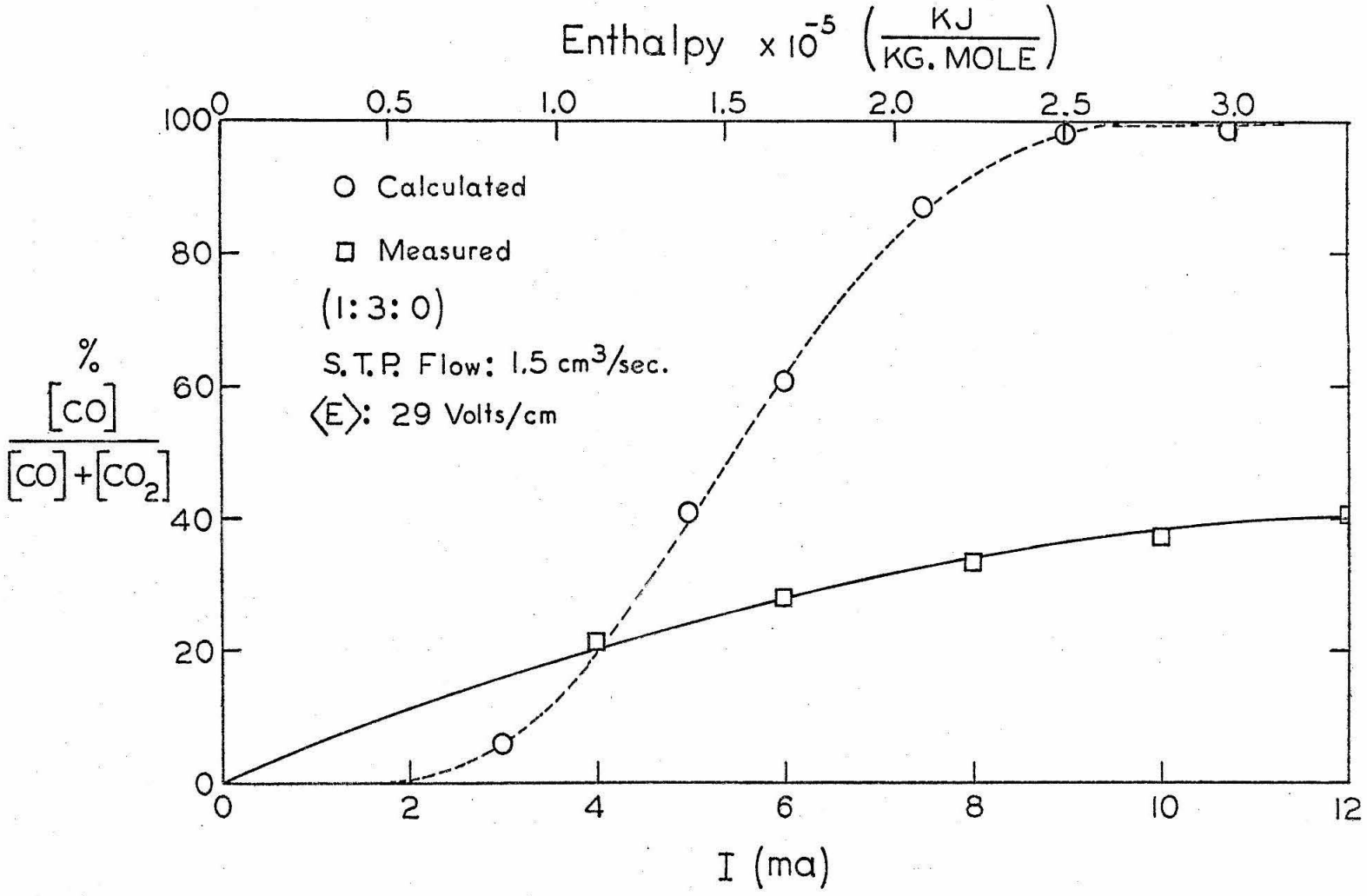

Fig 9.2: Calculated and Measured Dissociation.

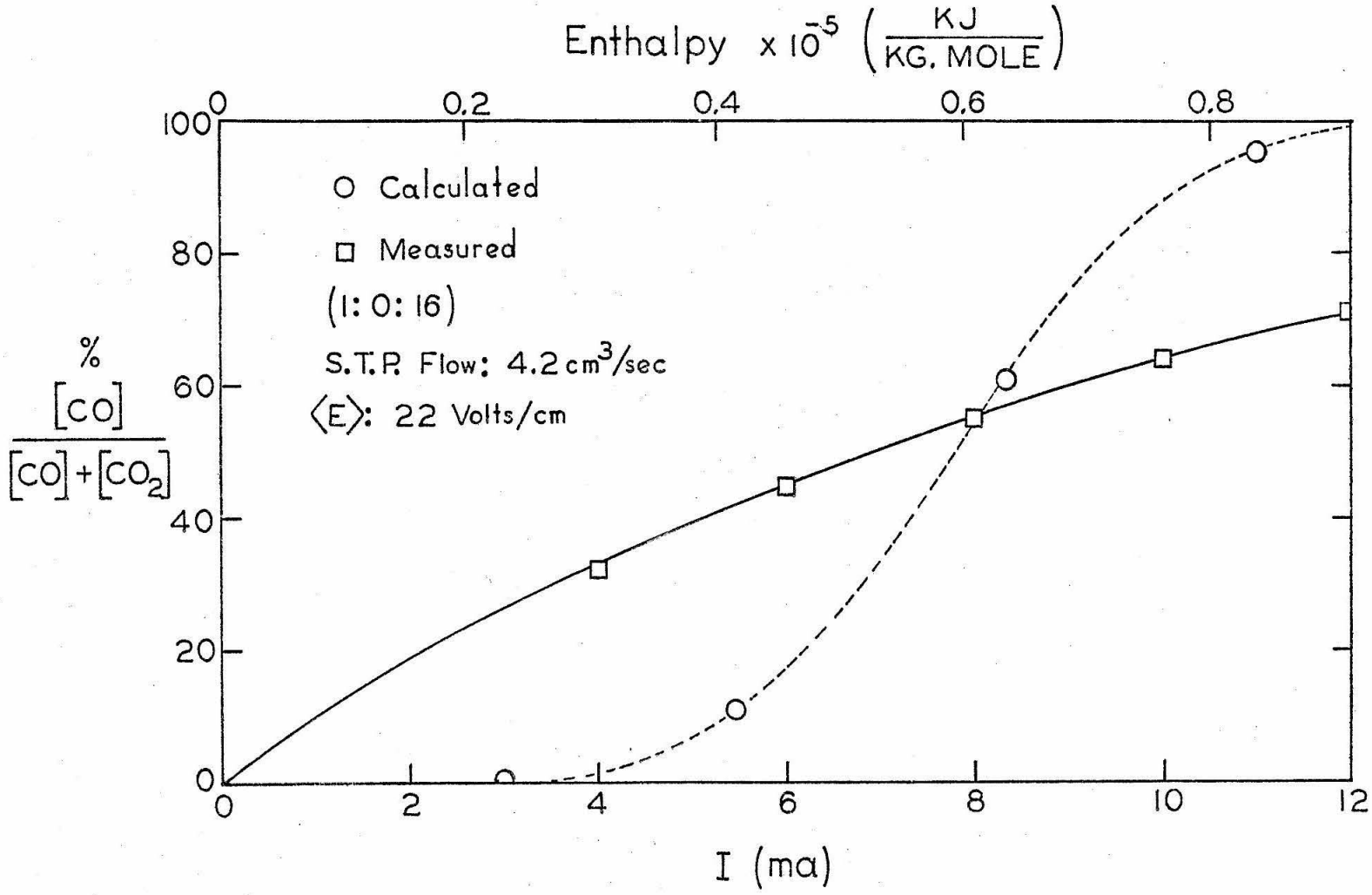

Fig. 9.3 ; Calculated and measured Dissociation.

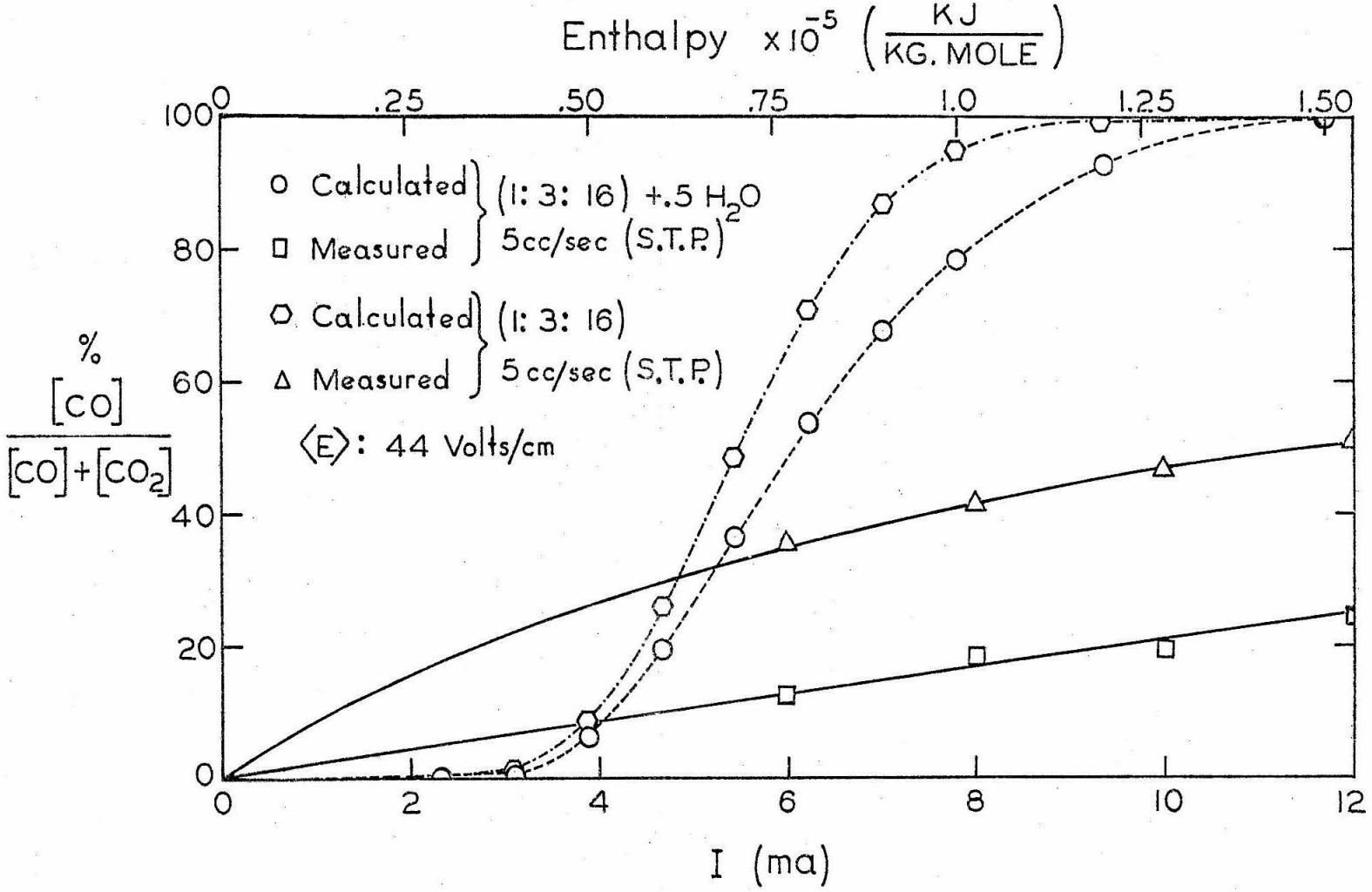

Fig. 9.4 : Calculated and Measured Dissociation.

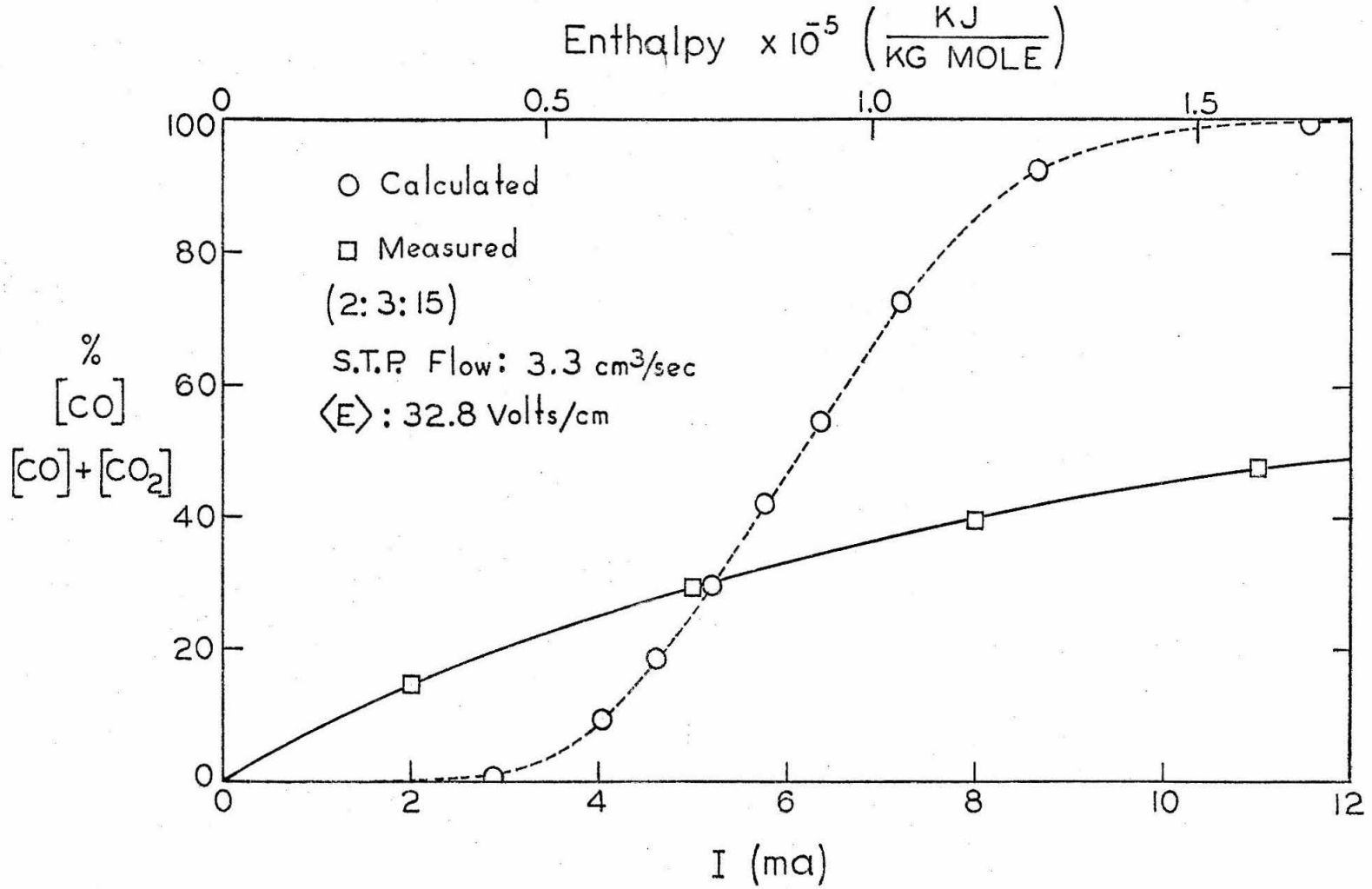

Fig. 9.5 : Calculated and Measured Dissociation.

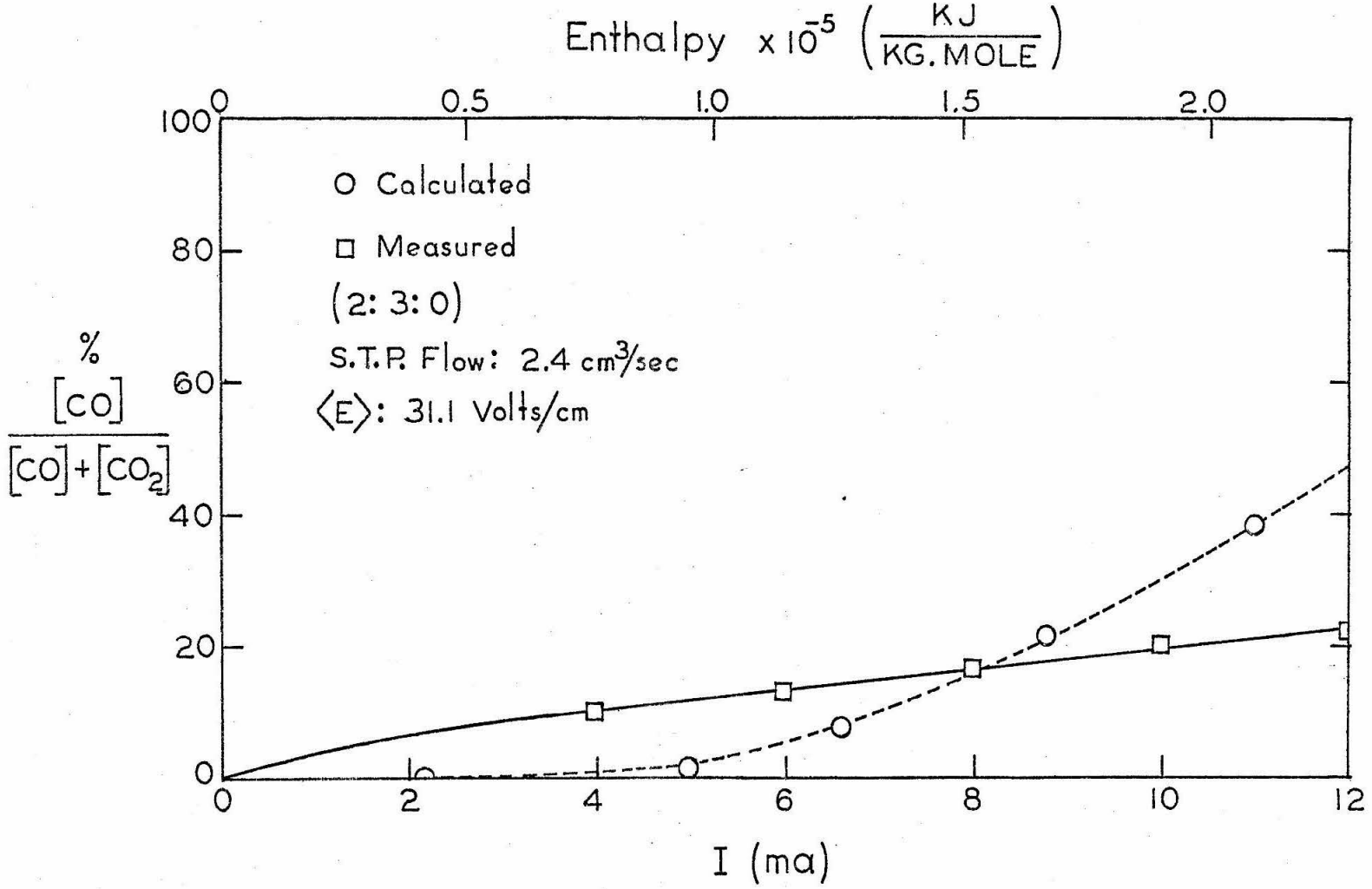

Fig. 9.6 : Calculated and Measured Dissociation.

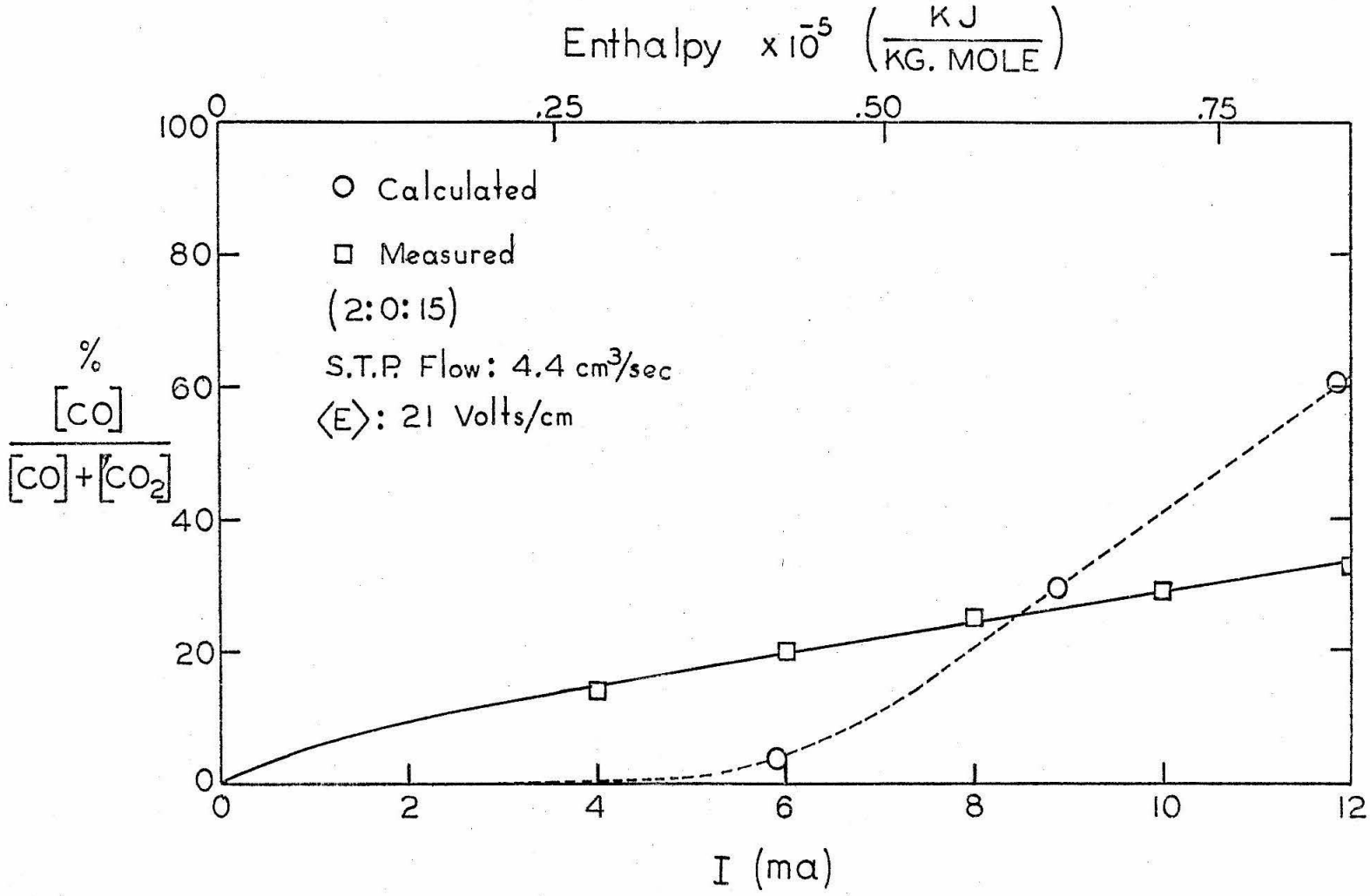

Fig. 9.7 : Calculated and Measured Dissociation.

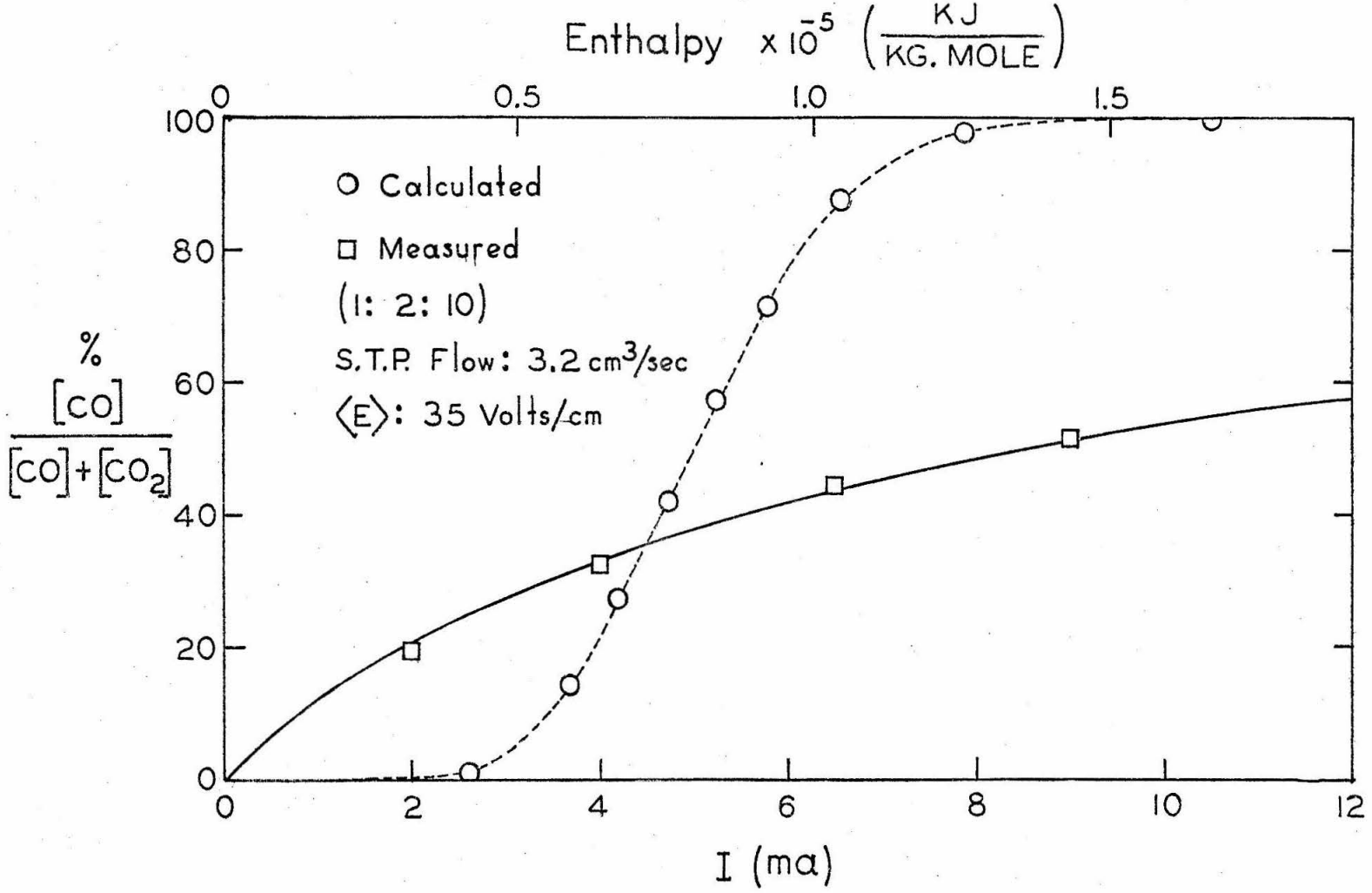

Fig. 9.8 : Calculated and Measured Dissociation.

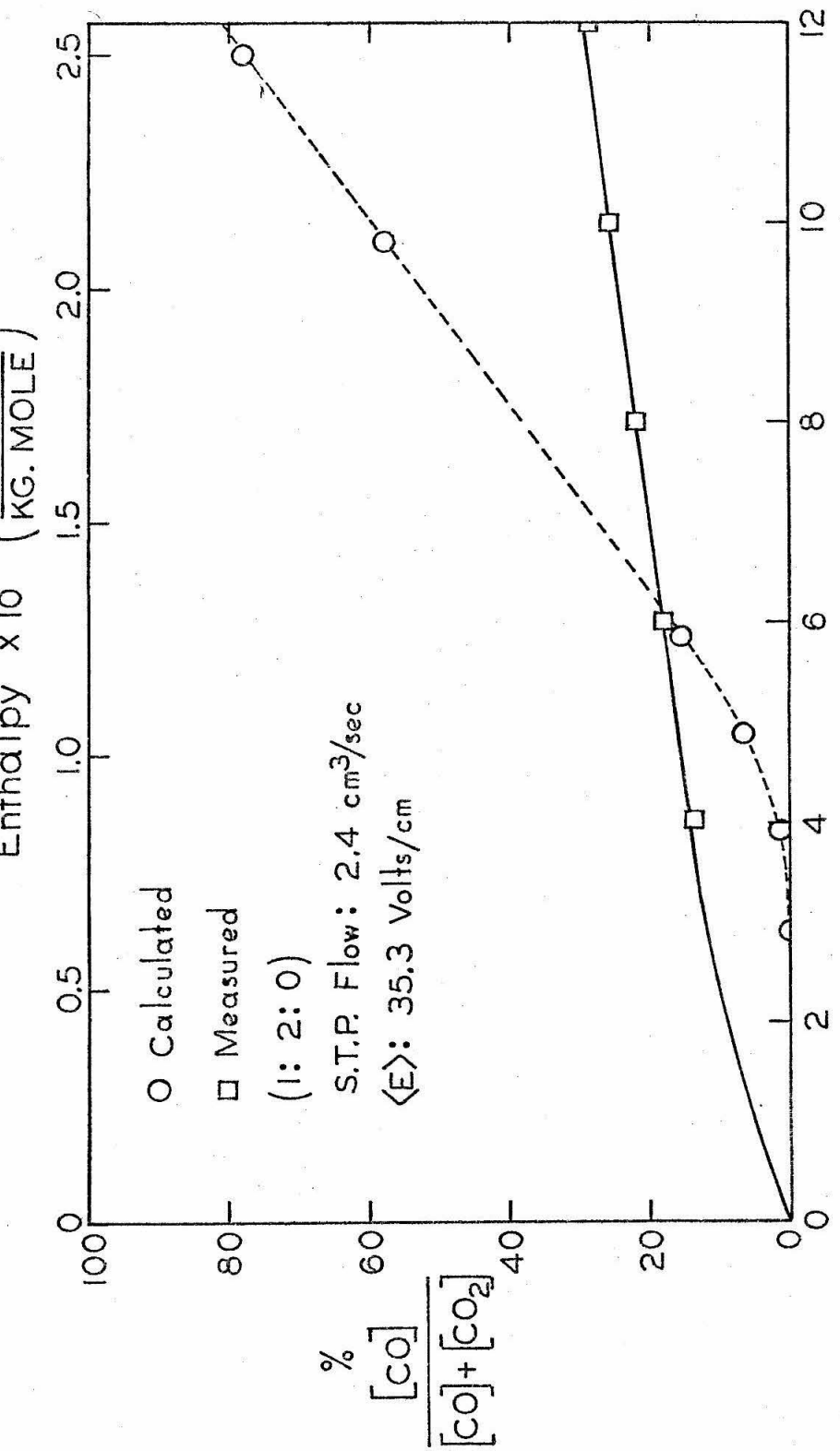

Fig. 9.9 : Calculated and Measured Dissociation .

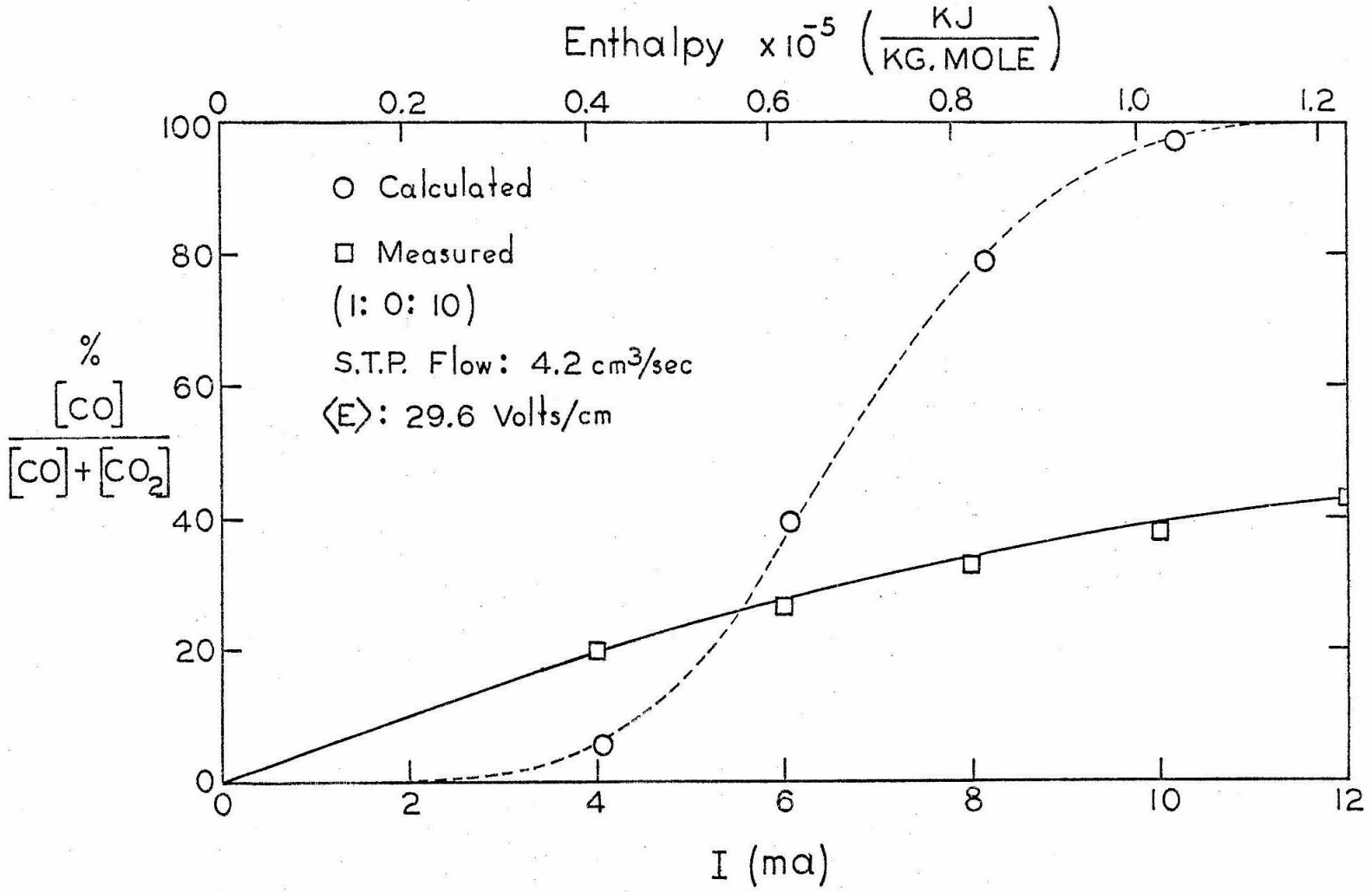

Fig. 9. 10 : Calculated and Measured Dissociation.

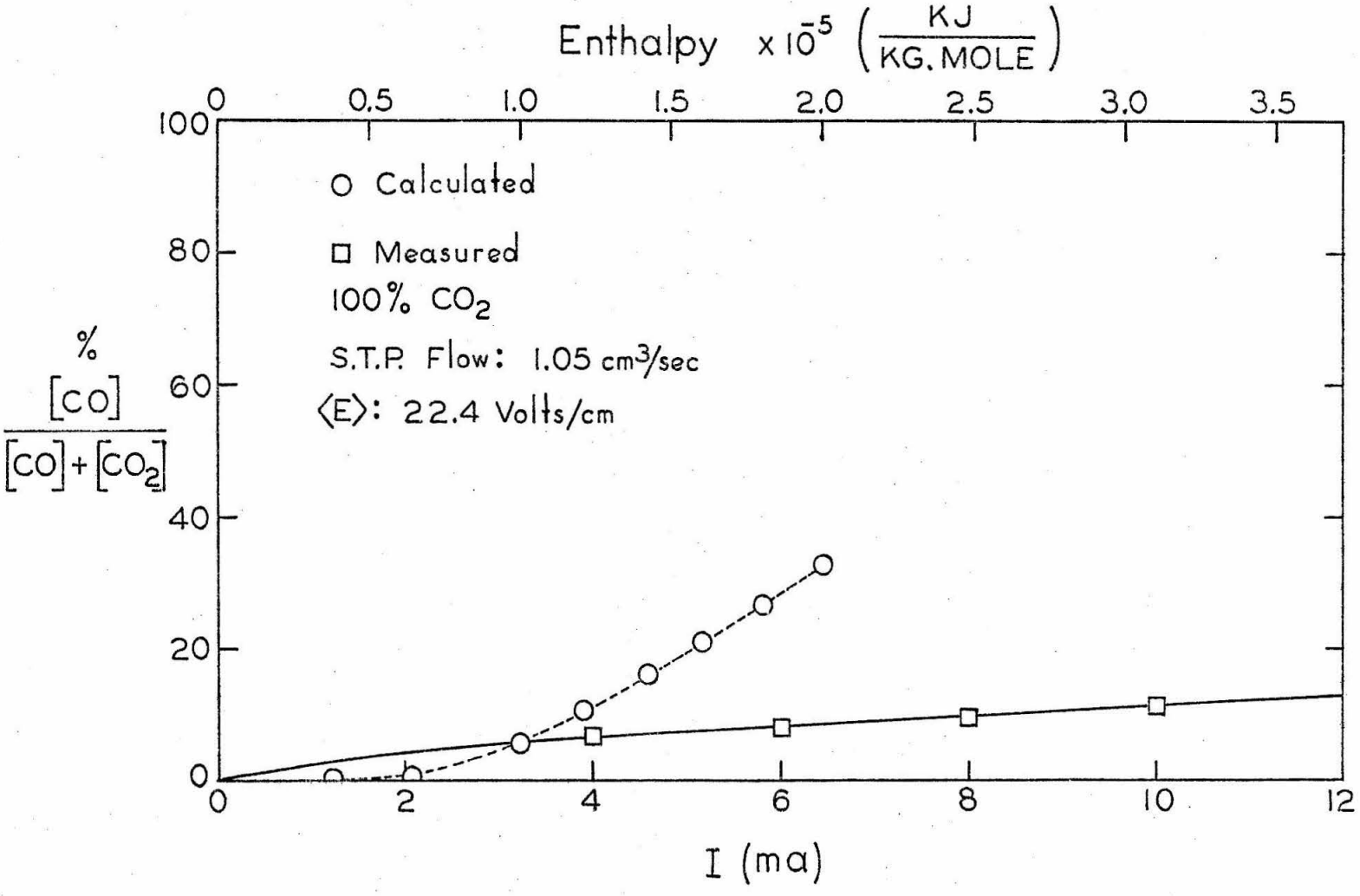

Fig. 9.11 : Calculated and Measured Dissociation.

Chapter X

SIMPLE KINETIC MODEL

In the present chapter a simple kinetic model will be developed. It will account for the major trends observed in the experimental results described in Chapter VIII and also by other authors.

Recapitulating, it was found that the dissociation of carbon dioxide molecules as function of average electron density was independent of the total laser pressure (for the range studied, 8 to 17 torr). It depended only on the initial composition of the mixture and the total mass flow rate (equivalent to the volume flow rate at standard conditions STP).

10.1 Plasma Kinetic Model

The number of reactions that must be considered in a model of the glow discharge in carbon dioxide lasers can be reduced considerably in the case of pulsed and flowing systems. In a flowing laser discharge many of the reactions can be eliminated due to the short residence time ($\tau \doteq .01 - .33$ sec) ; the dissociated or previously excited molecules do not have time to interact further with the electrons. Corbin and Corrigan (Ref. 10.1) and Buser and Sullivan (Ref. 10.2), after studying low pressure carbon dioxide discharges, concluded that the initial process responsible for the dissociation was given by:

$$CO_2 + e \rightarrow CO_2^* + e \rightarrow CO + O + e \qquad (10.1)$$

Corvin and Corrigan (Ref. 10.1) estimated from their results that the

coefficient of dissociation was two orders of magnitude greater than the ionization coefficient. From this they concluded that the dissociation must take place by way of uncharged species. It should also be noted that the ionization energy for carbon dioxide is 13.8 eV, while the dissociation energy is 5.4 eV. As mentioned previously, due to short residence times only initial processes are important because the gases would be outside the discharge by the time the secondary effects appear.

Reactions of the type (10.1) are called first order reactions, as they result from a single electron collision. Reactions of second order, that is, the molecule must collide twice with an electron before the dissociation would take place, were studied in Ref. 10.3. The sequence

$$\begin{aligned} CO_2 + e &\rightarrow CO_2^* + e \\ CO_2^* + e &\rightarrow CO + O + e \end{aligned} \tag{10.2}$$

was shown to have small influence up to current densities of at least 12 ma/cm^2 for pure carbon dioxide at 2 mm Hg. For the present experimental results, due to both the observed dissociation and the relatively short residence times, the process (10.2) is assumed to be small compared with the first order reaction (10.1).

Taking reaction (10.1) as the dominant one in the glow discharge of a flowing carbon dioxide laser, we may write the following equation governing the carbon dioxide concentration n_{CO_2}:

$$\frac{dn_{CO_2}}{dt} = -k_1 \bar{n}_e n_{CO_2} \tag{10.3}$$

Here k_1 is the rate constant for dissociation of carbon dioxide by direct electron impact and $\bar{n}_e$ is the average electron density. The rate constant k_1 is defined by:

$$k_1 = \frac{\int_0^\infty \sigma(\varepsilon)\ \sqrt{\varepsilon}\ f(\varepsilon)\ d\varepsilon}{2m_e \int_0^\infty f(\varepsilon)\ d\varepsilon} \qquad (10.4)$$

with $\sigma(\varepsilon)$ the cross section for carbon dioxide excitation and subsequent dissociation by electron collision. The electron energy distribution function is denoted $f(\varepsilon)$.

The model implicitly described by equations (10.3) and (10.4) is based on examining the CO_2-electron collisions in an element of gas as it moves through the laser tube. The CO_2 molecules are assumed stationary compared with the electrons. In this model diffusion, surface reaction, recombination, and all other rate processes except single collision dissociation (eq. 10.3) are neglected.

Integrating equation (10.3) for the characteristic time of the discharge, the residence time τ, we find:

$$\frac{n_{CO_2}(t)}{n_{CO_2}(0)} = e^{-k_1 n_e \tau} \qquad (10.5)$$

From the present experiments (Chapter VIII) and from previous work (Refs. 10.1, 10.3, 10.4, 10.5, for example) the dissociation of CO_2 in the discharge may be represented by the reaction $CO_2 \rightleftharpoons CO + \frac{1}{2} O_2$. Therefore,

$$n_{CO_2}(0) = n_{CO_2}(t) + n_{CO}(t) \tag{10.6}$$

and

$$\frac{n_{CO_2}(\tau)}{n_{CO_2}(0)} = \frac{n_{CO_2}(0) - n_{CO}(\tau)}{n_{CO_2}(\tau) + n_{CO}(\tau)} = e^{-\kappa_1 n_e \tau} \tag{10.7}$$

The dissociation fraction of carbon dioxide D, is defined as

$$D = \frac{n_{CO}(\tau)}{n_{CO_2}(\tau) + n_{CO}(\tau)} \tag{10.8}$$

with (10.6), this definition gives

$$1 - D = e^{-k_1 n_e \tau} \tag{10.9}$$

or

$$D = 1 - e^{-k_1 n_e \tau} \tag{10.10}$$

Equation (10.10) relates the reaction constant k_1, the electron average density and the characteristic time τ to the degree of dissociation of the carbon dioxide molecules in the glow discharge. This same equation was used in Ref. 10.4 to analyze dissociation results in flowing and pulsed lasers. However, because the electron density was not measured directly, its dependence on current and other variables rested on additional assumptions. Those assumptions are not required if the electron density in the dissociation process is measured. The result should be a more accurate description of the gas discharge.

10.2 Application of the Kinetic Model to the Present Work

The residence time τ as a function of the pressure P (in atm) of the plasma can be calculated from the volume flow rate at STP conditions

as:

$$(\text{sec}) = \frac{V_L(\text{cm}^3)\ P(\text{atm})}{Q_{STP}(\text{cm}^3/\text{sec})} \tag{10.11}$$

V_L is the volume of the active region of the plasma, in our case 51.4 cm^3 (65 cm by 1 cm I.D.), Q_{STP} is the total volume flow rate at STP conditions (300°K and 1 atm). Substitution of (10.11) in equation (10.10) gives:

$$D = 1 - e^{-\left(\frac{V_L k_1 P}{Q_{STP}}\right) \bar{n}_e} \tag{10.12}$$

therefore the constant K first defined in equation (8.7) is given by

$$K = \frac{V_L k_1 P}{Q_{STP}} \tag{10.13}$$

10.2.1 First Order Approximations

The rate constant k_1 given by equation (10.4) is not easily calculated except in simple cases. For example, for the hard sphere model ($\sigma_o = \sigma(\varepsilon) = \text{constant}$) and with a Maxwellian distribution gives $k_1 \propto \sqrt{\langle\varepsilon\rangle}$. In general, the form of these two functions $f(\varepsilon)$ and $\sigma(\varepsilon)$ cannot be measured or calculated simply.

If as an approximation we take $\sigma(\varepsilon) \propto \sqrt{\varepsilon}$ then equation (10.4) would give

$$k_1 = C_1\langle\varepsilon\rangle \tag{10.14}$$

where C_1 is a proportionality constant. This very crude approximation

of the cross section can be tolerated if we remember that the real cross section must also increase with energy. The dissociation process requires a minimum amount of energy (dissociation energy = 5.4 eV) in order to occur. Thus the dissociation cross section must go from 0 below but close to the dissociation energy level up to some local maximum value at above that level. Our assumption can thus be made to approximate this portion of the $\sigma(\varepsilon)$ curve. Experimental (Ref. 10.6) and theoretical (Ref. 10.7) evidence indicate that $f(\varepsilon)$ in CO_2 lasers drops in value at least exponentially (usually faster) with energy values above the mean energy. For a typical laser $\langle\varepsilon\rangle \simeq 1$ eV, thus at the energies at which the assumed $\sigma(\varepsilon)$ starts to depart significantly from the real cross section, the product $\sigma(\varepsilon)\sqrt{\varepsilon}\ f(\varepsilon)$ contributes less and less to the integral in equation (10.4) compensating for the error introduced in assuming such cross section dependence on energy ($\sigma(\varepsilon) \propto \sqrt{\varepsilon}$).

The average energy $\langle\varepsilon\rangle$ of the electrons in a glow discharge has been calculated by von Engel (Ref. 10.8, p.244) to be a universal function

$$\langle\varepsilon\rangle = F(c \cdot P \cdot R) \qquad (10.15)$$

Here c is a constant characteristic of each particular gas, P is the pressure in the discharge, and R is the radius of the tube. The agreement of this theory with experiments is quite good. Bekefi and Brown (Ref. 10.9) found that for helium and neon the agreement was good for the range $.2 < P \cdot R < 30$ (mmHg·cm). In the case of carbon dioxide laser mixtures, radiation temperature measurements by Tyte and

Sage (Ref. 10.10) and numerical calculations by Judd (Ref. 10.11) show that there is an inverse dependence of radiation temperature (average energy) with pressure and/or radius of the tube. Thus in the case of carbon dioxide laser discharges, the mean electron energy can be taken as inversely proportional to the product of gas pressure and the radius of the tube. For a given tube, equation (10.14) is taken as:

$$\langle \varepsilon \rangle = C_2/P \tag{10.16}$$

C_2 is a constant for a given mixture composition. Equations (10.13), (10.15), and (10.12) combine to give

$$D = 1 - e^{-K*n_e} \tag{10.17}$$

where

$$K = \frac{V_L * C_1 * C_2}{Q_{STP}} \tag{10.18}$$

Under the assumptions described in this section, the dissociation of carbon dioxide molecules versus average electron density would be independent of the total pressure and would only depend on the volume flow rate at STP conditions.

10.2.2 Comparison of Theory with Experimental Results

The qualitative implications of equation (10.17), mainly the inverse dependence of K with the total flow rate Q_{STP}, are fulfilled in the experimental results discussed in Section 8.3.1 and shown in Table 8.3.

A more striking relationship was found (Section 8.3.4 and Figs. 8.18 to 8.21) when the dissociation constant K was displayed as a

function of the CO_2 partial flow rate at STP . The resulting curve seemed to be the same under all conditions studied in which water vapor was not present. The resulting implications are far more complex to account for in our simple model. Assuming the gases to be ideal

$$\frac{P}{Q_{STP}} = \frac{P_{CO_2}}{Q_{CO_2}} \tag{10.19}$$

then equation (10.11) becomes

$$\tau = \frac{V_L P_{CO_2}}{Q_{CO_2}} \tag{10.20}$$

and K given by equation (10.13)

$$K = \frac{V_L P_{CO_2} k_1}{Q_{CO_2}} \tag{10.21}$$

Using equation (10.14), with its implicit approximation in (10.21), gives

$$K = \frac{V_L C_1 P_{CO_2}^{<\varepsilon>}}{Q_{CO_2}} \tag{10.22}$$

If this model were to predict the experimental results, the following relationship must hold:

$$<\varepsilon> = \frac{C_3}{P_{CO_2}} \tag{10.23}$$

where C_3 would be a constant independent of the mixture composition. Using this relationship in (10.22) gives

$$K = \frac{V_L C_1 C_3}{Q_{CO_2}} \qquad (10.24)$$

Again the limited experimental evidence on the subject seems to support this assumption. Tyte and Sage (Ref. 10.10), using a microwave radiometer, found the following results for the electron radiation temperature (T_r) for the following mixtures at 20.5 torr:

CO_2-N_2-He	T_r (eV)	P_{CO_2} (torr)
(1,4,36)	1.15	.5
(3,4,34)	.92	1.5
(5,4,32)	.87	2.5
(7,4,30)	.78	3.5

i.e., the temperatures decrease when the partial pressure of CO_2 is increased.

In conclusion, the foregoing arguments, although very rough approximations of physical processes in the plasma, give plausible qualitative explanations for the dissociation behavior encountered in the experiments. Rather than saying the final word on the subject, they suggest future areas of exploration both theoretical and experimental.

References

10.1 K. K. Corbin, S.J.B. Corrigan, "Dissociation of Carbon Dioxide in the Positive Column of a Glow Discharge", Physics 50, 2570 (1969).

10.2 R. G. Buser, J. J. Sullivan, "Initial Processes in CO_2 Glow Discharges", J. Appl. Phys. 41, 472 (1970).

10.3 Y. A. Ivanov, L. S. Polak, D. I. Slovetskii, "Kinetics of Carbon Dioxide Decomposition in the Glow Discharge", High Energy Chem. 5, 344 (1972).

10.4 A.L.S. Smith, J. M. Austin, "Dissociation Mechanism in Pulsed and Continuous CO_2 Lasers", J. Phys. D: Appl. Phys. 7, 314 (1974)

10.5 L. C. Brown, A. T. Bell, "Mass-Spectrometric Study of Ionic Species Present During the Oxidation of CO and the Decomposition of CO_2 in a RF Discharge", J. Chem. Phys. 61, 666 (1974).

10.6 M. Z. Novgorodov, A. G. Sviridov, N. N. Sobolev, "Electron Energy Distribution in CO_2 Laser Discharges", IEEE J. Quant. Elect. QE-7, 508 (1971).

10.7 W. L. Nighan, "Electron Energy Distributions and Collision Rates in Electrically Excited N_2, CO, and CO_2", Phys. Rev. A 2, 1989 (1970).

10.8 A. von Engel, Ionized Gases, 2nd Edition (Oxford, 1965).

10.9 G. Bekefi, S. Brown, "Microwave Measurements of the Radiation Temperature of Plasmas", J. Appl. Phys. 32, 25 (1961).

10.10 D. C. Tyte, R. W. Sage, "Electron Temperature Measurements in CO_2 Laser Plasmas", Proc. I.E.R.E. Conf. on Lasers and Optoelectronics, Southampton (1969).

10.11 O. P. Judd, "The Effect of Gas Mixture on the Electron Kinetics in the Electrical CO_2 Gas Laser", J. Appl. Phys. 45, 4572 (1974).

CHAPTER XI

SUMMARY OF THE CO_2 DISSOCIATION RESULTS

The most significant result of the $_2$ laser dissociation experiments is that the degree of dissociation measured as a function of the electron density, depends only on the STP partial flow rate of CO_2. This hypothesis was satisfied under a variety of conditions in several mixtures (with no water present). The carbon dioxide content ranged from 5% to 100%, thus the generalization appears justified. Since only one tube was used in the experiment (1 cm dia.), no generalizations to different diameter tubes can be made at this time. Partial flow rates of CO_2 ranged from .1 to 1.0 cm^3/sec at STP conditions.

The kinetic model developed in Chapter X to account for the experimental behavior generates new questions as to the characteristics of the electron distribution function. Many peculiar dependences of the distribution function (in the form of the average energy $\langle\varepsilon\rangle$) with mixture composition are taken as approximations of real behavior. Both theoretical and experimental investigations should be arrived at analyzing those dependences more closely. A suggested theoretical approach could be to solve the electron Boltzmann's transport equation with the carbon dioxide concentration in a mixture as a parameter. The function thus calculated could then be used to calculate the dissociation rate, assuming the dissociation cross section is known, or simply to calculate the dependence of the average energy with mixture composition to check with the assumptions made in Chapter X (equations

(10.16) and (10.23)) regarding the inverse dependence of average energy $\langle \varepsilon \rangle$ with pressure.

The wide variations in electron density for the same current density but different mixtures underscores to a lesser degree the pressure inaccuracies introduced when dissociation results are reported with current density as a parameter. The probable cause for the variations in electron density is assumed to be the different ionization rates of the various gases. This point should be explored more fully in the future.

APPENDIX A

A.1 EINSTEIN COEFFICIENTS FOR SPONTANEOUS AND STIMULATED EMISSION AND ABSORPTION

The purpose of this appendix is to review the derivation of the important result (2.3). The discussion here is based on Ref. A.1.

It was shown by Einstein (Ref. A.2) that three types of radiative processes may take place by which a photon of energy $\underline{h\omega}$ and momentum $\underline{h\vec{k}}$ can be emitted or absorbed: spontaneous emission, and stimulated emission and absorption. As a result of these processes, the particle that participates in the reaction changes from a state defined by energy and momentum $(\varepsilon', \vec{p}')$ to another, lower or higher state $(\varepsilon, \vec{p})$.

The electrons of a plasma are its most mobile constituents and therefore also the principal source of continuum radiation. Let $\eta_\omega(p,r,s)$ be the differential rate at which energy is emitted spontaneously, per unit solid angle and in unit frequency intervals by an electron with momentum in the range $(\vec{p}', d^3\vec{p}')$. Then with $f(\vec{p})$ the distribution function in momentum space,

$$j_\omega = \int \eta_\omega(\vec{p}')\, f(\vec{p}')\, d^3\vec{p}' \qquad (A.1)$$

is the total emission coefficient per unit volume. Let $\eta_{\omega s}(\vec{p}',r,s)$ be the differential rate of emission by an electron of momentum $\vec{p}'$ per unit intensity of incident radiation, per unit solid angle and per unit frequency interval. Then the coefficient for stimulated emission is defined by:

$$\alpha_{\omega S} = \int \eta_{\omega S}(\vec{p}') \; f(\vec{p}') \; d^3\vec{p}' \tag{A.2}$$

Finally, let $\eta_{\omega A}(\vec{p},r,s)$ be the differential rate of absorption per unit intensity of incident radiation. Then the absorption coefficient is given by:

$$\alpha_{\omega A} = \int \eta_{\omega A}(\vec{p}) \; f(\vec{p}) \; d^3\vec{p} \tag{A.3}$$

Note that this is not the absorption coefficient (a dimensionless quantity) that would be measured in the laboratory, which is given by

$$\alpha_{\omega} = \int \eta_{\omega A} \; f(\vec{p}) \; d^3\vec{p} - \int \eta_{\omega S}(\vec{p}') \; f(\vec{p}') \; d^3\vec{p}' \tag{A.4}$$

By the principle of detailed balancing the following relation is obtained:

$$\eta_{\omega}(\vec{p}') \; f(\vec{p}')d^3\vec{p}' = I(\omega)[\eta_{\omega A}(\vec{p}) \; f(\vec{p})d^3\vec{p} - \eta_{\omega S}(\vec{p}') \; f(\vec{p}')d^3\vec{p}'] \tag{A.5}$$

The scalar quantity I_{ω} is known as the specific intensity of radiation (or simply the intensity). In MKS it has the units of watts per square meter per steradian per radian frequency interval $d\omega$. Relation (A.5) is valid in general since no specific assumption has been made regarding the distribution function $f(\vec{p}')$ or the various rate coefficients.

Let us consider now the case of a plasma contained in an adiabatic shield of temperature T, and in a state of complete equilibrium. Then several of the plasma characteristics are known, namely:

-- The electrons are in their most random state and have a Maxwellian distribution

$$f(p) \propto e^{-\varepsilon/kT} \quad ; \quad \varepsilon = p^2/2m_e$$

-- The radiation intensity $I_\omega = B(\omega,T) = n_r^2 B_0(\omega,T)$ is that of a black body; where n_r is the "ray refractive index" and $B_0(\omega,T)$ is the black-body radiation in vacuum. $B_0(\omega,T)$ is a universal function that depends only on the frequency and temperature, and is given by Planck's formula.

By noting that $f(p)/f(p') = e^{\hbar\omega/kT}$ we can write equation (A.5) as

$$\eta_\omega(\vec{p}')d^3\vec{p} = B(\omega,T)\{\eta_{\omega A}(\vec{p})\, e^{\hbar\omega/kT}\, d^3\vec{p} - \eta_{\omega s}(\vec{p}')d^3\vec{p}'\} \qquad (A.6)$$

which gives $B(\omega,T)$,

$$B(\omega,T) = \frac{\eta_\omega(\vec{p}')}{\eta_{\omega s}(\vec{p}')\,\dfrac{\eta_{\omega A}(\vec{p})d^3\vec{p}}{\eta_{\omega s}(\vec{p}_1)d^3\vec{p}_1}\, e^{\hbar\omega/kT} - 1} \qquad (A.7)$$

From Bose statistics for photons,

$$B(\omega,T) = n_r^2 \frac{\hbar\omega^3}{8\pi^3 c^2}\left[\frac{1}{e^{\hbar\omega/kT} - 1}\right] \qquad (A.8)$$

and comparison of (A.7) and (A.8) gives

$$\frac{\eta_\omega(\vec{p}')}{\eta_{\omega s}(\vec{p}')} = \frac{n_r^2 \hbar\omega^3}{8\pi^3 c^2} \tag{A.9}$$

$$\frac{\eta_{\omega A}(\vec{p})\ d^3\vec{p}}{\eta_{\omega s}(\vec{p}')\ d^3\vec{p}'} = 1 \tag{A.10}$$

Equations (A.9) and (A.10) are independent of the distribution function and are assumed to be valid in general even when equilibrium does not prevail.

Using the above relations, the observed absorption coefficient (A.4) becomes:

$$\alpha_\omega = \frac{8\pi^3 c^2}{n_r^2 \hbar\omega^3} \int \eta_\omega(\vec{p}')\ [f(\vec{p}) - f(\vec{p}')]\ d^3\vec{p}' \tag{A.11}$$

The source function is defined as

$$S_\omega = \frac{j_\omega}{n_r^2\ \alpha_\omega} \tag{A.12}$$

and combination of equations (A.11) and (A.12)gives

$$S_\omega = \frac{\hbar\omega^3 \int \eta_\omega(\vec{p}')\ f(\vec{p}')\ d^3\vec{p}'}{8\pi^3 c^2 \int \eta_\omega(\vec{p}')[f(\vec{p}) - f(\vec{p}')]d^3\vec{p}'} \tag{A.13}$$

Expression (A.13) is the radiation intensity at frequency ω, emanating from the plasma. It is clear that, as the distribution function f(p) approaches a Maxwellian form, the source function S_ω approaches the black-body Planck distribution.

A.2 RADIATION TEMPERATURE

Assume that the plasma is emitting at frequency ω , with intensity S_ω . It is then possible to define a radiation temperature T_r, as the temperature of a black body which would emit with intensity S_ω at the same frequency and bandwidth.

Replace T by T_r in (A.8) and equate the result to (A.13)

$$kT_r = \hbar\omega \left\{ \ell n \left[\frac{\int \eta_\omega(\vec{p}') \; f(p) \; d^3p'}{\int \eta_\omega(\vec{p}') \; f(\vec{p}') \; d^3\vec{p}'} \right] \right\}^{-1} \tag{A.14}$$

With the relations (A.9), (A.10) and definitions (A.2 and (A.3) this becomes

$$kT_r = \hbar\omega \; \{ \ell n (\frac{\alpha_\omega A}{\alpha_{\omega s}}) \}^{-1} \tag{A.15}$$

In the classical limit $\hbar\omega << kT$ (Rayleigh-Jeans)

$$f(p') \doteq f(p) + \hbar\omega \frac{\partial f}{\partial \varepsilon} + \cdots \tag{A.16}$$

Substituting this in denominator of (A.13) we find:

$$S_\omega = \frac{-\omega^2 \int \eta_\omega(\vec{p}) \; f(\vec{p}) \; d^3\vec{p}}{8\pi^3 c^2 \int \eta_\omega(\vec{p}) \; \frac{\partial f}{\partial \varepsilon} \; d^3\vec{p}} \tag{A.17}$$

In equilibrium for the Rayleigh-Jeans limit of the Planck radiation function:

$$kT_r = \frac{8\pi^3 c^2}{\omega^2} S_\omega = \frac{-\int \eta_\omega(\vec{p})\ f(\vec{p})\ d^3\vec{p}}{\int \eta_\omega(\vec{p})\ \frac{\partial f}{\partial \varepsilon}\ d^3\vec{p}} \qquad (A.18)$$

If f(p) is a Maxwellian distribution, then T_r will be the true electron temperature. If we assume that η_ω varies as p^2 and evaluate the integrals in (A.18):

$$kT_r = \frac{\int p^2\ f(\vec{p})\ d^3\vec{p}}{\int 2m\ f(\vec{p})\ d^3\vec{p}} \frac{\langle p^2 \rangle}{2m} = kT_e \qquad (A.19)$$

The radiation temperature is found to be equal to the electron temperature if either of the two conditions is fulfilled. For instance (Ref. A.1) η_ω for helium varies as p^2 for electron energies greater than 1 eV.

References

A.1 G. Bekefi, Radiation Processes in Plasmas (John Wiley & Sons, New York, 1966).

A.2 A. Einstein, Zur Quantentheorie der Strahlung, Phys. Zeit 18, 121 (1917).

APPENDIX B

CHARACTERISTICS OF THE INSTRUMENTS USED IN THE MICROWAVE RADIOMETER

The problem of measuring low power microwave signals emitted by a pulsed discharge is a complicated one. It is necessary to amplify the microwave signal while at the same time shielding the instrumentation from the radiofrequency interference generated by the discharge and other associated circuits.

In order to isolate the instrumentation from the discharge, an enclosure made of copper mesh was built. Inside this enclosure all the instrumentation was located. The microwave emission from the laser was carried into the enclosure by standard waveguide (EIA-WR42) sections for a length of about six meters. A similar length of 50Ω coaxial cable carried the synchronizing signal from the control circuitry of the power supply. This signal was used to synchronize both the oscilloscope and the boxcar averager (for proper signal processing). Initially an optical isolator was used at the enclosure to coaxial interface but, since no difference could be detected, this circuit was removed from the system.

A block diagram of the system (Fig. 3.3) shows the major components of the system:

MIXER-PREAMPLIFIER

VARIAN KCH-760-10-50 SN 3539A

Crystals IN 26CMR

3 db Band Pass 12 mHz

Power gain 22 db

Intermediate frequency 60 mHz

R.F.V. SWR

(2) HP AMPLIFIERS

HP 461A

Frequency Response ± 1 db, 1 kHz-150 mHz

Gain 20 db ± 1 db or 40 db ± .5 db

Noise level -75 dbm (32×10^{-12}W)

(1) ATTENUATOR HP355C

Frequency Range dc-1 gHz

Attenuation 0-12 db, 1 db steps

(1) DIODE DETECTOR

HP 8471A

Frequency Range 100 kHz - 1.2 gHz

Although each element in the system was checked for accuracy, it was believed necessary to calibrate the system as a whole. With the instruments at our disposal, we could not check the microwave section and we had to rely on the factory calibration of the mixer-preamplifier (VARIAN KCH-7-60-10-50). The rest of the system was checked using a calibrated variable signal source at 60 mHz. It turned out that our diode detector was operating in a region between the linear and square law regimes, so calibration curves for different amplifier settings were drawn and were used in interpreting the data.

The microwave section was tested with a calibrated noise source:

AIRBORNE INSTRUMENTS LABORATORY

TYPE 71 NOISE GENERATOR

Power Supply 07111

This noise source had the equivalent temperature of 1.582 eV.

APPENDIX C

C.1 Theory of Microwave Measurements

A plane electromagnetic wave of frequency ω and propagation vector k can be described by

$$\vec{E} = \vec{E}_o \, e^{i(\omega t - \vec{k}\cdot\vec{r})} \tag{C.1}$$

The equation of motion of an electron that is acted upon by this wave and also undergoes collisions with the surrounding gas atoms is, according to Newton's second law

$$m_e \frac{d\vec{v}}{dt} + m_e \nu_m v = -e \, \vec{E}_o \, e^{i(\omega t - \vec{k}\cdot\vec{r})} \tag{C.2}$$

where m_e is the electron mass, ν_m is the collision frequency with gas atoms and e is the electron charge.

If the amplitude of the electron's resulting oscillatory motion is small compared with the wave, or if the wave is of transverse polarization (k perpendicular to E_o), the steady state solution is

$$\vec{v} = \frac{-e\vec{E}_o \, e^{i(\omega t - \vec{k}\cdot\vec{r})}}{m_e(i\omega + \nu_m)} \tag{C.3}$$

The current density then becomes

$$\vec{J} = n_e(-e)\vec{v} = \frac{n_e e^2 \vec{E}_o e^{i(\omega t - \vec{k}\cdot\vec{r})}}{m_e(i\omega + \nu_m)} \tag{C.4}$$

From Maxwell's equations, the wave equation for the electric vector is

$$\vec{\nabla} \times (\vec{\nabla} \times E) = -\mu_o \frac{\partial \vec{J}}{\partial t} - \frac{1}{c^2} \frac{\partial^2 \vec{E}}{\partial t^2} \tag{C.5}$$

Substitution of (C.1) and (C.4) into (C.5) gives

$$k^2 \vec{E} = - \frac{n_e e^2 \, i\omega\mu_o}{m_e(i\omega + \nu_m)} E + \frac{\omega^2}{c^2} \vec{E} \tag{C.6}$$

Then for nonzero $\vec{E}$ the wave number must be

$$k^2 = \frac{\omega^2}{c^2} \{1 - \frac{\omega_p^2}{\nu_m^2 + \omega^2} (1 + i \frac{\nu_m}{\omega})\} \tag{C.7}$$

The plasma frequency ω_p is given by

$$\omega_p^2 = \frac{n_e e^2}{m_e \varepsilon_o} = \frac{56.4}{2\pi} \sqrt{n_e} \text{ Hz } (n_e \text{ in cm}^{-3}) \tag{C.8}$$

and the square of the complex index of refraction of the plasma is

$$\mu^2 = 1 - \frac{\omega_p^2}{\nu_m^2 + \omega^2} (1 + \frac{\nu_m}{\omega} i) \tag{C.9}$$

To first approximation (Ref. C.1) the change in Q of a cavity into which a medium of index of refraction μ is introduced is

$$\frac{1}{Q} - \frac{1}{Q_o} = \frac{\int (\mu^2)_{Im} E_o \cdot E_o \, dV}{\int E_o \cdot E_o \, dV}$$

Then with (C.9),

$$\frac{1}{Q} - \frac{1}{Q_o} = - \frac{(\nu_m/\omega)}{\omega^2 + \nu_m^2} \frac{\int \omega_p^2 \vec{E}_o \cdot \vec{E}_o \, dV}{\int \vec{E}_o \cdot \vec{E}_o \, dV} \tag{C.10}$$

Similarly (Ref. C.1) the fractional shift in resonant frequency is

$$\frac{\Delta f}{f_o} = -\frac{1}{2}\frac{\int [(\mu^2)_R - 1]\, E_o \cdot E_o \, dV}{\int E_o \cdot E_o \, dV} \tag{C.11}$$

or

$$\frac{\Delta f}{f_o} = \frac{1}{2}\frac{1}{(\omega^2+\nu_m^2)}\frac{\int \omega_p^2 \, E_o \cdot E_o \, dV}{\int E_o \cdot E_o \, dV}$$

From (C.8) write the plasma frequency as

$$\omega_p^2(r) = \omega_{po}^2\left(\frac{n_e(r)}{n_o}\right) \tag{C.12}$$

where ω_{po} is the plasma frequency corresponding to n_o.

Now define the form factor η

$$\eta = \frac{\int \frac{n_e(r)}{n_o} E_o \cdot E_o \, dV}{\int E_o \cdot E_o \, dV} \tag{C.13}$$

and after using (C.12), equations (C.10) and (C.11) become

$$\Delta\left(\frac{1}{Q}\right) = \frac{(\nu_m/\omega)}{\omega^2 + \nu_m^2}\, \omega_{po}^2\, \eta \tag{C.14}$$

$$\frac{\Delta f}{f_o} = \frac{1}{2}\frac{\omega_{po}^2}{\omega^2 + \nu_m^2}\, \eta \tag{C.15}$$

These may be solved for ν_m and ω_{po} to give

$$\nu_m = \frac{\omega}{2}\frac{\Delta(1/Q)}{\left(\frac{\Delta f}{f_o}\right)} \tag{C.16}$$

$$\omega_{po}^2 = \frac{2}{\eta}\omega^2\left(\frac{\Delta f}{f_o}\right)\left\{1 + \left[\frac{\Delta(1/Q)}{2(\Delta f/f_o)}\right]^2\right\} \qquad (C.17)$$

after using (C.8),

$$n_o = \frac{2\omega^2 m_e \varepsilon_o}{\eta e^2}\left(\frac{\Delta f}{f}\right)\left\{1 + \left[\frac{\Delta(1/Q)}{2(\Delta f/f_o)}\right]^2\right\} \qquad (C.18)$$

C.2 Evaluation of the Form Factor - (Eq. C.13)

The microwave cavity is taken to be cylindrical, of radius R_o and length L. The plasma (glow discharge) is assumed to be contained in an infinite cylinder coaxial with the cavity and of smaller radius R ($R/R_o \simeq .10$)

The electron density in the plasma is assumed to be distributed as a Bessel function of zeroth order (von Engel, Ref. C.2)

$$n_e(r) = n_o J_o(x_{01}\frac{r}{R}) \qquad x_{01} = 2.40482\ldots \qquad (C.19)$$

where x_{01} is the first zero of the Bessel function. Note that the average density is

$$\bar{n}_e = .432 \times n_o$$

$$\bar{n}_e = \frac{n_o}{\pi R^2}\int_0^R J_o(x_{01}\frac{r}{R})\, 2\pi r\, dr = 0.432\, n_o \qquad (C.20)$$

The assumptions used to derive relations (C.16) and (C.15) limit us to conditions in which the electric field in the cavity is not very different from the value with no plasma present. In practice this limits the value of R/R_o to less than 0.2.

C.2.1 TM_{011} Mode

From Ref. C.3, for the TM_{011} mode in a cylindrical cavity of radius R_o and length L,

$$E_o \cdot E_o = E_o^2(r) \propto J_o^2(x_{01}\frac{r}{R_o}) + (\frac{\pi R_o}{x_{01}L})^2 J_1^2(x_{01}\frac{r}{R_o}) \qquad (C.21)$$

and $J_o(x_{01}) = 0$. Using (C.19) and (C.21) in (C.13) gives

$$\eta_{011} = \frac{\int_0^R J_o(x_{01}\frac{r}{R})\ J_o^2(x_{01}\frac{r}{R_o}) + (\frac{R_o}{Lx_{01}})^2 J_1^2(x_{01}\frac{r}{R_o})\ r\,dr}{\int_0^{R_o}\{J_o^2(x_{01}\frac{r}{R_o}) + J_1^2(x_{01}\frac{r}{R_o})(\frac{\pi R_o}{Lx_{01}})^2\}\ r\,dr} \qquad (C.22)$$

In Figure C.1 are shown the results of the numerical integration of equation (C.22) for a cavity of length L = 7.81 cm. The form factor η_{011} is shown as a function of R/R_o.

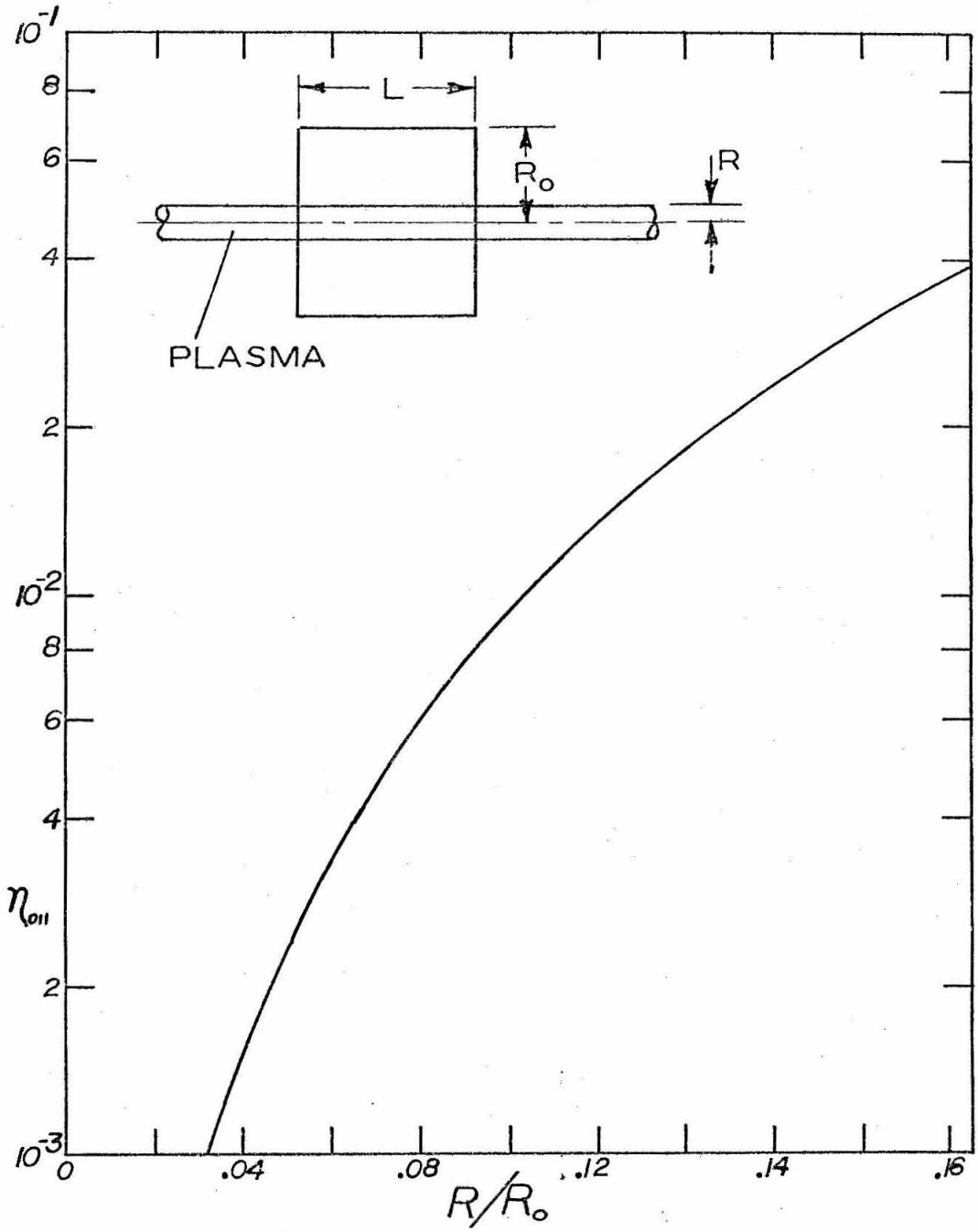

Fig. C-1: Calculated value of η for the TM_{011} mode of a cylindrical cavity. of length L = 7.81 cm.

References

C.1 Slater, J. C., "Microwave electronics", Rev. of Mod. Phys. 18, 441 (1946).

C.2 von Engel, A., Ionized Gases, 2nd Ed. (Oxford, 1965), p. 241.

C.3 Jackson, J. D., Classical Electrodynamics (John Wiley & Sons, Inc., 1962).

APPENDIX D

D.1 Numerical Solution of Boltzmann's Transport Equation for Electrons in the Glow Discharge

The electrons in a gas discharge can be fully described by the Boltzmann equation. However, the solution for the most general problem is too complex to do exactly. The distribution function $f(t,\vec{r},\vec{v})$ is found by solving the following differential equation:

$$\frac{\partial f}{\partial t} + (\vec{v}\cdot\vec{\nabla}_r)f + (\vec{a}_o\vec{\nabla}_v)f = \left(\frac{\delta f}{\delta t}\right)_{\text{collisions}} \qquad \text{(D-1)}$$

where $\vec{\nabla}_v$ is the gradient operator in velocity space and $\left(\frac{\delta f}{\delta t}\right)_{\text{coll}}$ gives the changes in the distribution function due to collisions.

Equation (D-1) can be reduced to a more manageable size if the following assumptions are made:

(1) The plasma is steady, isotropic and boundless. Thus, the distribution function depends on the velocity only, with no dependence on time.

(2) The Lorentz approximation is applicable (Ref. D-1):

$$f(v) \cong f_o(v) + \frac{\vec{v}}{|v|}\cdot\vec{f}_1(v) \quad \{f_o(v) >> |f_1(v)|\} \qquad \text{(D-2)}$$

i.e., the distribution function f can be expressed by an isotropic part $f_o(v)$ and by a small perturbation $\frac{\vec{v}}{|v|}\cdot\vec{f}_1(v)$ dependent on the velocity direction. This approximation implies that the collision frequency for momentum transfer is much larger than the collision frequency for excitation, and therefore for dissociation as well.

(3) Ionization is low, thus we can neglect e-e and e-ion interactions.

With the above assumptions, Boltzmann's transport equation, in the presence of an electric field $\vec{E}$, becomes:

$$\left(-\frac{e\vec{E}}{m} \cdot \nabla v\right) f = \left(\frac{\delta f}{\delta t}\right)_{coll} \tag{D-3}$$

With the Lorentz approximation (2), equation (D-3) gives the two equations for f_1 and f_o:

$$-\frac{e\vec{E}}{3mv^2} \cdot \left[\frac{\partial(v^2 f_1)}{\partial v}\right] = \left(\frac{\delta f_o}{\delta t}\right)_{coll} \tag{D-4}$$

$$-\frac{e\vec{E}}{m}\frac{\partial f_o}{\partial v} = \left(\frac{\delta \vec{f}_1}{\delta t}\right)_{coll} \tag{D-5}$$

The collision term in equation (D-5) is given by

$$\left(\frac{\delta f_1}{\delta t}\right)_{coll} = -\sum_j N_j Q_j^{(e)} \, v \, \vec{f}_1(v) \tag{D-6}$$

where $Q_j^{(e)}$ is the elastic cross section of the j^{th} element. If we change variables to energy, $u = mv^2/2e$, and substitute (D-6) into (D-5), this produces

$$\vec{f}_1(v) = \frac{e\vec{E}}{m \sum_j N_j Q_j^{(e)}} \cdot \frac{\partial f_o}{\partial v} \tag{D-7}$$

Equations (D-4) and (D-7) may now be combined to give

$$- \frac{E^2}{3} \frac{\partial}{\partial u} \left\{ \frac{u}{\sum_j N_j Q_j^{(e)}} \frac{\partial f_o}{\partial u} \right\} = \frac{u}{v} \left(\frac{\delta f_o}{\delta t} \right)_{coll} \qquad \text{(D-8)}$$

The inelastic collision term is given by

$$\frac{u}{v} \left(\frac{\delta f_o}{\delta t} \right)_{coll} = \sum_j \sum_k N_j [(u + \Delta_{jk}) \; f_o(u + \Delta_{jk}) \; Q_{jk}^{(i)}(u + \Delta_{jk})$$

$$- u \; f_o(u) \; Q_{jk}^{(i)}(u)] \qquad \text{(D-9)}$$

where $Q_{jk}^{(i)}(u)$ is the electron cross section for excitation (or de-excitation) of the k^{th} level of the j^{th} species with a corresponding energy loss (or gain) Δ_{jk}. The first integral of (D-8) is (Ref. D-1)

$$- \left(\frac{E}{N} \right)^2 \frac{u}{3} \frac{\partial f_o}{\partial u} \frac{1}{\sum_j \delta_j Q_j^{(e)}(u)} = \sum_j \sum_k \delta_j \int_u^{u+\Delta_{jk}} x \; f_o(x) \; Q_{jk}^{(i)}(x) \; dx \qquad \text{(D-10)}$$

where $\delta_j = \frac{N_j}{N}$. If we now define the functions ELAST(u), INTEG(u) and constant B,

$$\text{ELAST}(u) = \sum_j \delta_j Q_j^{(e)}(u) \qquad \text{(D-11)}$$

$$\text{INTEG}(u) = \sum_j \sum_k \delta_j \int_u^{u+\Delta_{jk}} x \; f(x) \; Q_{jk}(x) \; dx \qquad \text{(D-12)}$$

$$B = \left(\frac{E}{N} \right)^2 \times \frac{1}{3} \qquad \text{(D-13)}$$

then equation (D-10) can be integrated formally to give:

$$f(u) = -\int_{u}^{u_o} \frac{\text{ELAST}(u) \times \text{INTEG}(u)}{B * u}\, du \qquad \text{(D-14)}$$

For given N, δ_j, E, $Q_j^{(e)}(u)$, $Q_{jk}^{(i)}(u)$ and Δ_{jk}, the function f(u) in equation (D-14) can be calculated (at least in principle) by numerical techniques. A procedure suggested by Judd (Ref. D-2) starts with a boundary condition $f(u_o) = F$ at some high value of energy $u_o >> \bar{u}_e$; (D-14) is then integrated in small steps to lower energies. Judd found that if u_o is sufficiently high, $u_o/\bar{u}_e \simeq 40$, the solution converges to the same form independent of the boundary condition chosen at u_o.

D-2 Dissociation Processes and Boltzmann's Equation

In the event dissociation takes place, the number density of particles N is no longer fixed and will vary according to the degree of dissociation. Thus, suppose that the degree of dissociation is given by equation (10.5):

$$N_{CO_2}(\tau) = N_{CO_2}^{(0)}\, e^{-k_1 n_e \tau} \qquad \text{(D-15)}$$

where

$$k_1 = \sqrt{\frac{2e}{m}} \int u \cdot f(u) \cdot Q_d(u)\, du \qquad \text{(D-16)}$$

and $Q_d(u)$ is the dissociation cross section.

Assuming that the process $CO_2 \rightleftarrows CO + \frac{1}{2} O_2$ takes place, we can calculate the number densities of CO and O_2:

$$N_{CO}(\tau) = N_{CO_2}^{(0)}(1 - e^{-k_1 n_e \tau}) \qquad \text{(D-17)}$$

$$N_{O_2}(\tau) = \frac{N_{CO_2}^{(0)}}{2}\{1 - e^{-k_1 n_e \tau}\} \qquad (D\text{-}18)$$

Since $N = N_1 + N_2 + N_3 + \cdots + N_{CO_2} + N_{O_2} + N_{CO}$, and by using (D-15), (D-17) and (D-18), we find:

$$N = N^{(0)} + \frac{N_{CO_2}^{(0)}}{2}(1 - e^{-k_1 n_e \tau}) \qquad (D\text{-}19)$$

If the dissociation cross section were known accurately it would then be possible to obtain the degree of dissociation for any initial mixture by solving (D-14) with (D-15, D-17, D-18 and D-19) as additional constraints.

D-3 Calculation of the Dissociation Cross Section from Boltzmann's Equation and Experimental Results

Since the values of the dissociation cross section are not known accurately, the reverse problem of the one discussed in Section D-2 m might be of more practical importance. Namely, it should be possible to calculate the dissociation cross section by comparing the experimentally observed dissociation with the calculated distribution function through equation (D-16).

If we assume that we experimentally study "q" different conditions, then we would have "q" different values for k_1

$$\{k_1\} = \{k_1^{(1)}, k_1^{(2)}, k_1^{(3)}, k_1^{(4)}, \ldots, k_1^{(q)}\}$$

Since the degree of dissociation would be different in each case, we should also have "q" different distribution functions

$$\{f\} = \{f^{(1)}, f^{(2)}, f^{(3)}, \ldots, f^{(q)}\}$$

Therefore the following set of integral equations could be generated

$$\{k_1\} = \int_0^\infty \frac{2e}{m} u\, Q_d(u)\, \{f\}\, du \qquad \text{(D-20)}$$

Thus it is possible, although it might not be simply done, to solve (D-20) for the dissociation cross section $Q_d(u)$.

References

D-1 William L. Nighan, "Electron Energy Distributions and Collision Rates in Electrically Excited N_2, CO, and CO_2", Phys. Rev. A 2, 1989-2000 (1970).

D-2 C. J. Elliott, O. P. Judd, A. M. Lockett and S. D. Rockwood, "Electron Transport Coefficients and Vibrational Excitation Rates for Electrically Excited CO_2 Gas Lasers", Los Alamos Scientific Laboratory Research Report No. LA-5562 MS (1973).